CHARACTERIZATION AND MUTATION OF IODOTYROSINE DEIODINASE FROM *Haliscomenobacter hydrossis* FOR DETOXIFICATION OF IODOPHENOLS

by
Nattha Ingavat

A dissertation submitted to Johns Hopkins University in conformity with the requirements for the degree of Doctor of Philosophy

Baltimore, Maryland

March, 2017

Abstract

Iodotyrosine deiodinase (IYD) catalyzes deiodination of mono- and diiodotyrosines (I-Tyr and I_2-Tyr) to recycle iodide for proper thyroid function in mammals. IYD is also present in all animals and even some bacteria, although their function in lower organisms is not clear. In this study, a representative set of IYD from eukaryotes and prokaryotes was selected to assess their deiodination of iodophenols for bioremediation. Human IYD, bacterial IYD (hhIYD) and archaeal IYD (pfuIYD) exhibit different substrate binding recognition but their catalytic specificity is surprisingly conserved for iodotyrosines. Greater affinity of hhIYD for 2-iodophenol (2IP) compared to human IYD (~20 fold increased in affinity) indicated that interactions from the phenolate anion of 2IP can compensate for the lack of interactions established by the zwitterion of I-Tyr. Deiodination rates of 2IP by hhIYD are still very slow compared to that of I-Tyr suggesting that affinity is not diagnostic of catalytic efficiency. A crystal structure of hhIYD•I-Tyr shows the formation of an active site lid induced by interactions with the zwitterion of I-Tyr. However, the active site lid is not ordered in a structure of hhIYD•2IP indicating that 2IP cannot trigger closure of the active site lid. Reduction of hhIYD in the alternative presence of a substrate analog F-Tyr and 2IP also indicates differences in the ability of the zwitterionic substrate and 2IP to initiate IYD catalysis. A flavin semiquinone (FMN_{sq}) was detected during the reduction of hhIYD in the presence of F-Tyr but accumulation of this same intermediate was not observed in the presence of 2IP. Crystallographic and redox studies demonstrated that 2IP lacks an ability to initiate formation of the active site lid and cannot stabilize the one-electron chemistry for IYD catalysis, which explain its slow deiodination rates.

To enable IYD for bioremediation of iodophenols, three hhIYD mutants were generated in hopes of improving the k_{cat}/K_m values for iodophenol turnover. However, these mutants did not provide much increase in the catalytic efficiency for deiodination of iodopehnols as their k_{cat}/K_m values are ~3 – 17 fold lower than that of the wild-type hhIYD. However, the studies demonstrated

a repulsive interaction between Glu91 and the carboxylate of 4-hydroxy-3-iodobenzoate (2IPCOOH) can significantly increase the K_m for deiodination of 2IPCOOH. Removal of this repulsive interaction can significantly decrease the K_m as evident by a ~4 fold lower K_m for deiodination of 2IPCOOH by an E91R mutant compared to the wild type. This result suggests E91 is a potential mutation site for fine-tuning the K_m for deiodination of iodophenols.

In addition to hhIYD, two IYD-related enzymes (BluB and 3EO8) were selected to examine their native affinity for 2IP. Neither BluB nor 3EO8 bound 2IP with measurable affinity. Further structural analysis of 3EO8 indicated that its active site was relatively small to accommodate 2IP. 3EO8 mutants were therefore generated to enlarge its active site for 2IP coordination. However, the 3EO8 mutants did not improve the affinity for 2IP. A mutant with the highest affinity with 2IP demonstrated only a 20 % increase in affinity compared to the wild-type 3EO8.

Advisor: Prof. Steven E. Rokita

Readers: Prof.Craig A. Townsend

Prof. Marc M. Greenberg

Dedication

To my family, for their unconditional support

Acknowledgements

Coming to pursue the Ph.D. study in the US was quite a big transition for me. This journey could not be successful without love and supports from many people. Firstly, I would like to thank my advisor Professor Steven E. Rokita for accepting me into his research group. I really appreciate his efforts to train me how to think and ask myself specific questions before setting up each experiment and how to learn from the failed experiments. Also, thank you very much for spending a lot of time to teach me how to perform good scientific writing, which I think is one of the hardest communication skills. Especially, for me as English is not my first language. Lastly, thank you for allowing me to have such a good work-life balance during my Ph.D. study. I would like to thank Professor Criag A. Townsend and Professor Marc M. Greenberg for being my thesis advisory committees and spending time to read and give suggestions on my work.

My work could not be accomplished without training, assistance, guidance and facilities from our collaborator, Assistant Professor Jennifer M. Kavran at the Department of Biochemistry and Molecular Biology in the Bloomberg School of Public Health. She was the first person who introduced me to protein crystallography. She has also helped me a lot throughout for structural determination. Also, thank you my senior, Dr. Watchalee Chuenchor, at NIH and my friend, Dr. Leela Ruckthong, at the King Mongkut's University of Technology Thonburi in Thailand for providing me knowledge together with suggestions for protein crystallization.

I would like to thank all the present and former members of the Rokita lab. I am very grateful to Dr. Abhishek Phatarphekar, Dr. Blessing Deeyaa and Dr. Mark Hutchinson. We all joined the lab at the same year and have been helping each other a lot from research to other difficulties. I would like to thank again Dr. Abhishek Phatarphekar and Dr. Shalini Saha for helping me to get started on biochemistry and molecular biology work, as well as sharing their scientific experience to me. Their assistance allowed me to have a smooth transition from being a natural product chemistry to a biochemist. Also, thank you all younger generations in the lab (Zuodong Sun, Qi Su, Shane Byrne and Anton Kozyryev), who have such strong inspiration and intention towards

science. I also learned a lot from them. I would like to thank you my dear friends, Dr. Blessing Deeyaa, Darcie Long and Digs, Herdeline Ardoña, for their consolation, love and care. I also feel very grateful for all my Thai friends who are always around to give me helps and supports. Also, I feel very enjoyable to spend such wonderful moments with them, which really helps me from being homesick.

Lastly, but very importantly, I feel very grateful towards my family for their unconditional love, supports and contributions. To my parents who always give me encouragement, advices, unconditional love and supports by all means. To my two younger sisters for patiently listening to me and taking part of my responsibilities at home. To my uncles and antie for taking good care of my parents. To my grandmother who always gave me love and care, as well as kept motivating me for education. She was my huge inspiration for my Ph.D. study. Unfortunately, she did not have a chance to appreciate it since she passed away in the middle of my Ph.D. journey.

Table of Contents

List of Tables

Chapter 1: Introduction

None

Chapter 2: Analysis of binding and catalysis specificity for IYD homologs

Chapter 3: Structural and functional analysis for the slow turnover of 2-iodophenol by hhIYD

Chapter 4: Mutation of hhIYD to improve catalytic efficiency of turnover of 2-iodophenols

Chapter 5: Analysis of IYD-related enzymes for affinity of 2-halophenols

Chapter 6: Conclusions

None

List of Figures

Chapter 1 :Introduction

Chapter 2: Analysis of binding and catalysis specificity for IYD homologs

Chapter 3: Structural and functional analysis for the slow turnover of 2-iodophenol by hhIYD

Chapter 4: Mutation of hhIYD to improve catalytic efficiency of turnover of 2-iodophenols

Chapter 5: Analysis of IYD-related enzymes for affinity of 2-halophenols

Chapter 6: Conclusions

None

List of Abbreviations

AUC - Area under curve

4A2IP - 4-amino-2-iodophenol

BLAST - Basic Local Alignment and Search Tool

BluB - bacterial flavin destructase

Br-Tyr - 3-monobromotyrosine

2BP - 2-bromophenol

Cl-Tyr - 3-monochlorotyrosine

2CP - 2-chlorophenol

DDT - dichlorodiphenyltrichloroethane

FAD - Flavin adenine dinucleotide

FMN - flavomononucleotide

FMN_{hq}- FMN hydroquinone

FMN_{ox} - FMN in an oxidized form

FMN_{sq} - FMN semiquinone

FRP - flavin reductase P

F-Tyr - 3-monofluorotyrosine

2FP - 2-fluorophenol

GSH -glutathione

hhIYD - IYD from *Haliscomenobacter hydrossis*

ID -iodothyronine deiodinase

IS - internal standard

I-Tyr - 3-monoiodotyrosine

I_2-Tyr -diiodotyrosine

IYD - iodotyrosine deiodinase

2IP -2-iodophenol

2IPCN - 4-hydroxy-3-iodobenzonitrile

2IPCOOH - 4-hydroxy-3-iodobenzoate

K_d - dissociation constants

LB - Luria-Bertani media

NOX - NADH oxidase

NTR - nitroreductase

PCBs -polychlorinated biphenyls

PCP - pentachlorophenol

pfuIYD - IYD from *Pyrococcus furiosus*

PMSF - phenylmethylsulfonyl fluoride

RT - room temperature

SEC - size-exclusion chromatography

TCBQ -tetrachloro-1,4-benzoquinone

TCHQ -tetrachlorohydroquinone

TH -thyroid hormone

tnIYD – IYD from *Thermotoga neopolitiana*

TriCHQ -trichlorohydroquinone

X-Tyr - 3-halotyrosines

2XP - 2-halophenols

Chapter 1: Introduction

1.1 Halogenated aromatics: Significance, concerns and biological remediation

Bioremediation is the use of microorganisms and enzymes to degrade environmental pollutants.[1] This process was initially developed through defense mechanisms of microorganisms thriving in contaminated sites. Halogenated compounds present in nature allow microorganisms to evolve their metabolic pathways to use organohalides as a new carbon and energy source.[2] Several anaerobic bacteria are able to consume chlorinated benzenes[3] or polychlorinated dibenzodioxins[4] as terminal electron acceptors for their energy metabolism. These bacteria utilize reductive dehalogenation for their electron transport process.[5] Development of microbial strains has been done for implementing detoxification of halogenated wastes. As bioremediation involves enzymatic processes, it is normally operated at neutral pH and mild temperature without producing more toxic wastes.[2, 6] Lately, bioremediation has been developed to rival the efficiency of chemical treatments but offers a more environment-friendly alternative.[6] For example, a lignin peroxidase from *Phanerochaete chrysosporiumhas* has been used for bioremediation of polycyclic aromatic hydrocarbons (PAHs), which provides similar product ratios to those found from chemical degradation.[6] However, certain classes of substances are resistant to biodegradation, and thus discourage application of biological processes. Among the most problematic non-biodegradable compounds are haloaromatics because the halogens may block many dioxygenase enzymes which normally initiates degradation of aromatic rings.[2, 7-9] Haloaromatics are used in many applications such as polychlorinated biphenyls (PCBs) used in electrical transformers, coolants and hydraulic fluids,[2, 7] pentachlorophenol (PCP) used as pesticides[2, 7, 10] and dichlorodiphenyltrichloroethane (DDT) used commonly as pesticide (Figure 1-1).[2, 7] Large-scale consumption coupled with poor disposal practice of halogenated aromatics have liberated a large amount of these compounds into the environment. Their persistence together with intrinsic toxicity consequently harm the surroundings and human health.[2, 7-9] Many efforts have been directed at replacing haloaromatics with other less harmful materials. However, the unique physiochemical properties of halogenated compounds dim the feasibility.[2]

Accordingly, research is currently directed at eliminating non-biodegradable halogenated aromatics, especially, the most widely-used chlorinated ones.[2, 7-9] Development of new enzymes to eliminate different classes of non-biodegradable substances would provide more alternatives and enhance the efficiency of bioremediation. Studies on degradation of haloaromatic compounds by microorganisms have led to discovery and characterization of several dehalogenases that play key roles in detoxification of haloaromatic substances.

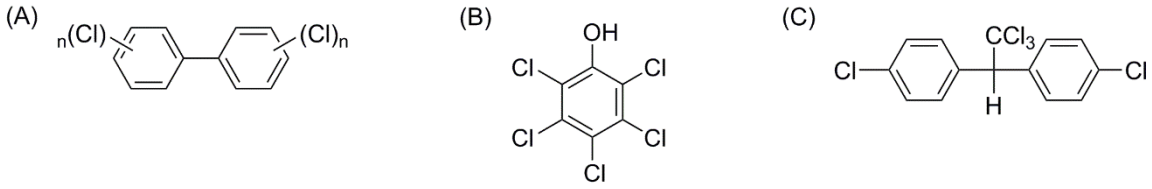

Figure 1-1. Structures of (A) polychlorinated biphenyls, PCB (B) pentachlorophenol, PCP and (C) dichlorodiphenyltrichloroethane, DDT.

1.2 Types of aromatic dehalogenases

There are three classes of aromatic dehalogenases that have different mechanisms and different net reactions.[2, 7] Examples below are aromatic dechlorinating enzymes as they are the best studied for bioremediation.

1.2.1 Hydrolytic dehalogenases

Hydrolytic dehalogenases catalyze replacement of halide with a hydroxyl group.[2, 7] An example is 4-chlorobenzoyl CoA dehalogenase found in a number of aerobic soil bacteria catalyzing dechlorination of 4-chlorobenzoyl CoA, an intermediate formed in certain PCB degradation pathways.[2, 11] The mechanism for catalysis involves nucleophilic aromatic substitution, which is normally unfavorable due to the introduction of a nucleophile to an electron-rich aromatic ring. However, with a *para* electron-withdrawing thioester group in the substrate, 4-chlorobenzoyl CoA dehalogenase can mediate catalysis by delocalizing electrons from an attacking Asp-145 into thioester prior to expulsion of chloride (Figure 1-2). A catalytic cycle is then completed by hydrolysis of an acyl-enzyme intermediate complex. The mechanism shows 4-chlorobenzoyl CoA

dehalogenase requires the substrate to contain a thioester group at the *para* position of a hydroxylated site to achieve dechlorination.[2, 7]

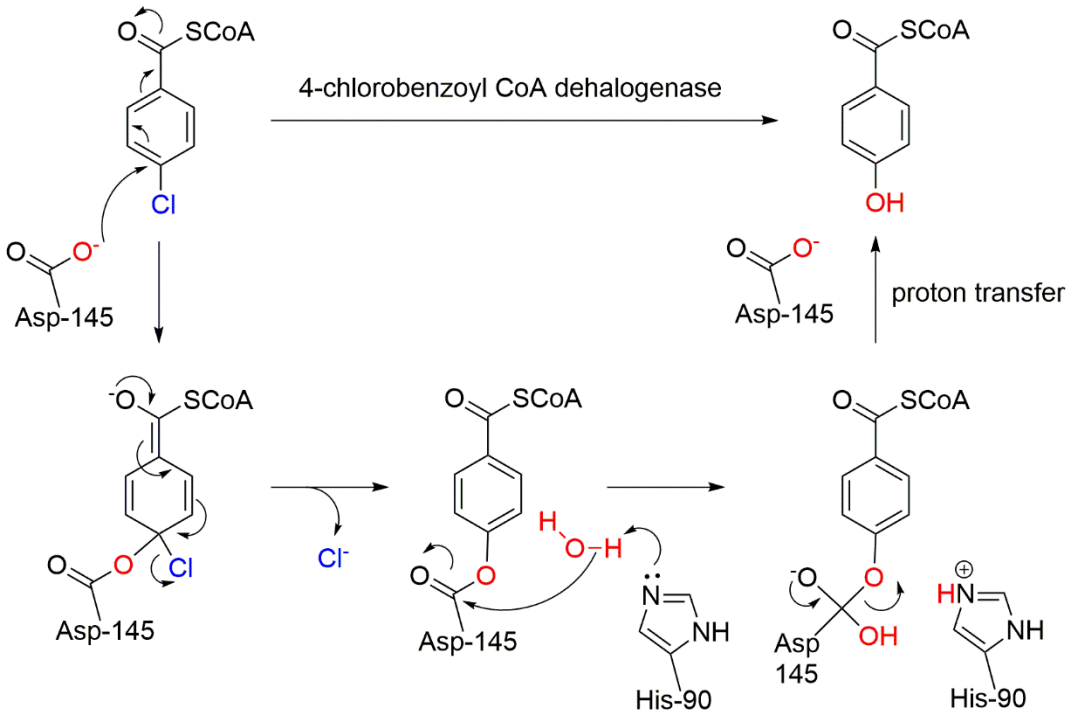

Figure 1-2. Mechanism of 4-chlorobenzoyl CoA dehalogenase.

1.2.2 Oxidative dehalogenases

Oxidative dehalogenases catalyze replacement of a halide with a hydroxyl group derived from molecular oxygen.[2, 7] An example is pentachlorophenol monooxygenase (PCP monooxygenase), containing flavin adenine dinucleotide (FAD) as a cofactor.[7] PCP monooxygenase catalyzes the first step of PCP degradation, which transforms PCP to tetrachlorohydroquinone (TCHQ) in the presence of oxygen and 2 equivalents of NADPH (Figure 1-3A).[7]

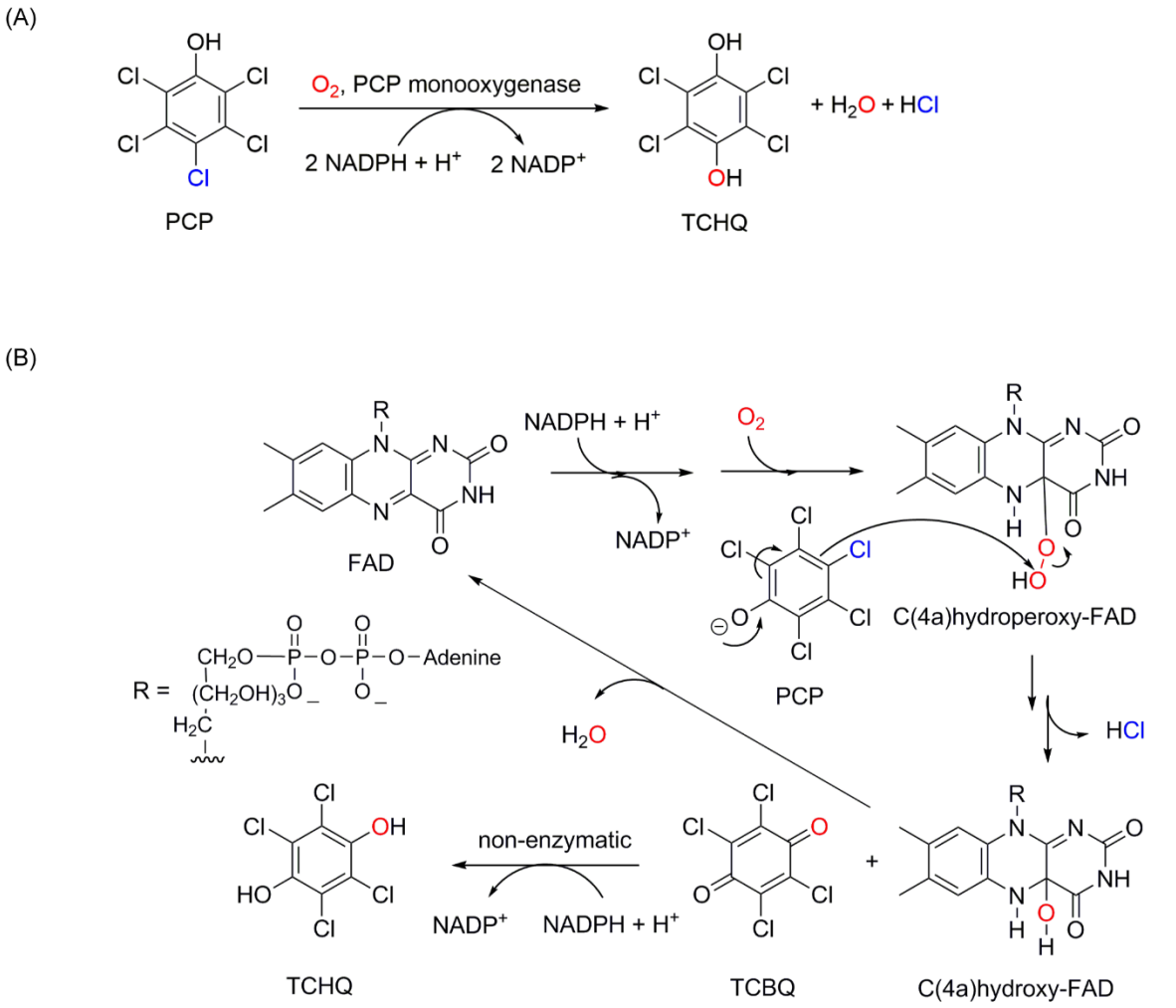

Figure 1-3. (A) Degradation of PCP to TCHQ by PCP monooxygenase (B) Proposed mechanism of PCP monooxygenase.

The mechanism illustrated in Figure 1-3B shows that PCP monooxygenase requires a substrate (PCP) to have a *para*-hydroxyl group to mediate hydroxylation. The *para*-hydroxyl substituent helps with bond reorganization to react with the C(4a)hydroperoxy-FAD to produce tetrachloro-1,4-benzoquinone (TCBQ). This product is then reduced by NADPH to yield TCHQ.[2] This observation suggests PCP monooxygenase is applicable for a substrate with a different substituted position from that of 4-chlorobenzoyl CoA dehalogenase.

1.2.3 Reductive dehydrogenases

Reductive dehydrogenases replace a halosubstituent with a hydrogen atom.[2, 7] An example is tetrachlorohydroquinone dehydrogenase (TCHQ dehydrogenase), which catalyzes reductive dechlorination of TCHQ to trichlorohydroquinone (TriCHQ). This is the second step in a PCP degradation pathway and uses glutathione (GSH) as a reducing equivalent.[2, 7] The proposed mechanism in Figure 1-4 shows chloride is removed during transformation of TCHQ to trichlobenzoquinone (TriCBQ), suggesting necessity for the presence of two *para*-hydroxyl groups in the substrate for dechlorination. TriCBQ then undergoes 1,4-nucleophilic addition with GSH and is reduced by Cys-13 in an active site of the enzyme to yield TriCHQ as a product. A catalytic cycle is completed by oxidation of another GSH to exchange a disulfide bond with a mixed glutathione-Cys13 complex.[12]

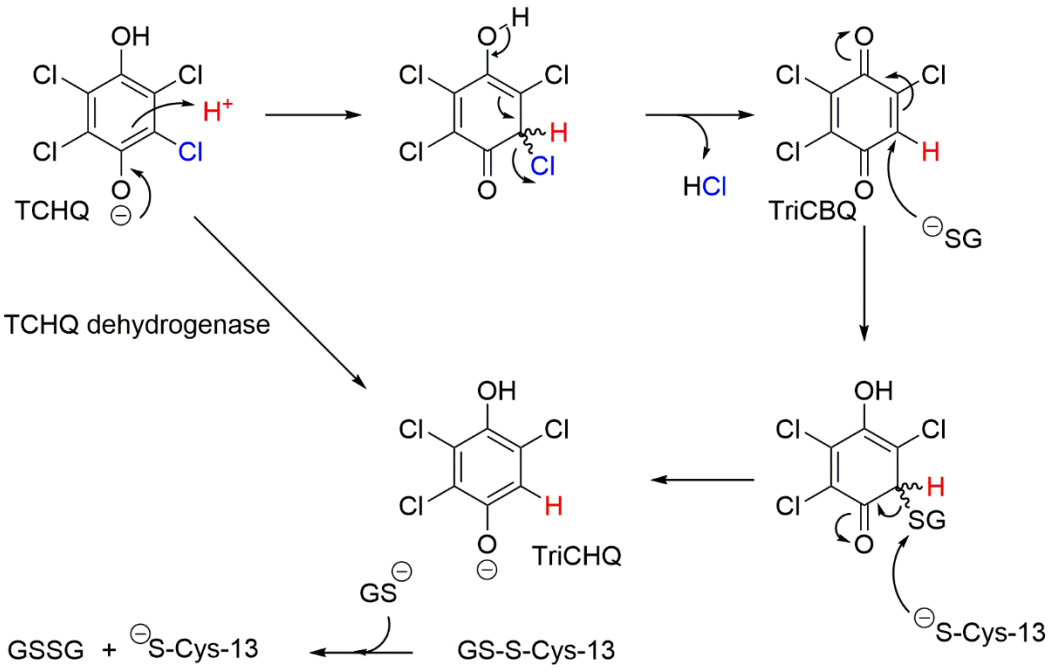

Figure 1-4. Proposed mechanism of reductive dechlorination of TCHQ by TCHQ dehaloganase.

As illustrated in three mechanisms above, each enzyme requires substrates with different groups and/or different substituent positions. Additional mechanisms of dehalogenases may provide

additional alternatives for detoxification of the halogenated aromatics. For example, an iodotyrosine deiodinase (IYD) may be used in bioremediation of haloaromatics.

1.3 Introduction to iodotyrosine deiodinase (IYD)

IYD is a dimeric flavoprotein responsible for recycling iodide from the byproducts of thyroid hormone biosynthesis, monoiodotyrosine (I-Tyr) and diiodotyrosine (I_2-Tyr) (Figure 1-5), which otherwise would be liberated as waste.[13, 14] Iodide is a micronutrient essential for production of thyroid hormones (THs) (Figure 1-5), which play important roles in development during early childhood and control of metabolism in adults.[15, 16] The recommended intake of iodide is relatively small (150 μg per day),[16] but IYD is crucial to recycle iodide to ensure a sufficient amount of iodide for TH synthesis. Mutations of the IYD gene have shown evidence of serious birth deficiency, cognitive defects and diseases associated with the thyroid gland.[17]

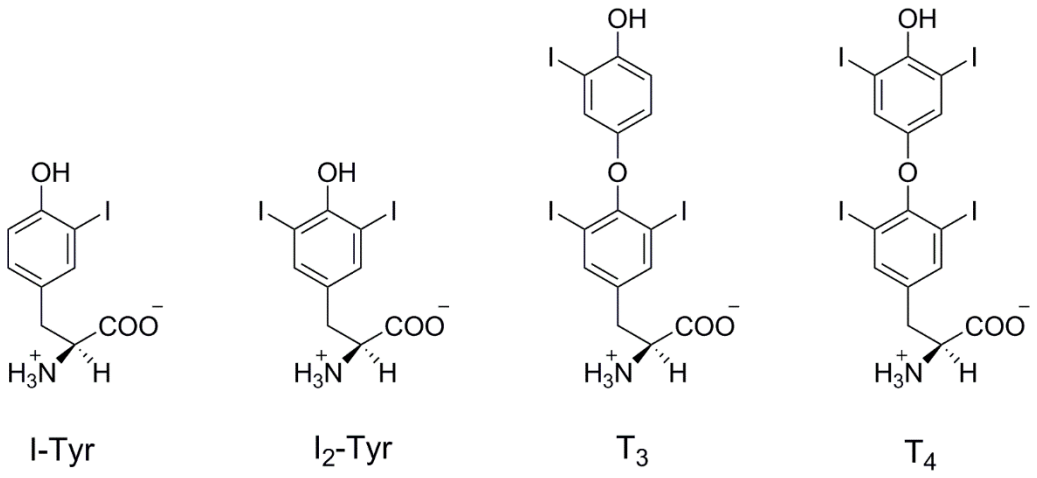

Figure 1-5. Structures of monoiodotyrosine (I-Tyr) and diiodotyrosine (I_2-Tyr) along with thyroid hormones T_3 and T_4.

IYD reduces a C-X bond of I-Tyr and I_2-Tyr using a flavin mononucleotide (FMN) cofactor (Figure 1-6).[13, 14] This reductive dehalogenation is very rare in aerobic organisms. Iodothyronine deiodinase (ID) is the only one other enzyme that catalyzes a similar reaction during its catalytic deiodination of THs (Figure 1-5).[18] IYD and ID have quite different evolutionary origins and mechanisms. ID is in the thioredoxin superfamily[19] while IYD belongs to the nitro-FMN reductase

superfamily (previously known as the NADH oxidase/Flavin reductase superfamily).[20] Deiodination performed by ID relies on an active site selenocysteine in contrast to IYD that uses FMN cofactor.

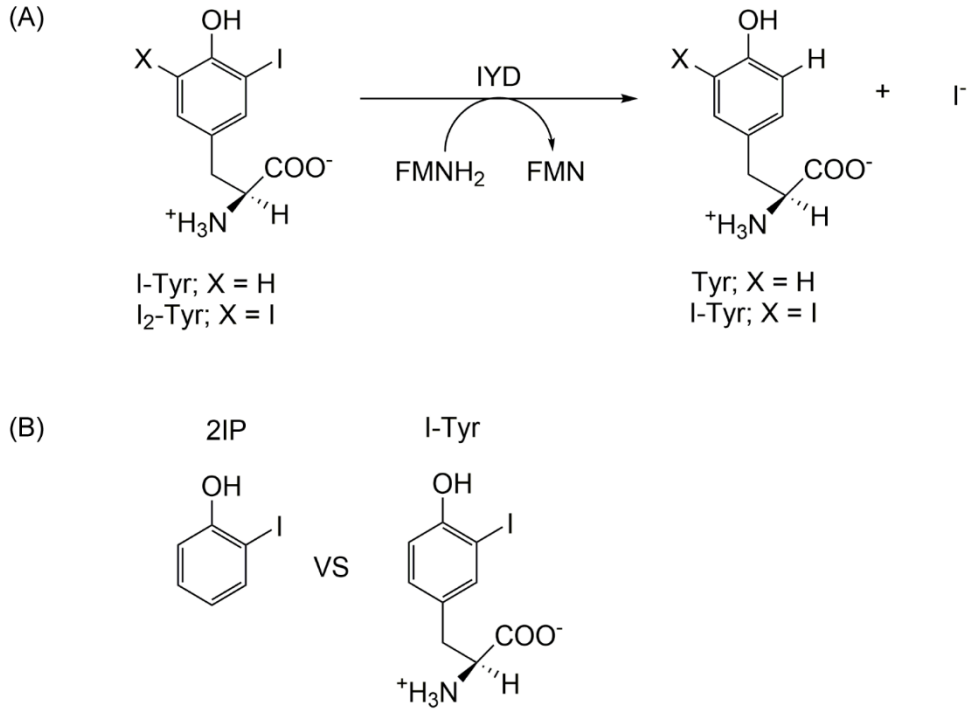

Figure 1-6. (A) Reductive deiodination of I-Tyr and I_2-Tyr by IYD. (B) Structures of 2IP and I-Tyr.

IYD intrigued us to study this enzyme for bioremediation of halogenated aromatic compounds as it has similar activity as reductive dehalogenases. However, an advantage of IYD over some reductive dehalogenases is it is oxygen stable in contrast to cobalamin-dependent reductive dehalogenases, which are oxygen sensitive.[21] A structure of an IYD substrate, I-Tyr, includes a subcomponent of 2-iodophenol. These properties of IYD raise the propensity of engineering IYD to accept halophenols as new substrates. Moreover, previous studies reported the ability of IYD to promote debromination and dechlorination of bromo- and chlorotyrosine.[22, 23] This finding broadens the possibility of developing a modified engineered IYD to detoxify the most problematic chlorinated aromatic compounds. Furthermore, IYD catalyzes substrates with a hydroxyl group ortho to the C–I bond, which offers a different regiochemistry from the three dehalogenases

described above. Hence, success of IYD engineering would provide alternative catalytic machinery to perform dehalogenation of a different substrate architecture.

1.4 Challenges of engineering nIYD to perform dehalogenation of halophenols

Crystal structures of mouse IYD demonstrate that IYD exists as a homodimer with FMN bound at the interface (Figure 1-7 A).[24] The zwitterion of I-Tyr is key to induce formation of an active site lid, which is disordered in the absence of I-Tyr (Figure 1-7).[24] The ordering of the lid is caused by bridging between the zwitterion of I-Tyr and three residues in the active site lid (Glu153, Tyr157 and Lys178) and FMN (Figure 1-8).[24] Besides, these electrostatic interactions from the zwitterion of I-Tyr, the co-crystal complex is likely to be stabilized by π-stacking between an aromatic ring of I-Tyr and FMN, hydrogen bonding of the phenolate of I-Tyr to an amide backbone of Ala126 and 2'OH-ribityl of FMN (Figure 1-8).

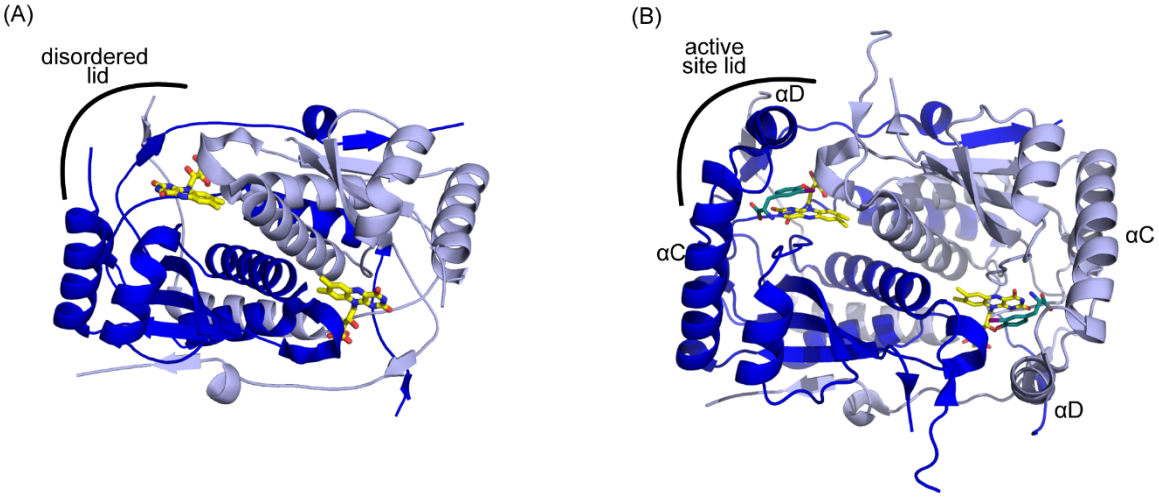

Figure 1-7. Crystal structure of (A) mouse IYD (PDB 3GB5) and (B) mouse IYD with I-Tyr (PDB 3GFD). An active site lid consists of C-terminus of αC and αD helices. Two different shades of blue represent two individual polypeptides. FMN and I-Tyr are presented in yellow and blue (carbon atoms).

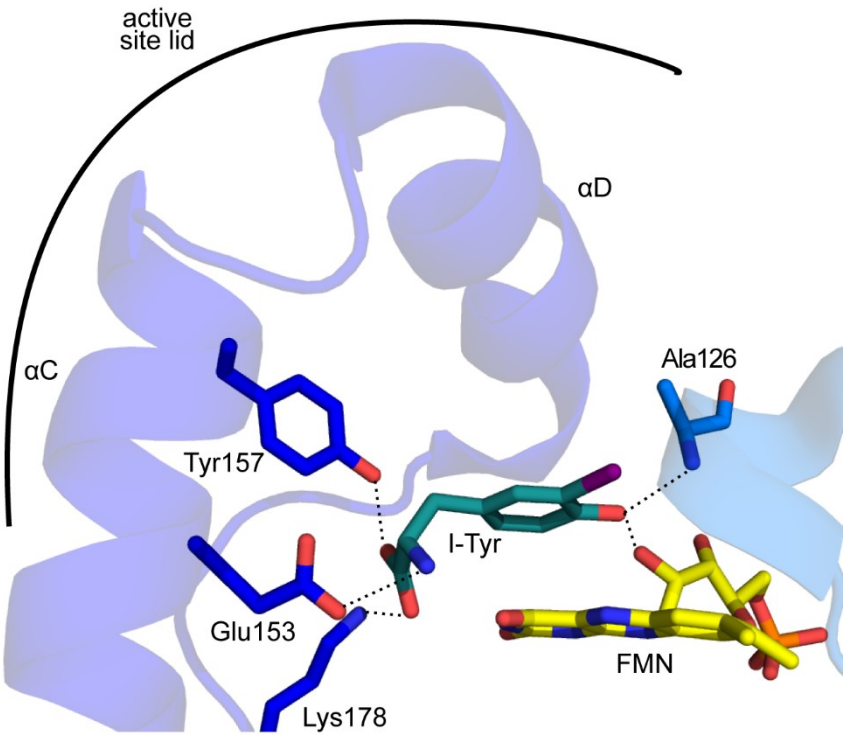

Figure 1-8. Active site of mouse IYD with I-Tyr. Two different shades of blue represent two individual polypeptides. FMN and I-Tyr are presented in yellow and blue (carbon atoms) respectively. Black dashed lines represent hydrogen bonding within 2.4 – 3.1 Å.

Site-directed mutagenesis of each active site lid residue confirmed the importance of the zwitterion of the substrate for binding and catalysis. Studies on two mutants mouse IYD, E153Q and Y157F, demonstrated decreases in both binding affinity and catalytic efficiency (k_{cat}/K_m). E153Q has an undetectable level of both affinity to I-Tyr and a deiodination of I_2-Tyr.[25] The results correspond to recent binding and kinetic studies of IYD from *Drosophila*.[23] Previous studies have raised the challenges for engineering IYD for deiodination of 2IP as it lacks the zwitterion to stabilize the lid as well as to mediate IYD binding and catalysis.

1.5 Specific aims

The ultimate goal for this study is to engineer IYD for deiodination of iodophenols. As a prelude to IYD engineering, the basal binding and catalysis of IYD for iodophenols were studied. My first research objective was to investigate basal binding and catalysis of IYD with iodophenols compared to that of I-Tyr to learn how the absence of the zwitterion affects binding and catalysis.

My second objective was to engineer IYD and an IYD-related enzyme within the nitro-FMN reductase superfamily to accept iodophenols as a substrate. This dissertation describes the following. First, an IYD homolog from bacterium, *Haliscomenobacter hydrossis*, (hhIYD) was selected for engineering IYD for deiodination of iodophenols by performing binding and catalytic activity of a representative set of three IYDs from eukaryotes and prokaryotes with 2IP and I-Tyr. Second, binding and catalytic activity of a set of 2-iodophenol derivatives were studied to establish a correlation between substrate binding affinity and catalysis. Third, crystallographic studies of hhIYD in the alternative presence of I-Tyr and 2IP were pursued to compare coordination of I-Tyr and 2IP to hhIYD, which explains slow deiodination of 2IP. Fourth, three hhIYD mutants were generated using rational designs based on a predicted structure of hhIYD aiming to improve catalytic efficiency (k_{cat}/K_m) for deiodination of 2IP and 4-hydroxy-3-iodobenzoic acid (2IPCOOH). Fifth, binding affinity of 2IP with two IYD-related enzymes in the nitro-FMN reductase superfamily (BluB and 3EO8) and eight 3EO8 mutants was measured to assess possibilities of installing deiodinase activity in their scaffold for iodophenol turnover.

Chapter 2: Analysis of binding and catalysis specificity for IYD homologs

2.1 Introduction

The discovery that IYD is pervasive throughout metazoan and some prokaryotes has raised a question, what are the functions of IYD in organisms without thyroid hormones. Examples are prokaryotic IYDs found in bacteria and those found in even more primitive organisms like archaea. Their functions are still unknown although there is evidence that a few bacterial strains accumulate iodide.[26] IYD is likely involved in catabolism or detoxification allowing bacteria and archaea to survive environments containing toxic halogenated compounds. This implies bacterial and archaeal IYD may not have I-Tyr or I_2-Tyr as their primary substrates. Hence, IYD from bacteria and archaea may exhibit substrate promiscuity that may enable IYD to function in bioremediation.

Three IYD homologs were selected to study substrate binding and catalysis specificity of IYD from eukaryotes and prokaryotes. Human IYD was chosen as a representative from eukaryotes. IYDs from the bacterium, *Haliscomenobacter hydrossis*, (hhIYD) and a hyperthermophilic archaea, *Pyrococcus furiosus* (pfuIYD), were selected as representatives of IYDs from prokaryotes. In addition, *H. hydrossis* is commonly found in waste water after sewage treatment.[27] Hence, its function may be related to dehalogenation of halogenated pollutants. The pfuIYD has an advantage over other homologs as it can function at high temperature at which increased catalytic activity can be expected. As discussed below, pfuIYD may display some level of substrate promiscuity based on sequence alignment and phylogenetic analysis.

IYD is a subclass within the nitro-FMN reductase superfamily that also includes other subclasses such as NADH oxidase (NOX) and flavin reductase P (FRP). The structure of mouse IYD shows most structural similarity to a bacterial flavin destructase (BluB) responsible for biosynthesis of a lower ligand for vitamin B_{12}.[24, 28] As IYD and BluB share a unique active site lid position different from NOX and FRP, they were categorized as a new subclass in the superfamily.[24, 28] Sequence analysis of mammalian IYDs exhibited an N-terminal membrane anchor, an intermediate domain and a catalytic domain.[29] The first two domains show higher

variability and lack homology to known protein domains while the catalytic domain is more conserved and shows homology to members of the nitro-FMN reductase superfamily.[20, 30] Fewer domains were found in hhIYD, which lacks the predicted membrane anchor while pfuIYD expressed only the catalytic domain.[31] Sequence alignment of catalytic domains of mammalian IYDs, hhIYD and pfuIYD reveals that hhIYD and pfuIYD still contain the three active site lid residues (Glu153, Tyr157, Lys178 of mouse IYD) and Thr interacting with O^4 and N5 of the FMN cofactor (Thr235 of mouse IYD), which are excellent predictors for deiodinase activity (Figure 2-1).[30, 31] Both prokaryotic IYDs also have conserved FMN binding residues except for Lys11 of pfuIYD, which substitutes a conserved Arg. This change may explain the weak affinity of FMN in pfuIYD as discussed in a result session. In addition, phylogenetic sequence analysis of IYD and other members in the superfamily also implied that pfuIYD may exhibit more substrate promiscuity as its position on the phylogenetic tree is distant from IYD homologs, but closer to other enzymes in the superfamily (BluB, NOX and FRP) (Figure 2-2).[30]

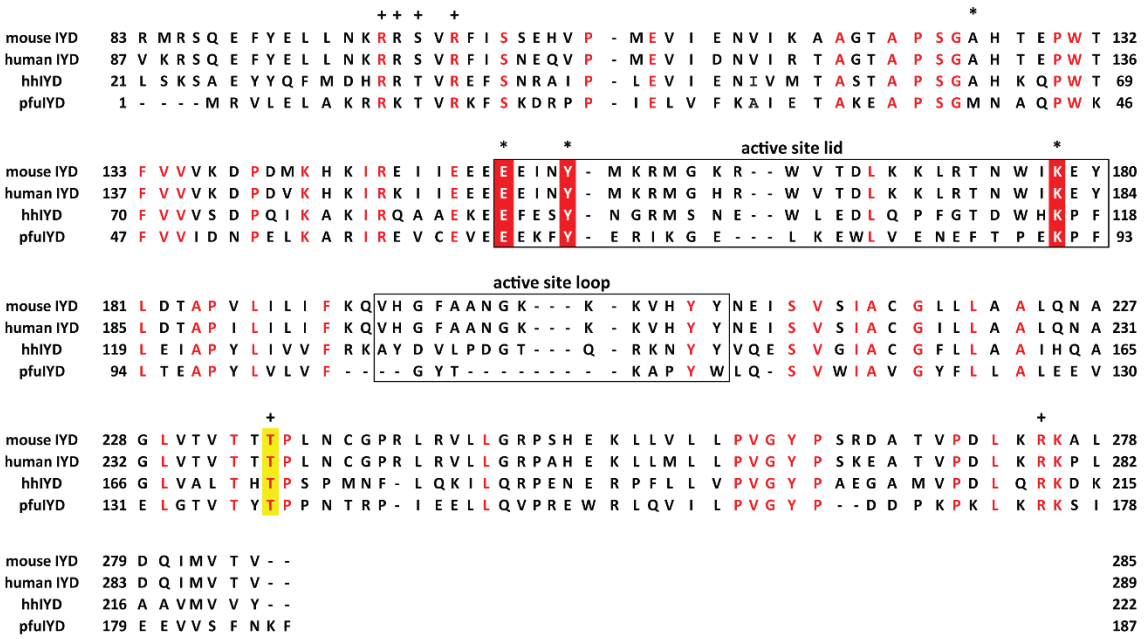

Figure 2-1. Sequence alignment of the catalytic domains of mouse IYD, human IYD, hhIYD and pfuIYD. Numbers on the left and right indicate numbering for amino acid residues. Residues in red and white are fully conserved. FMN and substrate coordinating residues are indicated with (+) and (*), respectively. Columns highlighted in red indicate residues that coordinate with the substrate zwitterion. A column highlighted in yellow indicates a residue that coordinates with the O^4 and N^5 positions of the FMN cofactor. The figure was modified from that created by Dr. Abhishek V Phatarphekar and Zuodong Sun.

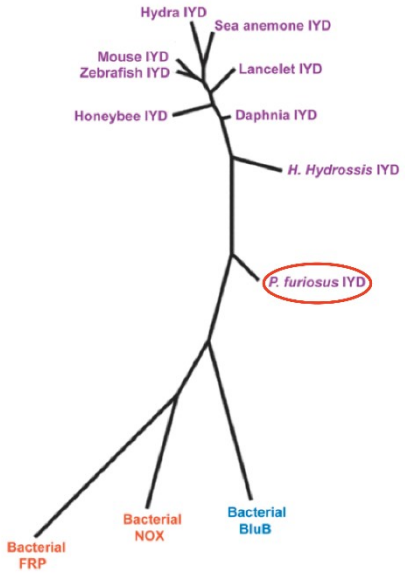

Figure 2-2. Phylogenetic analysis of the IYD branch of the nitro-FMN reductase superfamily. The figure is adapted from the literature.[30] The branch lengths are proportional to the number of amino acid substitutions per aligned residue. IYD from *P. furiosus* (pfuIYD) is circled in red.

This Chapter describes specificity of substrate recognition and turnover for three different IYD homologs using 2-iodophenol (2IP) and mono-iodotyrosine (I-Tyr) as substrates. 2IP was selected because it is a representative of haloaromatics and has the most structural similarity to I-Tyr. The C–I bond is the weakest carbon-halide bond, hence is the easiest C–X bond to cleave. In addition, both 2IP and I-Tyr are mono-iodinated compounds, which reduce complexity for product analysis (compared with diiodophenol and I_2-Tyr). Further investigations on binding and catalysis of halotyrosine and halophenol derivatives were performed to study the correlation between an active site binding and deiodinase activity.

2.2 Experimental Procedures

2.2.1 Materials

Expression plasmids (pSMT3) containing human IYD and hhIYD genes (pSMT3-His_6-SUMO-IYD-His_6) were kindly provided by former graduate students, Dr. Jimin Hu[32] and Dr. Jennifer Buss,[33] respectively. The pfuIYD expression plasmid (pET24a-pfuIYD-His_6) was kindly provided by another former graduate student, Dr. Abhishek V Phatarphekar.[31] The SUMO specific protease Ulp1 expression plasmid (pET28b-Ulp1) was kindly provided by Dr. C. Lima (Memorial Sloan-Kettering Institute, New York, NY). All expression plasmids containing IYD genes are under the T7 promoter, hence IPTG was used to induce protein expression. All DNA primers were synthesized by IDT (Coralville, IA). The pET24a plasmid and Rosetta 2 DE3 *E. coli* cells were purchased from Novagen (Darmstadt, Germany). Electrocompetent Genehogs (*E. coli*) cells were obtained from Invitrogen (Carlsbad, CA). Pfu Turbo polymerase and its buffer were obtained from Agilent (Santa Clara, CA). T4 DNA ligase, all restriction enzymes and their buffers were purchased from New England BioLabs Inc. (NEB) (Ipswich, MA). PageRuler broad range unstained protein standards, GeneRuler 1 Kb plus DNA standards, Genejet plasmid miniprep kit, His-Pur Ni-NTA resin and ScintiSafe Plus 50% scintillation cocktail were obtained from Thermo Fisher Scientific (Waltham, MA). QIAquick gel extraction kit was purchased from QIAGEN. The Sephacryl S-200

HR resin for size exclusion chromatography (SEC) was obtained from GE Healthcare (Piscataway, NJ).

Reagents of the highest grade available were used without purification. 3-Bromo-L-tyrosine was purchased from AEchem Scientific Corporation (Naperville, IL). 3-Chloro-L-tyrosine (Cl-Tyr), 3,5-diiodo-L-tyrosine (I_2-Tyr), 2-bromophenol (2BP), 4-aminophenol, 4-amino-2-iodophenol (4A2IP) and 4-cyanophenol were obtained from Sigma-Aldrich (Madison, WI). 3-Fluoro-L-tyrosine (F-Tyr) was purchased from Astatech, Inc (Bristol, PA). Formic acid (88%), 3-iodo-L-tyrosine (I-Tyr), 2-iodophenol (2IP) and *m*-cresol were obtained from Acros Organics (Morris Plains, NJ). 2-Chlorophenol (2CP), 2-fluorophenol (2FP) and 4-hydroxylbenzoic acid were purchased from Alfa Aesar (Tewksbury, MA). 4-Hydroxy-3-iodobenzonitrile (2IPCN) was purchased from Pharmabridge, Inc (Doylestown, PA). Benzoic acid was obtained from Mallinckrodt Chemical Work (St. Louis, MO).

2.2.2 General methods

Plasmids were purified from cultures grown from selected single colonies of Genehogs *E. coli* cells using the Genejet plasmid miniprep kit. All PCR reactions were performed using an Eppendorf Mastercycler gradient (Hauppauge, NY). *E. coli* cells were transformed with the plasmid of interest using an Eppendrof Eporator at 2500 V. Restriction digestion reactions for all PCR products and plasmids were performed at 37^{o}C for 1 h. The digested PCR products and linearized plasmids were purified and visualized through 1% agarose gel electrophoresis operated at 100 V for 50 min. The digested products were extracted from agarose gels using the QIAquick gel extraction kit (QIAGEN). Ligation reactions were carried out using T4 DNA ligase.

Purification of all IYDs was carried out with Ni^{2+} column chromatography (a flow rate of 1 ml/min) and size exclusion chromatography (a flow rate of 0.3-0.4 ml/min) using an AKTA Prime FPLC (GE Healthcare). Centrifugation steps were performed using the Beckman Coulter centrifuge. Protein concentration was performed using Amicon Ultra-15 centrifugal filter with 10 kDa MW cut off (Millipore). Proteins were analyzed by SDS-PAGE (12% resolving and 5%

stacking acrylamide layers) at 220 V for 45 min. The ε_{280}, theoretical pI and molecular weight of purified IYD homologs were determined from their amino acid sequences using ExPASy ProtParam.[34] All UV measurements were performed by a Hewlett-Packard 8453 spectrophotometer. For pfuIYD, protein concentration was determined from the A_{280} after subtracting an absorbance contributed from free FMN at 280 nm, using A_{280}/A_{450} = 1.57 for calculation[30] and the FMN occupancy per enzyme active site was determined by measuring the absorbance of FMN at 450 nm ($\varepsilon_{450\ [FMN]}$ = 12,500 M^{-1} cm^{-1}).[35] The A_{280}/A_{450} and extinction coefficients of FMN inside IYD at 450 nm ($\varepsilon_{450\ [IYD]}$) for human IYD and hhIYD were determined and used to calculate their protein concentration and FMN occupancy. To determine A_{280}/A_{450} of FMN and $\varepsilon_{450\ [IYD]}$, IYD was diluted in 100 mM potassium phosphate, pH 7.4 to contain at least ~80 μM of FMN (200 μl). The solution was separated into two equal aliquots. One of the aliquots was used to extract free FMN from the FMN-bound protein through heat denaturation (110 ºC for 10 min). The heated solution was cooled to room temperature and centrifuged for 3 – 5 min to remove precipitated and denatured protein. The supernatant was then loaded on the Ni^{2+} affinity column (0.2 – 0.3 ml) to retain soluble IYD on the Ni^{2+} resin. Free FMN was eluted using the same potassium phosphate buffer. The concentration of free FMN was determined ($\varepsilon_{450\ [FMN]}$ = 12,500 M^{-1} cm^{-1}). Then, the $\varepsilon_{450\ [IYD]}$ was calculated using the concentration of free FMN and A_{450} of the nature protein. The concentration of IYD was calculated using A_{280} after correcting with a dilution factor created by eluting the FMN. Protein concentration of human IHD and hhIYD was determined from the A_{280} after subtracting an absorbance contributed from free FMN at 280 nm, using A_{280}/A_{450} = 1.9 ± 0.1 (human IYD) and 1.72 ± 0.04 (hhIYD) for calculation. The FMN occupancy per enzyme active site was determined by measuring the absorbance of FMN at 450 nm ($\varepsilon_{450\ [human\ IYD]}$ = 13,000 ± 300 $M^{-1}cm^{-1}$ and $\varepsilon_{450\ [hhIYD]}$ = 13,600 ± 300 $M^{-1}cm^{-1}$). Enzyme concentration used for each experiment was determined based on FMN concentration to represent the enzyme in an active form.

2.2.3 Cloning of hhIYD

An hhIYD construct without a SUMO fusion was generated to optimize purity of hhIYD for protein crystallization. The hhIYD gene was amplified from the pSMT3 construct containing an hhIYD-SUMO fusion using the recommended concentration of Pfu Turbo polymerase as suggested by the manufacturer. A forward primer 5'-AATTAATCATATGAAGCAAAAGCCTGCTT-3' and a reverse primer 5'-AATTAATCTCGAGCTAGTGATGGTGATG-3' containing NdeI and XhoI restriction sites (underlined) were used for gene amplification. The hhIYD gene was subcloned using the NdeI and XhoI sites into the pET24a vector for expression without the SUMO fusion.

2.2.4 Site-directed mutagenesis

The pET24a-pfuIYD-His_6 was used as a template for site-directed mutagenesis and Pfu turbo polymerase was used for amplification. K11R was introduced by the forward primer 5'-GCCAAACGTCGTCGCACTGTTCGCAAA -3' and its reverse complement. The mutated codon is indicated in red. Amplification of the mutated plasmid was confirmed through 1% agarose gel electrophoresis before transformation into electrocompetent Genehogs *E. coli* cells (Invitrogen). The plasmid was purified from a culture grown from the selected single colonies and the mutation was confirmed by DNA sequencing (Genwiz).

2.2.5 Expression and purification of IYD homologs

Human IYD without its N-terminal transmembrane sequence (residues 2-31) was expressed with a SUMO fusion as described previously.[32] hhIYD and pfuIYD were expressed without a SUMO fusion in its full-length native sequence.[31] Rosetta 2 (DE3) *E. coli* cells were transformed with the plasmid containing the IYD gene of interest. Single colonies were picked and inoculated into a small culture of Luria-Bertani media (LB) (25 ml) containing kanamycin (50 µg/ml) and chloramphenicol (34 µg/ml). The culture was incubated with shaking for 14-16 h at 37 ºC. The small culture was then diluted by approximately 50-fold into a culture of LB medium (1 L) with the same concentration of the antibiotics described above and incubated with shaking at 37 ºC until

OD_{600} of 0.6-0.8 was obtained. Riboflavin (10 μM) was supplemented in the 1 L culture of media containing IYD when their FMN occupancy is low (≤ 60 %) in attempt to increase the FMN occupancy of the final protein. Protein expression was performed by addition of IPTG (20 μM) and incubation with shaking at 16 ºC for 12 – 14 h.[31] Cells were harvested by centrifugation (5000 xg for 10 min) and either were used for purification right away or frozen in liquid nitrogen and stored at -80 ºC.

For IYD purification, cells were resuspended in lysis buffer (500 M NaCl, 25 mM imidazole, 10% glycerol, 0.5 mM TCEP and 50 mM sodium phosphate, pH 7.9) and supplemented with FMN (100 μM). The cells were then lyzed by passage through a French press at a pressure of 1,000 psi or an Emulsiflex C3 homogenizer (Avestin) (Ottawa, ON, Canada) at a pressure of 20,000 psi for 3 – 4 times. Cell lysates were centrifuged at 45,000 x g for 0.5 – 1 h to precipitate cell debris. With one trial, cell lysates containing pfuIYD were heated at 80 ºC for 20 min and cooled to room temperature prior to centrifugation with an aim to increase FMN occupancy of the pfuIYD. Both SUMO-IYD and non-SUMO tagged IYD was purified in two steps using Ni-NTA affinity and size-exclusion chromatography (SEC). The supernatant (25 – 35 ml) was first introduced onto a Ni-NTA column (10 ml) that was pre-equilibrated with lysis buffer (3 column volumes). The loaded sample was washed with lysis buffer containing 25 mM, 60 mM and 100 mM imidazole for 2 – 4 column volumes each. IYD was then eluted with lysis buffer containing 300 mM imidazole. The purified SUMO-IYD protein were incubated with Ulp1 (approximately, 1:100 w/w for 10-12 h) for 12 – 14 h at 4 ºC for SUMO lysis. The protein solution was concentrated using an Amicon Ultra-15 centrifugal filter (10 kDa MW-cut off, Millipore) until reaching a volume of ~ 1 ml.

Both SUMO-IYD and non-SUMO tagged IYD solutions were supplemented with FMN (100 μl of 10 mM FMN) before applying to a size-exclusion column (volume = 220 ml), pre-equilibrated with buffer (300 M NaCl, 15% glycerol, 0.5 mM TCEP and 50 mM sodium phosphate, pH 7.4). Fractions with desired protein were collected and analyzed by SDS-PAGE. Note that the final

buffer used for pfuIYD was maintained at pH 6.8 to avoid a possibility of protein precipitation due to zero net charge on the protein (pI = 7.8).

2.2.6 Synthesis of 4-hydroxy-3-iodobenzoic acid (2IPCOOH)

4-Hydroxybenzoic acid (830 mg, 6.0 mmol) was dissolved in conc. NH_4OH solution (29% w/w, 100 ml) and stirred at 4 °C. Iodine (1.5 g, 6.0 mmol) in EtOH (18 ml) was added dropwise over 1 h and the mixture was stirred for another 2.5 h at 4 °C. The mixture was rotoevaporated to a volume of 40 ml and then acidified to pH 2 using HCl (1 N). The mixture was further rotoevaporated until dry. The solid was dissolved in EtOAc (20 ml), washed twice with H_2O (20 ml). The organic phase was rotoevaporated again to yield pale yellow solid. The solid was dissolved in 20% aq. acetonitrile with 0.44% formic acid (v/v) and purified by reverse-phase HPLC (Econosphere C18 column; 250 x 10 mm, 10 µm) using a gradient of 20 – 30% of aq. acetonitrile with 0.44 % (v/v) formic acid over 15 min at a flow rate of 5 ml/min. Fractions containing the product (t_R = 6.8 min) were lyophilized to yield 2IPCOOH as a white solid (360 mg, 23 % yield). ^{1}H NMR (400 MHz, acetone-d_6) δ 7.05 (d, 1H, J = 8.4 Hz), 7.92 (dd, 1H, J = 2.0, 8.5 Hz), 8.40 (d, 1H, J = 2.0 Hz) (Appendix Figure A1); ^{13}C NMR (101 MHz, acetone-d_6) δ 82.90, 114.5, 123.8, 131.6, 141.2, 160.7, 165.4 (Appendix Figure A2). Both the ^{1}H and ^{13}C NMR spectra are consistent with the literature.[36]

2.2.7 Catalytic activity assay with ^{125}I-[I_2-Tyr]

Deiodination rates of I_2-Tyr by IYD were determined by quantifying the release of [^{125}I]-iodide from the radiolabeled ^{125}I-[I_2-Tyr] as previously described.[20, 37] In brief, reaction mixtures contained 200 mM KCl, 50 mM 2-mercaptoethanol, 0.05 mM methimazole and 0.033 mM FMN, 100 mM potassium phosphate pH 7.4, I_2-Tyr and the indicated enzyme concentrations. The ^{125}I-[I_2-Tyr] was added to each reaction mixture (15,000-20,000 cpm). The reactions were then initiated by addition of 10% sodium dithionite in 5% sodium bicarbonate (100 µl) to reach a final volume of 1 ml. The reactions were conducted at 25 °C and quenched by addition of 0.1% I_2-Tyr in 0.1 N NaOH (100 µl). An aliquot from each reaction (850 µl) was applied onto a column containing AG 50W-X8 cation exchange resin (Bio-Rad Labs), which was pre-equilibrated with 10% acetic acid. The

column was eluted with 4.15 ml of 10% acetic acid and the eluate was collected in a scintillation vial (fraction A). The column was further washed with 5 ml of 10% acetic acid and the eluate was collected in another scintillation vial (fraction B). The rest of the reaction mixture (250 µl) was transferred to a new scintillation vial containing 4.75 ml of 10% acetic acid (fraction S). Fraction A, B and S were then added with scintillation cocktail (10-12 ml) and the radioactivity (cpm) of each fraction was measured using a Tri-Carb 2910TR liquid scintillation counter (Perkin Elmer). The released radioactive iodide (F) was determined from equation 2-1.[37] The initial rate (V) was determined from equation 2-2[37] (F_0 = background radioactivity from a control reaction without enzyme). The initial rates (nmol h^{-1}) were then fit against substrate concentrations (S, µM) into the Michaelis-Menten equation 2-3 using Origin 6.0.

$$F = \frac{\frac{\text{cpm A} + \text{cpm B}}{0.85}}{\frac{\text{cpm S}}{0.25}} \qquad \text{Equation } 2-1$$

$$V = (F - F_0) \times \left(2 \times \frac{1}{\text{time (min)}} \times \frac{60 \text{ min}}{1 \text{ h}} \times [S]\right) \qquad \text{Equation } 2-2$$

$$V = \frac{V_{max}\,[S]}{K_m + [S]} \qquad \text{Equation } 2-3$$

2.2.8 Binding affinity determination

Binding affinity for ligands of IYD was determined by their ability to quench the fluorescence of the oxidized FMN (FMN_{ox}) in the active site of IYD (λ_{ex} = 450 nm and λ_{em} = 523 nm) as previously described.[22, 32] The fluorescence signal was measured using a Fluoromax-4 fluorescence spectrophotometer (Horiba Scientific). IYD in 100 mM potassium phosphate, pH 7.4 (pH 6.9 for pfuIYD) was stirred for 15 – 30 min prior to ligand addition (See Figure 2-4, 2-5 and Appendix Figure A7 for more details). Binding affinity was monitored over 4 log concentration units, centered at the concentration that provides 50% fluorescence quenching. Observed fluorescence

intensities (F) were divided with an initial fluorescence signal without addition of ligand (F_0). The ratios of F/F_0 were then plotted against log units of ligand concentrations (S_0). The dissociation constant (K_d) values were determined by non-linear least squares fitting of the data to equation 2 – 4[38] using Origin 6.0. ΔF is the total change in fluorescence intensity and E_0 is enzyme concentration.

$$\frac{F}{F_0} = 1 + \frac{\Delta F}{F_0}\left(\frac{(K_d + E_0 + S_0) - \sqrt{(K_d + E_0 + S_0)^2 - 4E_0S_0}}{2E_0}\right) \qquad \text{Equation } 2-4$$

2.2.9 Catalytic dehalogenation of mono-halogenated compounds by IYDs

Catalytic turnover of IYD for mono-halogenated compounds was observed by quantifying the product of dehalogenation after separation by reverse-phase HPLC as previously described.[23, 31] In brief, mono-halogenated substrates were incubated with IYD in 111 mM potassium phosphate pH 7.4 (900 µl) (unless specified otherwise) and the reaction was initiated by addition of 5% dithionite in 5% sodium bicarbonate (100 µl). This mixture was incubated at 25 ºC (unless specified otherwise) prior to quenching with 88% formic acid (50 µl). An internal standard (IS) of either *m*-cresol or benzoic acid was used to quantify formation of the product. The entire reaction mixture (1050 µl) was applied to a Microsorb MV 300-5 C18 (250 x 4.6 mm) analytical column (Varian) to measure product formation. See Appendix Figures A3, A9 and A11 for the HPLC solvents and gradients used for deiodination reactions of each substrate. Concentration of the dehalogenated product was determined from the standard curve created by addition of known amounts of product into the reaction mixture lacking the substrate. The ratios of the area under curve (AUC) of the product to AUC of IS were plotted against known concentrations of the spiked product (Appendix Figure A4). An equation showing the relationship between AUC and amounts of standard was determined by linear regression and used to calculate concentrations of dehalogenated products generated by the enzymatic reactions. The kinetic parameters were determined by fitting the data into the Michaelis-Menten equation 2-3 using Origin 6.0. The substrate 2IP had phenol as impurity (< 1 %). The contribution of the impurity contaminated in each substrate was subtracted from the product signal prior to analysis.

2.3 Results

2.3.1 Expression and purification of IYD homologs

The development of His_6-tagged-SUMO fusion constructs successfully provided expression systems for mammalian IYDs in *E. coli*, which had been problematic in the past.[25, 32] Consequently, the SUMO fusion has been used for IYD homologs from other organisms to enhance protein solubility. However, the IYD-SUMO fusion expression often results in later co-elution of IYD and the SUMO tag during SEC purification. Hence, a hhIYD construct without the SUMO tag was generated in an attempt to optimize its purity for crystallization (Chapter 3). Previously, IYD from *Drosophila melanogaster* was successfully expressed without the SUMO fusion,[23] and hhIYD provided similar success. PfuIYD was initially expressed as a SUMO fusion protein by Dr. Abhishek V Phatarphekar, however SUMO lysis by Ulp1 was incomplete. Hence, the same non-SUMO expression system was also implemented for pfuIYD and the protein was successfully expressed. The purified human IYD from the IYD-SUMO fusion and native hhIYD lacking SUMO were both obtained in yields of 15 – 24 mg per 1 L of culture. Soluble pfuIYD was expressed without a SUMO tag to a yield of about 7 mg per 1 L of culture. All three homologs were obtained with purity of > 98% (human IYD and hhIYD) and > 95% (pfuIYD) as evident from SDS-PAGE, Coomassie staining and ImageQuantTL analysis (Figure 2-3**)**. Human IYD and hhIYD contained FMN at an occupancy of 95 – 105 % but only 55 – 75 % FMN occupancy of pfuIYD was observed among different purification batches. Several attempts were made to increase FMN occupancy of pfuIYD mainly to optimize protein homogeneity for crystallization trials. The efforts included supplementing cultures with riboflavin (10 μM) during protein expression, heat-mediated uptake after cell lysis,[39] optimization of final buffer conditions, heat and FMN incubation with different temperature and time (Table 2-1). However, none of the trials above improved the FMN occupancy of pfuIYD. The final FMN occupancy of pfuIYD after these procedures still ranged between 59 – 77 % which is similar to the protein yielded after purification (55 – 75 %).

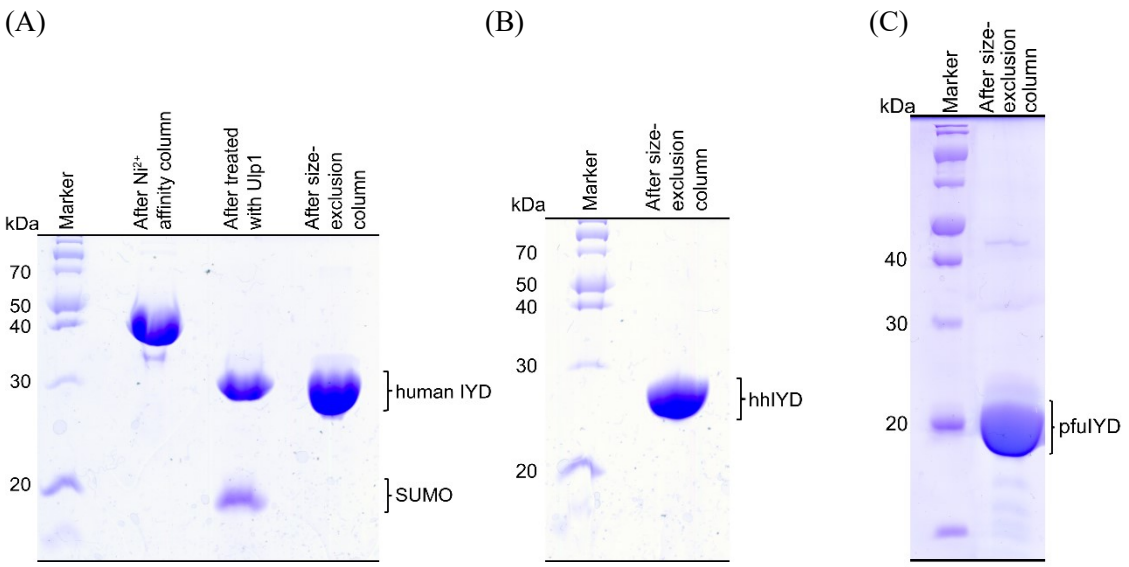

Figure 2-3. SDS-PAGE gels of the purified IYD homologs. Lane 1 is marker with molecular weights of protein (kDa) indicated on the left. (A) human IYD; Lane 2 is the human IYD-SUMO fusion protein obtained after Ni^{2+} affinity chromatograpphy. Lane 3 shows human IYD and SUMO proteins after treated with Ulp1. Lane 4 is the purified human IYD after SEC. (B) hhIYD and (C) pfuIYD.

Table 2-1. Conditions of buffer, temperature and time used to increase FMN occupancy of pfuIYD.

Buffer (pH 6.8)	NaCl (mM)	Temp (°C)	Incubation time (h)	FMN occupancy (%)
50 mM sodium phosphate	300	80	0.5	77
50 mM sodium phosphate	300	80	2	68
50 mM Bis-tris	300	RT	12-14	75
50 mM Bis-tris	300	80	0.5	59
25 mM Bis-tris	-	RT	12-14	77
25 mM Bis-tris	100	RT	12-14	77
25 mM Bis-tris	200	RT	12-14	77

PfuIYD (~150 μM) was incubated with supplemented FMN (~750 μM) and buffer at the indicated temperature and time prior to centrifugation (5000 × g) using an Amicon Ultra-15 centrifugal filter (10 kDa MW-cut off, Millipore). Then, a cycle of buffer addition and centrifugation was repeated until the filtrate contained no FMN as measured by UV (ε_{450} = 12,500 M^{-1} cm^{-1}).[35] The FMN occupancy represents the final FMN content of pfuIYD after each treatment. RT is abbreviated for room temperature.

Elution of FMN during purification of pfuIYD by SEC suggested weak affinity of FMN for the pfuIYD homolog and resulted in quite different FMN occupancy (50-80 %) in different protein fractions eluted from the SEC. Sequence analysis of pfuIYD suggested that weak affinity of FMN for pfuIYD may arise from a non-conserved FMN binding residue, Lys11, which appears as Arg in other homologs in this study (Figure 2-1). Difference in bulkiness and length of these two amino

acid side chains may affect FMN affinity with the protein. Hence, pfuIYD K11R mutant was generated to introduce the conserved Arg back to the pfuIYD sequence with the aim to increase FMN affinity to the protein. The pfuIYD K11R construct was generated by site-directed mutagenesis and expressed about 18 mg per 1 L of culture with ~95 % purity as evident from SDS-PAGE, Coomassie staining and ImageQuantTL analysis (Appendix Figure A5**)**. However, variation of FMN occupancy (60 – 75 %) of the pfuIYD K11R protein was still observed in different protein fractions during SEC purification. The final pfuIYD K11R protein contained similar FMN occupancy (up to 78%) compared to that of the wild-type (55 – 75 %).

2.3.2 Catalytic deiodination of I_2-Tyr by IYD homologs

Deiodination of I_2-Tyr by IYD homologs was first compared by their catalytic efficiency (k_{cat}/K_m) to that previously reported for other IYD homologs.[30, 31] Kinetic studies were performed using our routine radioactivity assay to measure $^{125}I^-$ release from radiolabeled ^{125}I-[I_2-Tyr]. Human IYD, hhIYD and pfuIYD (WT) exhibited k_{cat}/K_m values ranging from 0.4 – 3.4 min^{-1} μM^{-1} (Table 2-2), which are comparable to those previously reported.[30-32] Their catalytic efficiency also fell into the range of the k_{cat}/K_m values for other IYD homologs from eukaryotes to prokaryotes.[30-32] The k_{cat} values of the selected IYDs ranged between 0.44 – 7.3 min^{-1} while the K_m values ranged between 1 – 15 μM. Deiodination rates of I_2-Tyr by pfuIYD at 25 °C was performed by Dr. Abhishek V Phatarphekar and displayed the lowest k_{cat} and K_m. Since pfuIYD is found in an thermophilic archaea, its kinetics for I_2-Tyr turnover was also performed at high temperature (60 °C) to determine the relative deiodination rates to those measured at 25 °C. The k_{cat} value of pfuIYD at 60 °C increased by ~16 fold while its K_m increased by 2 fold compared to that determined at 25 °C to give the highest k_{cat}/K_m for I_2-Tyr turnover (T = 60 °C) among the three IYD homologs.

Table 2-2. Catalysis deiodination of I_2-Tyr by IYD homologs.

IYD homolog	Temp (°C)	k_{cat} (min^{-1})	K_m (μM)	k_{cat}/K_m (min^{-1} μM^{-1})
human IYD[a]	25	7.3 ± 0.2	15 ± 1	0.49 ± 0.04
hhIYD[a]	25	6.7 ± 0.8	6 ± 2	1.1 ±0.4
pfuIYD (WT)[b,c]	25	0.442 ± 0.008	1.0 ± 0.1	0.4 ± 0.1
pfuIYD (WT)[a,c]	60	7.2 ± 0.3	2.1 ± 0.4	3.4 ± 0.7

[a]Determined from the data of Appendix Figure A6 and the kinetic parameters are comparable to that previously reported.[30-32] Errors derive from least square fitting. [b]Experiment performed by Dr. Abhishek V Phatarphekar. [c]Assays performed at pH 6.8 – 6.9.

2.3.3 Affinity of halotyrosine and halophenol derivatives to IYD

2.3.3.1 Determination of binding specificity for IYD homologs

Binding affinity of ligands to IYD was determined by monitoring the ability of each ligand to quench the fluorescence of FMN_{ox} in an active site of IYD. To determine binding specificity of human IYD, hhIYD and pfuIYD (WT), binding assays of I-Tyr and 2IP for each IYD homolog were performed. The K_d values of I-Tyr to all IYDs ranged from 0.03 – 8.2 μM (Figure 2-4). The K_d values of I-Tyr for human IYD and pfuIYD fell into a sub-μM range, which is similar to that previously observed in mouse IYD.[25] Interestingly, the affinity of pfuIYD for I-Tyr at 60 °C maintained the same as that observed at 25 °C (Table 2-3, Appendix Figure A7). On the other hand, the affinity of hhIYD for I-Tyr is ~90- and 200-fold less than that of human IYD and pfuIYD, respectively. Lower stringency of hhIYD affinity for I-Tyr implied that the enzyme may share its affinity with other ligands besides halotyrosines.

Table 2-3. Catalysis deiodination and binding affinity of IYD homologs.

IYD homolog	Substrate	pK_a	K_d (μM)[c]	k_{cat} (min^{-1})[d]	K_m (μM)[d]	k_{cat}/K_m ($min^{-1}\ \mu M^{-1}$)[d]
human IYD	I-Tyr	8.4[a], 8.3[b]	0.09 ± 0.02[g]	6.9 ± 0.4	7.3 ± 0.8	1.0 ± 0.2
	2IP[g]	8.4[a], 8.5[b]	1,410 ± 70	0.26 ± 0.01	4,100 ± 400	(6.3 ± 0.7)×10^{-5}
pfuIYD[h]	I-Tyr (25° C)	8.4[a], 8.3[b]	0.04 ± 0.02	-	-	-
	I-Tyr (60°C)		0.03 ± 0.02	-	-	-
	2IP (25 ° C)	8.4[a], 8.5[b]	79 ± 4	-	-	-
	2IP (60 ° C)		270 ± 20	1.0 ± 0.2	4,000 ±2,000	(3 ± 1)×10^{-4}
hhIYD	I-Tyr	8.4[a], 8.3[b]	8.2 ± 0.5	16 ± 1	12 ± 2	1.3 ± 0.3
	2IP	8.4[a], 8.5[b]	67 ± 2	0.17 ± 0.02	4,100 ± 800	(4 ± 1)×10^{-5}
	2BP	8.5[b]	260 ± 20	<0.002[e]	-	-
	2IPCOOH	8.6[a]	24.1 ± 0.7	0.186 ± 0.006	7,100 ± 600	(2.6 ± 0.2)×10^{-5}
	4A2IP	9.3[a]	96 ± 3	-	-	(2.6 ± 0.2)×10^{-4}
	2IPCN	6.7[a]	1.44 ± 0.05	< 0.001[f]	-	-

[a]pK_a values of the phenolic protons were calculated with the ACE and JChem acidity and basicity calculator (https://epoch.uky.edu/ace/public/pKa.jsp). [b]pK_avalues were also determined experimentally as published previously.[40-42] [c]K_d values were determined from Figure 2-4 to 2-6 and Figure A7. [d]Kinetic parameters were determined from Appendix Figures A8. [e]k_{cat} value was estimated from Figure A11. [f]k_{cat} value was estimated from Figure A9. Errors derive from least squares fitting. [g]Experiments performed by Zuodong Sun. [h]Assays performed at pH 6.9.

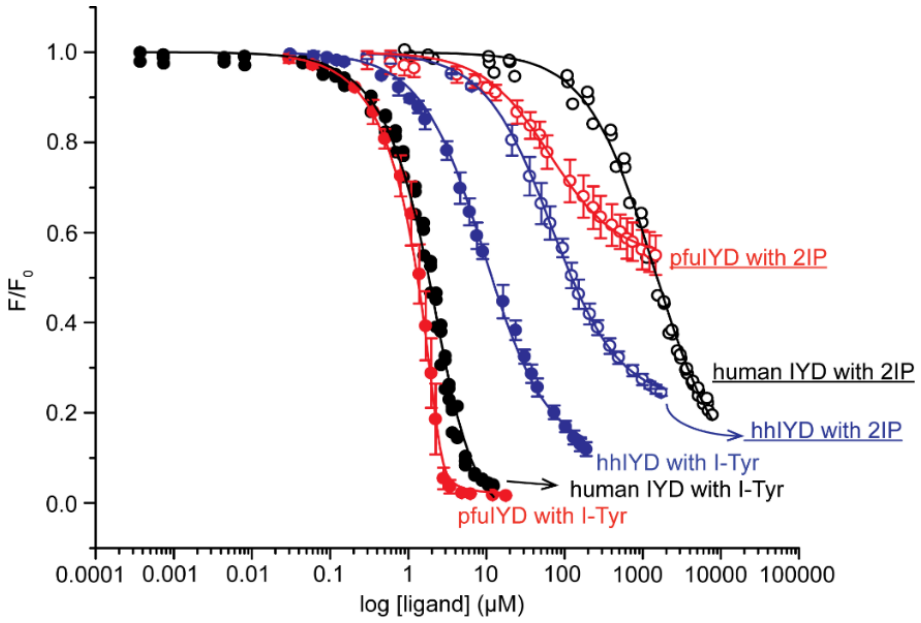

Figure 2-4. Quenching of FMN_{ox} fluorescence upon ligand binding to IYD at 25 °C. Human IYD (4.3 μM, 200 mM KCl), hhIYD (2.5 μM) in 100 mM potassium phosphate, pH 7.4 and pfuIYD (2.5 μM) in 100 mM potassium phosphate, pH 6.9 were stirred at 25 °C for 30 min prior to addition of the indicated ligand. The K_d values derived from the best fit of the data (solid lines) to equation 2-4. Complete fluorescence quenching by 2IP was limited by its solubility.

The three IYD homologs exhibited different affinities for 2IP with K_d values ranging from 67 – 1,410 μM (Table 2-3, Figure 2-4). hhIYD and pfuIYD showed similar affinities with 2IP (K_d = 65

– 80 μM) while human IYD expressed the weakest affinity with a K_d almost 20-fold more than that of pfuIYD and hhIYD. Binding of pfuIYD with 2IP was also performed at 60 °C. In contrast to I-Tyr, a decrease in the affinity for 2IP was observed with the K_d of ~3.5 fold more than that determined at 25 °C (Table 2-3, Appendix Figure A7).

The binding studies of I-Tyr and 2IP showed that human IYD exhibited almost 16,000-fold increase in the K_d for 2IP versus I-Tyr while hhIYD exhibited the smallest difference (~8 fold). PfuIYD expressed the greatest binding promiscuity as it clearly binds I-Tyr as tightly as human IYD but still binds 2IP with similar affinity as hhIYD. Different binding selectivity among the three IYD homologs suggested that IYD from bacteria and archaea may express substrate promiscuity for different purposes of dehalogenation while human IYD maintains high substrate specificity toward I-Tyr to maintain iodide homeostasis.

2.3.3.2 The contribution of the zwitterion on binding different halotyrosines to hhIYD

The results from binding specificity suggested that affinity of hhIYD has the least dependence on the zwitterion of all selected IYD homologs. Small differences in binding strength between I-Tyr and 2IP for hhIYD (~8-fold difference in the K_d values) stimulated further analysis of its affinity for a series of 3-halotyrosines (X-Tyr) and 2-halophenols (2XP) to assess the contribution of the zwitterion on binding of different halo-substituents

Previously, affinities of X-Tyr for mouse IYD and human IYD were determined with K_d values of I-Tyr, Br-Tyr and Cl-Tyr were all in the sub-μM while that of F-Tyr bound with a K_d about 10-fold higher (Table 2-4). A similar trend was observed for hhIYD, but its K_d value for each X-Tyr is one order of magnitude higher than those of the mammalian IYDs (Table 2-4). Weaker binding of X-Tyr to hhIYD also suggested that the zwitterion of X-Tyr had less effect on binding to hhIYD compared to mammalian IYDs. However, the zwitterion was still essential to maintain binding of different halotyrosines since their K_d values range within less than an order of magnitude (Table 2-4, Figure 2-5). The difference in affinity of X-Tyr may in part be affected by different abilities of the halo-substituents to shift acidity of the phenol (Table 2-4). Previous studies with human IYD

demonstrated the preferential binding of human IYD to the phenolate form of I_2-Tyr.[32] Hence, changes in the pK_a caused by different halo-substituents can potentially affect affinity of X-Tyr and hhIYD as the proportion of the phenolate changes. Most affinity of X-Tyr to hhIYD followed this trendency except for Cl-Tyr. Its affinity may be more influenced by the size of a chloro-substituent. Otherwise, increased affinity to hhIYD was observed when the phenolic proton is more acidic (Table 2-4). However, the results are not very obvious due to fairly small differences among the pK_a (8.48 - 8.86) and the K_d values of X-Tyr (Table 2-4).

Table 2-4. Binding affinity of halotyrosines (X-Tyr) and halophenols (2XP) for IYD

Halogen (X)	pK_a [a] (2-halophenol)	K_d (μM)				
		X-Tyr			2XP	
		mouse IYD[b]	human IYD[b]	hhIYD[c]	human IYD[d]	hhIYD[c]
I	8.53	0.09 ± 0.04	0.09 ± 0.02	8.2 ± 0.5	1,410 ± 70	67 ± 2
Br	8.48	0.15 ±0.02	0.10 ± 0.01	2.1 ± 0.3	-	260 ± 20
Cl	8.35	0.11 ± 0.03	0.14 ± 0.02	6.2 ± 0.3	-	410 ± 30
F	8.86	1.3 ± 0.20	1.3 ± 0.40	51 ± 2	-	22,700 ± 900

[a]Values determined previously.[41] [b]Determined previously.[32, 43] [c]Determined from the data of Figure 2-5. [d]Determined from the data of Figures 2-4. Errors derive from least squares fitting.

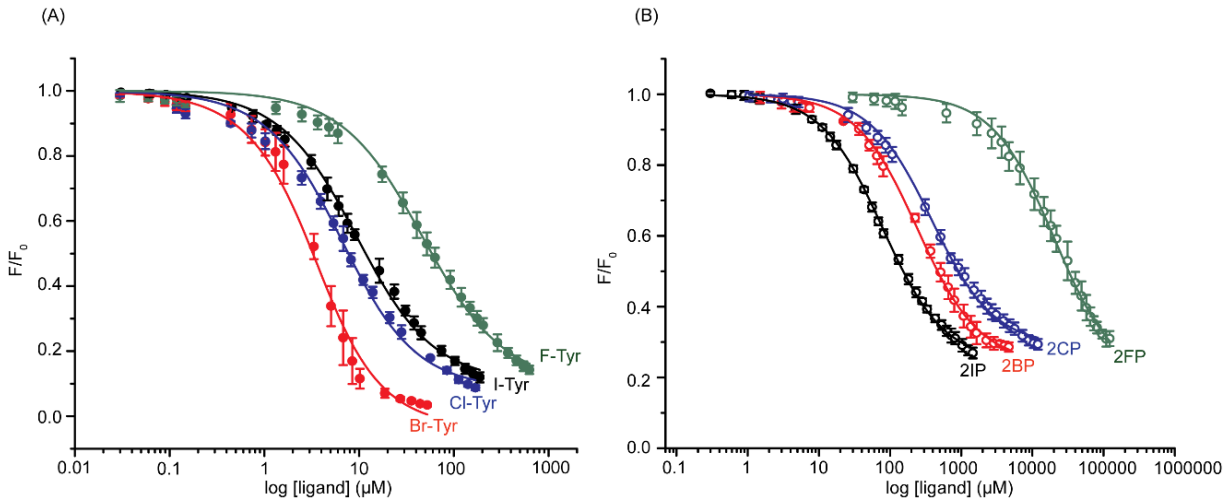

Figure 2-5. Quenching of FMN_{ox} fluorescence upon ligand binding to hhIYD. hhIYD (2.5 μM) in 100 mM potassium phosphate, pH 7.4 was stirred at 25 °C for 30 min prior to addition of the indicated ligand. The K_d values derived from the best fit of the data (solid lines) to equation 2-4. Complete fluorescence quenching by 2XP was limited by their solubility.

In contrast to X-Tyr, contribution of the halogens to the binding affinity is more pronounced for halophenols as their binding strength for hhIYD dramatically dropped from 2-iodophenol to 2-

fluorophenol (Table 2-4, Figure 2-5). This change is evident by their widely distributed K_d values from 67 μM to 23 mM. The results suggested that the zwitterion is more significant on binding to hhIYD when the halogens are smaller in size.

2.3.3.3 Determination of binding affinity of iodophenol derivatives to hhIYD

The binding studies of different halotyrosines for hhIYD showed that hhIYD has the greatest promiscuity for the iodo-substituted derivatives (I-Tyr and 2IP). Hence studies of hhIYD binding promiscuity were extended to three additional iodophenol derivatives, including ones with an electron donating group (4-amino-2-iodophenol, 4A2IP), an electron withdrawing group (4-hydroxy-3-iodobenzonitrile, 2IPCN) and an extra charge (4-hydroxy-3-iodobenzoate, 2IPCOOH). Previously, the phenolate rather than phenol form showed preferential binding to human IYD. The derivatives with the amino and cyano groups were used to shift the acidity of the phenolic proton (Table 2-3). The estimated pK_a for 4A2IP is slightly higher than that of 2IP (~0.3 pK_a unit). As speculated, its affinity for hhIYD is slightly weaker than 2IP (~1.45 fold) (Table 2-3, Figure 2-6) as its phenolic proton is less acidic than that of 2IP. 2IPCN exhibited a more substantial difference in a K_d value compared to 2IP (~46 fold) because of a greater difference in pK_a (2 pK_a units) (Table 2-3, Figure 2-6). The affinity of 2IPCN was even stronger than I-Tyr, which implied that the zwitterion may not be necessary for substrate recognition and turnover for hhIYD. The K_d of 2IPCOOH is intermediate between 2IPCN and 2IP and the negative charge of the carboxylate anion is not likely to affect its affinity for hhIYD (Table 2-3, Figure 2-6).

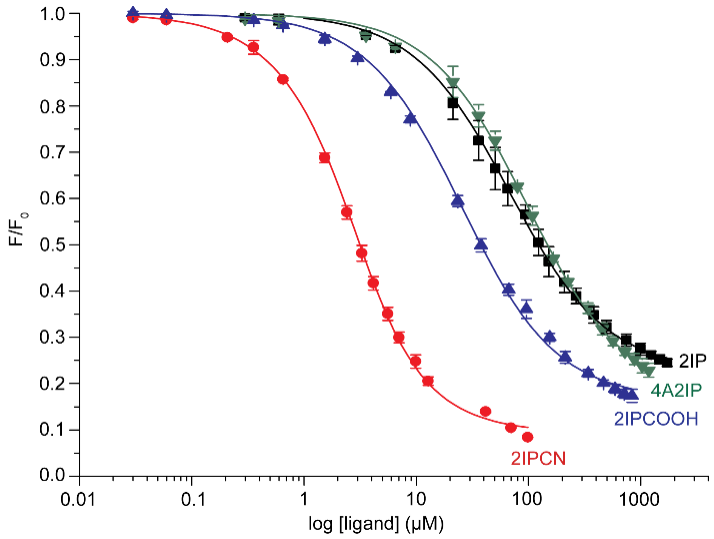

Figure 2-6. Quenching of FMN_{ox} fluorescence upon ligand binding to hhIYD. hhIYD (2.5 μM) in 100 mM potassium phosphate, pH 7.4 was stirred at 25 °C for 30 min prior to addition of the indicated ligand. The K_d values derived from the best fit of the data (solid lines) to equation 2-4.

2.3.4 Catalytic deiodination of I-Tyr and mono-halophenols

Enzyme turnover of each mono-halogenated compound was determined by measuring formation of its deiodinated product after separation by reverse-phase HPLC (Appendix Figure A3, A9 and A11). The initial rates as a function of substrate concentrations were used to determine the kinetic parameters (Appendix Figure A8). A k_{cat}/K_m of deiodination of I-Tyr by human IYD is 2-fold more than that recently determined for *Drosophila* IYD.[23] Their k_{cat} values are almost identical and the K_m for human IYD is only ~1.5 fold-less than that of *Drosophila* IYD. The catalytic efficiency of I-Tyr turnover by human IYD is only 2-fold higher than that of I_2-Tyr (Table 2-2 and 2-3). Their k_{cat} values are experimentally indistinguishable and the K_m of I-Tyr is only ~2-fold lower than that of I_2-Tyr. Lacking the zwitterion greatly decreased efficiency of deiodination of 2IP by human IYD with a k_{cat}/K_m five orders of magnitude lower than that of I-Tyr (Table 2-3). Its k_{cat} is lower by 20-fold and the K_m is higher by 560 fold compared to that of I-Tyr.

HhIYD exhibited almost identical catalytic efficiency (k_{cat}/K_m) for deiodination of I-Tyr as human IYD, despite about 90-fold weaker affinity with I-Tyr (Table 2-3). Again, loss of catalytic

efficiency was also observed for deiodination of 2IP although its affinity is about 20-fold greater than human IYD. The k_{cat} of 2IP turnover by hhIYD is even lower than that of human IYD (~45%) while their k_{cat}/K_m values are still in the same order of magnitude. The binding and kinetic results of human IYD and hhIYD with I-Tyr and 2IP exhibited no correlation between affinity and catalysis. A k_{cat} of 2IP turnover by pfuIYD at 60 ^oC is ~4- and ~6-fold higher than that of human IYD and hhIYD at 25 ^oC. An increase in the k_{cat} of pfuIYD is expected for rates at higher temperature. However, its K_m is almost identical to that of human IYD and hhIYD, resulting in one order of magnitude higher k_{cat}/K_m. All IYD homologs expressed low deiodination rates of 2IP. However, their slow rates were confirmed to derive from enzymatic activity by performing deiodination of 2IP in the presence of free FMN instead of IYD. The reaction containing FMN (2.5 μM), 2IP (5 mM) and dithionite (0.5%) was performed under a standard condition. If phenol was generated, the amount was below the detection threshold of 3 nmol after 2 h (Appendix Figure A10). Turnover of 2-bromophenol (2BP) was further investigated but very slow debromination rates were observed with the detected phenol less than threshold of 3 nmol after 4 h. (Appendix Figure A11).

Catalytic activity of hhIYD with three iodophenol derivatives was further determined to study whether active site affinity or a charge group of a substrate will have an influence on catalysis. 2IPCOOH has slightly tighter affinity with hhIYD than 2IP. However, its k_{cat}/K_m is still within an order of magnitude with that of 2IP. The results implied the rate of catalysis does not correlate with substrate affinity. More obvious results were shown by the last two examples where a k_{cat}/K_m of 4A2IP turnover is ~6-fold increased from that of 2IP which contrasts to its weaker affinity to hhIYD. Surprisingly, no 4-cyanophenol product was detected over the detection threshold from the deiodination of 2IPCN by hhIYD (Appendix Figure A9) although the ligand binds hhIYD even more tightly than I-Tyr. The binding and catalysis studies suggested that tight active site binding does not necessarily increase the catalytic efficiency of hhIYD.

2.4 Discussion

The binding of human IYD, hhIYD and pfuIYD to I-Tyr and 2IP suggested different binding specificity between IYDs from eukaryotes and prokaryotes. Despite their binding differences, all three IYDs have similar catalytic specificity as their k_{cat}/K_m values for iodotyrosines distributed within an order of magnitude and are 4 – 5 orders of magnitude higher than those of 2IP. Clearly, human IYD controls both binding and catalytic selectivity to iodotyrosines for efficient maintenance of iodide for a thyroid function. The bacterial IYD and archaeal IYD share more promiscuity for binding 2IP but low deiodination rates of 2IP suggested that 2IP is not their primary substrate. Both prokaryotic IYDs still reserve their deiodinase activity for iodotyrosines which may be physiologically relevant. However, their function is still unknown. The higher k_{cat} of I_2-Tyr turnover by pfuIYD at 60 ^oC versus 25 ^oC is expected for IYD from thermophilic *P. furriosus* thriving at an optimal temperature of 100 ^oC.[44] Interestingly, its K_d for I-Tyr and K_m for I_2-Tyr at 25 ^oC and 60 ^oC are maintained but the K_d for 2IP at 60 ^oC is increased from that of 25 ^oC by ~3.5 fold. These observations suggested that at high temperature, the enzymatic machinery of pfuIYD is designated for recognition and catalysis of halotyrosines over 2IP. It is still a mystery but very tempting to believe that the truncated loop of pfuIYD may in part mediate binding and catalysis of halotyrosines at high temperature. Investigations on substrate specificities of the selected IYDs suggest that an increase in binding stringency was evolved from the archaeal IYD to human IYD but the catalytic selectivity for halotyrosines was already fine-tuned and exists in the primitive organism like archaea.

Further investigations on active site binding for hhIYD revealed that substrate affinity can be altered by two features. Initially, only an ~8 fold-difference in the K_d of I-Tyr and 2IP for hhIYD implied that the zwitterion may not contribute much to its affinity. However, the drastic decrease in affinity of hhIYD with a series of phenols with different halo-substituents demonstrated that the zwitterion is still essential for ligand affinity to hhIYD especially when the halo-substituents become smaller. The necessity of the zwitterion was also illustrated by crystallographic studies of

mouse and human IYD showing bridging interactions from the zwittion of iodotyrosines to three active site lid residues and the isoalloxazine ring of FMN.[32, 43] Mutations of each individual active site residue or modifications of the carboxylate or amino group of I-Tyr to remove charges also exhibited decreases in substrate binding affinity.[23, 25, 45] However, binding studies of iodophenol derivatives for hhIYD revealed that the zwitterion is not the only key feature for active site binding as changes in acidity of the phenolic pK_a introduced by different *para*-substituents is also important for ligand affinity. 2IPCN binds more tightly than 2IP and even more than I-Tyr potentially because its phenolic proton is significantly more acidic than that of 2IP and I-Tyr (Table 2-3), leading to a greater proportion of the phenolate anion to provide an electrostatic interaction to the backbone Ala64 (equivalent to Ala126 in mouse IYD as described in Chapter 1). The importance of the acidity of the phenolic proton was evident in the weak affinity of a methyl-tyrosine to mouse IYD (K_d > 1.5 mM) due to high pK_a (pK_a = 10.4)[45] of its phenolic proton.[22, 32]

However, high affinity of the active site does not ensure an increase in deiodination rates by IYD. This behavior is evident by the failure to improve catalytic efficiency of I-Tyr for human IYD and pfuIYD, which exhibited stronger affinity for I-Tyr than hhIYD. Also, high affinity of 2IP to hhIYD and pfuIYD compared to human IYD does not increase their k_{cat}/K_m for 2IP turnover. Substrate affinity and steady-state kinetics of 2-iodophenol derivatives for hhIYD demonstrated that 2IPCOOH binds hhIYD almost 3-fold more tightly than 2IP but showed slightly lower k_{cat}/K_m (~1.6 fold). On the contrary, 4A2IP showed weaker affinity by hhIYD versus 2IP but exhibited a larger k_{cat}/K_m by ~6 fold. The most striking evidence demonstrating no correlation between binding and catalysis is that affinity for 2IPCN by hhIYD is even stronger than I-Tyr but no detectable turnover was observed. These results clearly confirmed that tight binding is not the only determinant for IYD catalysis. This observation implied IYD has additional requirements upon substrate coordination to trigger FMN chemistry for its reductive deiodination. Since lack of the zwitterion is the only difference 2IP has compared to I-Tyr, the absence of the zwitterion in 2IP is a potential reason for loss of IYD activity.

2.5 Summary

The k_{cat}/K_m values of I_2-Tyr turnover for human IYD, hhIYD and pfuIYD fell within the range reported for other IYD homologs from different eukaryotes and prokaryotes. Their catalytic efficiency for I-Tyr is also within an order of magnitude from that of I_2-Tyr despite being determined from different assays. Binding studies of 2IP compared to I-Tyr for all three IYDs displayed different substrate recognition between the selected eukaryotic and prokaryotic IYDs. As expected, human IYD exhibited the highest binding specificity for I-Tyr with an almost 16,000 fold difference in the K_d of I-Tyr and 2IP. PfuIYD and hhIYD shared more binding promiscuity with 2IP. Their K_d values for I-Tyr and 2IP (~2,000 fold and ~8 fold, respectively) are much less than the 16,000 fold. The increase in affinity of both prokaryotic IYDs for 2IP was thought to potentially increase their catalytic efficiency for 2IP. However, their k_{cat}/K_m values for 2IP turnover are still low and within an order of magnitude to that of human IYD. Hence, all selected IYDs displayed the same catalysis preference for I-Tyr with k_{cat}/K_m of 4 – 5 orders of magnitude higher than that of 2IP. Low deiodination rates of 2IP suggested that it is not the primary substrate for IYDs including those from bacterium and archaea. Different binding specificity but similar catalytic selectivity also suggested that IYD has different criteria for binding and turnover. Tight substrate binding does not ensure IYD catalysis as apparently evident by no detectable 2IPCN turnover despite its strongest affinity to hhIYD. The phenolate anion is key for affinity of iodophenol derivatives to hhIYD, however it cannot increase the catalytic efficiency for deiodination of iodophenols.

Chapter 3: Structural and functional analysis for the slow turnover of 2-iodophenol by hhIYD

3.1 Introduction

Flavoproteins catalyze a very broad spectrum of redox processes by different mechanisms based in part by its ability to participate in both one- and two-electron processes.[46-49] The oxidized FMN (FMN_{ox}) can be reduced via either a single two-electron process to generate a fully reduced-state hydroquinone (FMN_{hq}) or by two single electron steps to first form its one-electron reduced semiquinone (FMN_{sq}) and then proceed to the fully-reduced FMN_{hq} (Figure 3-1).[50]

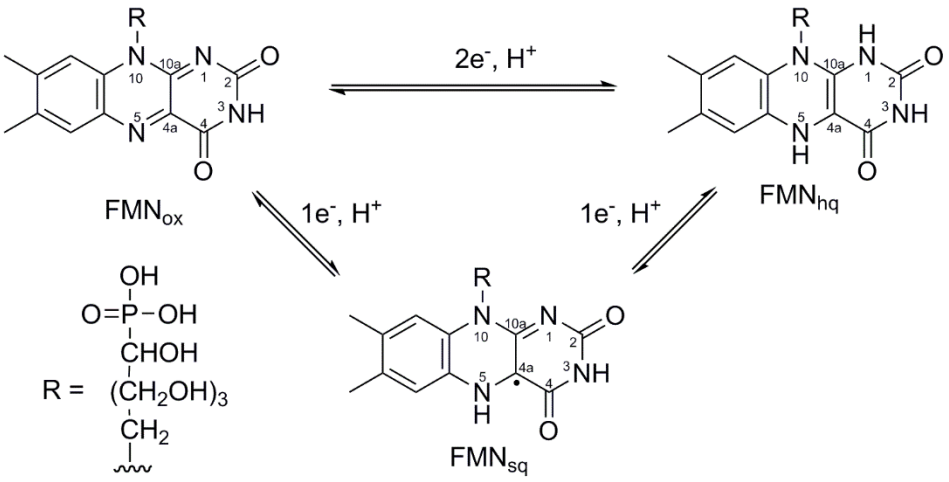

Figure 3-1. Interconversion of the three oxidation states of FMN.

Enzymes within the nitro-FMN reductase superfamily can be distinguished by their ability to promote one and two electron chemistry. For example, reduction of nitroaromatic compounds is catalyzed by nitroreductases via a two electron pathway[51-53] and reductive dehalogenation of halotyrosines is catalyzed by IYD via a one-electron pathway.[22, 32] These two processes are often distinguished by the patterns of hydrogen bonding to N5-FMN. The crystal structures of nitroreductases show hydrogen bonding between the amide backbone and N5-FMN, which may in part be related to stabilizing the two-electron process.[51, 53] Alternatively, hydrogen bonding to N5-FMN in IYD is established from the side chain hydroxyl group of Thr and this hydrogen bonding

pattern is often associated with activation of the one-electron pathways which consequently promotes FMN_{sq} formation.[24, 32]

The crystal structures of human IYD•I-Tyr demonstrated that hydrogen bonding to N5-FMN is established upon coordination of halotyrosine substrates.[32] Binding of I-Tyr to the active site of human IYD allows the Thr235 side chain to approach N5-FMN within hydrogen bonding distance (Figure 3-2). Further studies on the redox properties of FMN in human IYD revealed that association of the substrate analog fluorotyrosine (F-Tyr) to human IYD can switch the redox chemistry of FMN from two- to one-electron processes.[32] This change is evident by accumulation of FMN_{sq} during the reduction of FMN in human IYD in the presence of F-Tyr. However, this same stabilization is not detected when F-Tyr is absent.[32] The crystallographic and redox studies suggested that IYD requires coordination of the substrate to initiate one-electron chemistry for its deiodination take place.

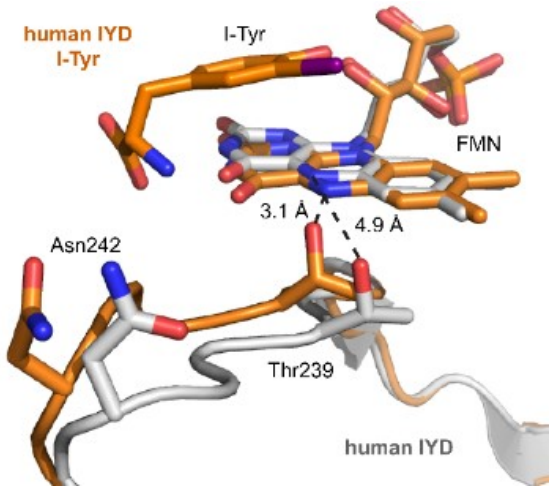

Figure 3-2. Conformational change upon association of I-Tyr with human IYD. Superimposition of human IYD in the absence (gray) and presence of I-Tyr (orange).

It is explained in this Chapter why catalytic turnover of 2IP is still very low ($k_{cat}/K_m = (4 \pm 1)\times10^{-5}$ min^{-1} μM^{-1}) despite its high affinity for hhIYD (K_d = 67 ± 2 μM). Crystallographic studies and redox titration of hhIYD in the alternative presence of 2IP and I-Tyr were also used for hhIYD to contrast the ability of these two substrates to template the active site of hhIYD for its catalysis.

3.2 Experimental Procedures

3.2.1 Materials

Sparse matrix screens including Index HR2-144 (Hampton Research), Cryos Suite (QIAGEN) and PEGs II (QIAGEN) were used for crystal screening. All other reagents used for crystallization were purchased from Hampton Research. Xanthine and xanthine oxidase were obtained from Sigma-Aldrich. Other materials are described in Chapter 2 (2.2.1).

3.2.2 Expression and purification of hhIYD

Expression, purification and concentration determination of hhIYD are described in Chapter 2 (2.2.2 and 2.2.5) Enzyme concentration used for each experiment was determined based on FMN concentration to represent the native active site.

3.2.3 Crystallization

Crystallization conditions were determined using sparse matrix screening with commercially available screens and a Phoenix crystallization robot. Crystals of hhIYD without ligand were grown by mixing 1 µl of protein (14 mg/ml, in 50 mM sodium phosphate pH 7.4, 100 mM NaCl, 0.5 mM TCEP and 10 % glycerol) in 0.8 µl of well solution containing 80 mM Tris-HCl pH 8.5, 100 mM $MgCl_2$, 24% (w/v) PEG 4000 and 20% glycerol. To obtain a co-crystal of hhIYD and I-Tyr, hhIYD (14 mg/ml (final) in 25 mM HEPES pH 7.4, 0.5 mM TCEP and 10 % glycerol) was incubated with 2 mM (final) of I-Tyr overnight at 4 ^{o}C. Crystals were grown by mixing 0.8 µl of the hhIYD•I-Tyr mixture in 1 µl of a well solution containing 100 mM HEPES pH 7.5, 150 mM $MgCl_2$, 25% (w/v) PEG 3350, 2 mM I-Tyr and 15% glycerol. To obtain a co-crystal of hhIYD with 2IP, hhIYD (16 mg/ml (final) in 25 mM HEPES pH 7.4, 0.5 mM TCEP and 10 % glycerol) was incubated with 2 mM (final) of 2IP overnight at 4 ^{o}C. Crystals were grown by mixing 1 µl of hhIYD•2IP mixture in 0.8 µl of a well solution containing 100 mM Tris-HCl pH 9, 200 mM $MgCl_2$, 2 mM 2IP, 17% (w/v) PEG 8000, 17% glycerol and 10% (v/v) ethylene glycol. All crystals were grown at 20 ^{o}C using

hanging drop vapor diffusion. The crystals appeared within 3 days. Each crystal was then flash frozen in liquid nitrogen directly from the drop.

3.2.4 Data Collection and Structure Determination

Diffraction data were collected at the 12-1 and 7-1 beamlines at the Stanford Synchrotron Radiation Lightsource (SSRL). The diffraction data were processed using either XDS/Aimless[54] (for PDB: 5KO7 and 5KO8) or HKL2000/Scalepack[55] (for PDB: 5KRD). Phases were determined by molecular replacement using PHASER[56] and the mouse IYD (PDB: 3GB5) was used as the search model.[24] All three structures were built and refined by iterative rounds of model-building in COOT[57] and refinement in PHENIX.[58] All structural figures were drawn in PyMOL (Schrödinger, LLC). X-ray diffraction and data processing were performed by Dr. Jennifer Kavran.

3.2.5 Anaerobic Redox Titration.

Anaerobic titration of hhIYD was performed using a xanthine/xanthine oxidase system as previously described.[32, 59, 60] Solutions of hhIYD (20 μM), potassium phosphate (100 mM, pH 7.4), NaCl (500 mM), glycerol (10% v/v), xanthine (1 mM) and methyl viologen (13 μM) were purged by bubbling with Ar for 30 min to remove molecular oxygen. Reduction was initiated by addition of xanthine oxidase (140 μg/ml). Reduction of hhIYD was repeated in the alternative presence of F-Tyr (500 μM) and 2IP (800 μM) to study the effect of ligand on the redox properties of hhIYD.

3.3 Results

3.3.1 Structural studies of hhIYD

Crystal structures of hhIYD in the absence and alternative presence of I-Tyr and 2IP were established for structural comparison to study a correlation between active site binding and turnover of 2IP. All the structures were determined by X-ray diffraction and molecular replacement using mouse IYD as a model (PDB: 3GB5).[24] The crystals of hhIYD, hhIYD•I-Tyr and hhIYD•2IP diffracted X-ray with the resolution of 2.3 Å, 2.2 Å and 2.1 Å, respectively. Data collection and refinement statistics are summarized in Table 3-1. All three hhIYD structures have two polypeptide

chains per asymmetric unit but only the structure of hhIYD without a ligand existed in a biological dimer with two identical chains. The biological dimer forms of hhIYD•I-Tyr and hhIYD•2IP were generated using the crystal symmetry feature in PyMOL.

Table 3-1. Data collection and refinement statistics

Protein	hhIYD	hhIYD•I-Tyr	hhIYD•2IP
Ligands	FMN	FMN and I-Tyr	FMN and 2IP
Protein Data Bank code	5KO7	5KO8	5KRD
Data collection			
Space group	P 2_1 2_1 2	P 6_2 2 2	P 6_4 2 2
Unit cell parameters			
a, b, c (Å)	92.18, 110.88, 43.29	152.72, 152.72, 87.20	154.70, 154.70, 88.88
α, β, γ (°)	90, 90, 90	90, 90, 120	90, 90, 120
Resolution (Å)[a]	36.96–2.25 (2.32–2.25)	38.18–2.15 (2.22–2.15)	20.00–2.10 (2.17–2.10)
Wavelength (Å)	1.127	0.980	0.980
No. of unique reflections[a]	21,635 (1,685)	33,077 (2,795)	36,523 (3,607)
No. of observed reflections	149,492	647,766	267,636
Completeness (%)[a]	98.9 (88.4)	99.9 (100)	98.8 (99.5)
Redundancy[a]	6.9 (5.1)	19.6 (20.4)	7.3 (7.2)
R_{sym} (%)[a,b]	7.5 (145)	14.7 (375)	10.7 (100)
$R_{p.i.m}$ (%)[a,c]	3.1 (69.4)	3.4 (84.0)	5.7 (100)
$I/\sigma I$[a]	15.2 (1.1)	16.8 (1.1)	15.2 (1.0)
Refinement			
Resolution used in refinement (Å)	35.4–2.3	38.2–2.2	20.0-2.1
R_{work} (%)/R_{free} (%)[d]	21.6/25.4	19.1/23.2	17.7/22.1
No. of atoms			
Protein	6,336	6,925	6,401
Heteroatoms	100 (FMN)	174 (FMN and I-Tyr)	116 (FMN and 2IP)
Solvent	62	128	126
Mean *B*-factor (Å^2)			
Protein	71.25	62.44	60.16
Waters	53.47	50.96	56.18
FMN	56.22	44.21	45.74
I-Tyr	–	62.57	–
2IP	–	–	65.46
RMSD from ideality			
Bond lengths (Å)	0.003	0.005	0.014
Bond angles (°)	0.707	0.842	1.386
Ramachandran analysis			
Favored (%)	99.49	98.60	99.49
Allowed (%)	0.51	1.40	0.51
Outliers	0	0	0

[a] The values in parentheses are for the highest resolution shell.

[b] $R_{sym} = \Sigma hkl \Sigma i |Ii - \langle I \rangle| / \Sigma hkl \Sigma i Ii$, where Ii is the intensity of an individual reflection and <I> is the mean intensity obtained from multiple observations of symmetry related reflections.

[c] $R_{p.i.m} = \Sigma hkl \sqrt{((1/(n-1))} \Sigma i |Ii - \langle I \rangle| / \Sigma hkl \Sigma i Ii$, where Ii is the intensity of an individual reflection and <I> is the mean intensity obtained from multiple observations of symmetry related reflections.

[d] $R_{work} = \Sigma hkl (|F_{obs}| - |F_{calc}|) / \Sigma hkl |F_{obs}|$ where F_{obs} is an observed amplitude and F_{calc} a calculated amplitude; R_{free} is the same statistic calculated over a subset of the data that has not been used for refinement.

3.3.1.1 Structure of hhIYD

The structure of hhIYD in the absence of ligand is consistent with the mammalian IYDs that have common features of the nitro-FMN reductase superfamily, to which IYD belongs to.[24, 32] The biologically relevant form of hhIYD is an α_2 dimer with α-β fold and domain swaps at each N and C terminus. The FMN cofactor is non-covalently bound in active sites formed by the dimer interface (Figure 3-3A). The hhIYD structure is superimposable on both mouse and human counterparts (mouse IYD: RMSD of 0.85 Å for 304 Cα atom comparison of PDB: 5KO7 versus 3GB5; human IYD: RMSD of 0.77 Å for 321 Cα atom comparison of PDB: 5KO7 versus 4TTB) (Appendix Figures B1-A and B1-B). Similar to both mammalian IYDs, an active site lid of hhIYD (residues 95 – 112) is unstructured as indicated by the lack of electron density for the active site lid region (Figure 3-3 A). However, the loop of hhIYD (residue 133 – 145) is present despite the absence of I-Tyr. The equivalent loop in human IYD is detected only when I-Tyr is bound while the entire loop of mouse IYD was barely built even in the presence of I-Tyr (Appendix Figure B2). The presence of the loop of hhIYD is rationalized by substitution of Ala in mammalian IYDs with Pro137[61, 62] in hhIYD that can introduce rigidity into the region. In addition, Asp138 and Thr140 of hhIYD (substituted with Gln and Lys in mammalian IYDs) are within hydrogen bonding distance, which could help to stabilize the loop.

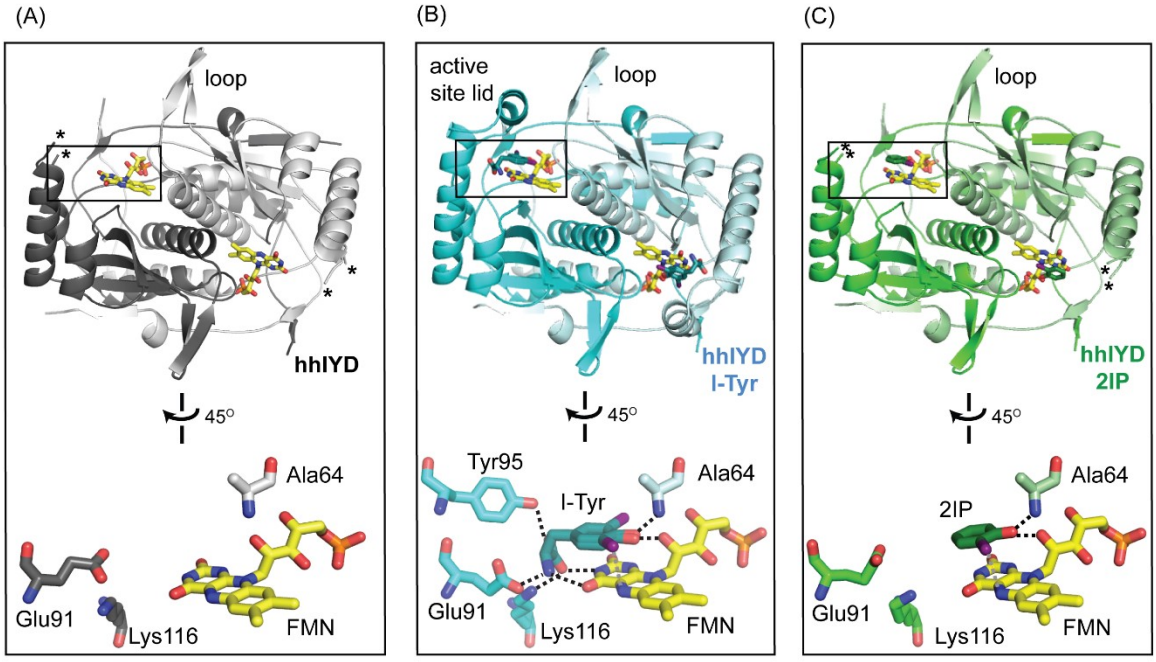

Figure 3-3. Structures of hhIYD and the active site environment. (A) hhIYD (gray) (B) hhIYD•I-Tyr (cyan) and hhIYD•2IP (green). The associated FMN_{ox} co-factor is present in yellow (carbon atom). Black dashed lines represent hydrogen bonding within 2.5 – 2.9 Å and gray dashed lines indicate a distance of 4 Å. The unstructured active site lids in (A) hhIYD and (C) hhIYD•2IP generate two discontinuous ends as indicated by (*).

3.3.1.2 Structure of hhIYD•I-Tyr

The structure of hhIYD•I-Tyr is nearly superimposable with the structure of hhIYD in the absence of I-Tyr (RMSD of 0.23 Å for 345 Cα comparison of PDB: 5KO8 versus 5KO7) (Appendix Figure B1-C) except for the detectable active site lid (residues 95 - 112) (Figure 3-3 B). The lid was also observed in the co-crystal complexes of mouse and human IYDs with I-Tyr. Coordination of I-Tyr stabilizes the lid by using its zwitterion to establish interactions with the side chains of three active site lid residues, Glu91, Tyr95 and Lys116 (Figure 3-3 B). The zwitterion also offers hydrogen bonding through its ammonium to the O^4-FMN and its carboxylate to the N3-FMN. Besides, electrostatic interactions from the zwitterion of I-Tyr, the hhIYD•I-Tyr complex is likely to be stabilized by π-stacking between an aromatic ring of I-Tyr and FMN, hydrogen bonding of the phenolate of I-Tyr to an amide backbone of Ala64 and 2'OH-ribityl of FMN. All these interactions are also present in both mammalian crystal complexes with I-Tyr.

The entire lid of hhIYD•I-Tyr could be built for one chain but not for the other due to insufficient electron density for residues 98-100. This behavior implied that the lid is somewhat dynamic even when I-Tyr is bound. In addition, I-Tyr in the active site of hhIYD is present in two conformations as evident by an unbiased difference map of I-Tyr and an anomalous signal from the iodo atom (Figure 3-4 A). In more prevalent conformation, the aromatic ring stacks over FMN with the C-I bond aligning over a C4a-N5 bond of FMN (4.0 Å from an iodo atom to N5-FMN) (Figure 3-3 B and Figure 3-4 A), which is similar to the single conformation observed with the mouse and human IYD. The second conformation contains I-Tyr with its aromatic ring flipped by ~180° with the C-I bond pointing toward Phe110. The presence of this alternative conformation is likely explained by the π-interaction given by Phe110 to the C–I bond.[63] An equivalent Phe is not found in either mammalian IYDs.[24, 32]

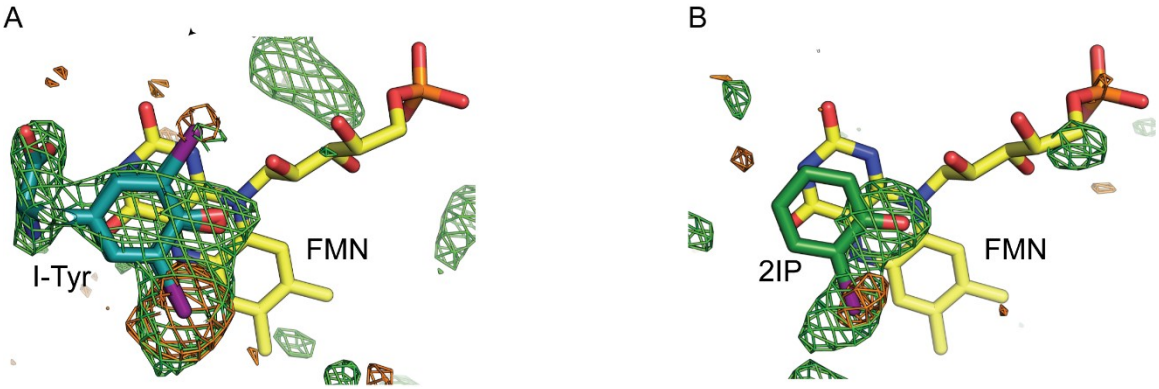

Figure 3-4. Substrates and FMN_{ox} complex in the active site of hhIYD (A) Two configurations of I-Tyr (B) Single configuration of 2IP. FMN_{ox} is presented in yellow (carbon atoms). The unbiased difference map (Fo-Fc) countoured at +3σ are indicated in green mesh. The anomalous difference maps contoured at +3σ are shown in orange mesh.

3.3.1.3 Structure of hhIYD•2IP

The co-crystal structure of hhIYD with 2IP is nearly superimposable with the structure of hhIYD in the absence of ligand with RMSD of 0.30 Å for 337 Cα atom comparison of PDB: 5KRD versus 5KO7 (Figure B1 D). Unlike I-Tyr, 2IP lacks the zwitterion to establish interactions with the lid residues and FMN, hence no detectable active site lid was observed (Figure 3-3 C). The unbiased difference map and the anomalous difference map showed the electron density for a hydroxyl group

and one position of an iodo atom indicating that 2IP is located with a single orientation. Undetectable electron density for an aromatic ring of 2IP suggested that 2IP is dynamic in the active site of hhIYD (Figure 3-4 B). However, 2IP resides in the active site with a similar orientation to I-Tyr in the mammalian IYDs having its aromatic ring above FMN and its C–I bond aligns over C4a-N5 bond of FMN (4 Å). A distance from the iodo atom of 2IP to N5-FMN is also similar to that observed in hhIYD•I-Tyr (4.0 Å) (Figure 3-1 B-C). The complex of hhIYD•2IP is likely stabilized by π-stacking between the aromatic rings of 2IP and FMN together with a hydrogen bonding from the phenolate to Ala64 backbone and 2'OH-ribityl of FMN.

3.3.2 Reduction of FMN in the active site of hhIYD

Previous studies demonstrated that deiodination by IYD is driven by an one-electron process.[22, 32, 52] This is evident by detection of the one-electron reduced FMN_{sq} during the reduction of mammalian IYDs in the presence of either I-Tyr or an inert substrate analog fluorotyrosine (F-Tyr). To investigate slow deiodination of 2IP by hhIYD, similar redox titration studies were repeated with hhIYD in the presence of 2IP to learn how its active site coordination affects FMN chemistry compare to F-Tyr.

Reduction of hhIYD was performed using xanthine/xanthine oxidase.[59, 60] In the absence of ligand, FMN_{ox} bound to hhIYD (λ_{max} = 446 nm and shoulder near 470 nm) was reduced without detection of the FMN_{sq} (λ_{max} = 590 nm) (Appendix Figure B3) suggesting a preferential two-electron process. Then, reduction of hhIYD was performed in the presence of an inert substrate analog F-Tyr. Binding studies confirmed that this analog binds hhIYD (K_d = 46 ± 2 μM) (Figure B4) but is not subject to dehalogenation.[22, 32] About 10-fold excess of K_d was used for the redox titration. FMN_{sq} was detected during reduction of hhIYD with F-Tyr present, indicating a switch from two-electron to one-electron chemistry as observed in human IYD (Figure 3-5 A).

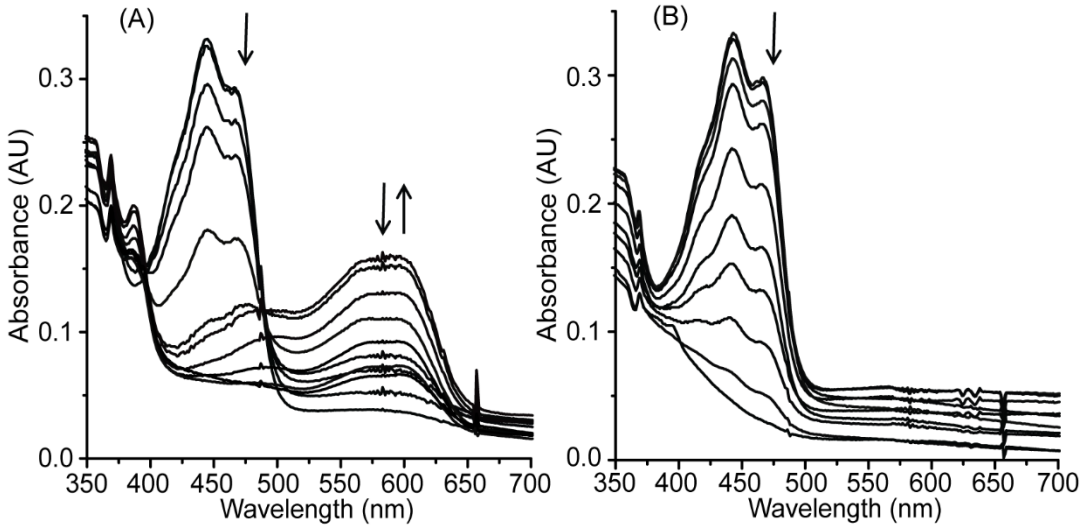

Figure 3-5. UV spectrum monitoring reduction of FMN bound to hhIYD in the presence of ligands (A) F-Tyr and (B) 2IP. FMN_{ox} (446 nm) decreases upon reduction and accumulated FMN_{sq} (590 nm) is detected in (A) but not in (B).

2IP was used to assess its ability to stabilize FMN_{sq} as it is not practical to use the analog 2FP due to its very weak affinity for hhIYD (K_d = 20 ± 1 mM) (Appendix Figure B4). 2IP was used instead due to its slow deiodination by hhIYD with the turnover number less than one during the time needed for its redox titration experiment (40 min). Unlike F-Tyr, accumulation of FMN_{sq} was not observed during the reduction of hhIYD when 2IP is present (Figure 3-5 B). This finding suggested 2IP lacks the ability to shift the chemistry of FMN from a two- to one-electron process.

3.4 Discussion

Success in co-crystallization of hhIYD•2IP and the redox titration studies provided an explanation for the slow deiodination of 2IP by hhIYD. Crystallographic studies demonstrated that 2IP resides in the active site of hhIYD but is mobile. It does mimic the orientation of I-Tyr. Unlike I-Tyr, 2IP lacks ability to order the active site lid. Both I-Tyr and 2IP stack over FMN and their C–I bonds are aligned over a reactive center C4a–N5 bond of FMN. In several flavoproteins, π-stacking either from the protein or substrate to an isoalloxazine ring of FMN is essential to fine-tune flavin redox chemistry.[64, 65] In addition, close proximity of substrates to a highly-reactive region, C4a-N5 bond of FMN, is also likely to modulate their enzymatic activity.[28, 51, 66] For instance, a co-crystal of nitroreductase NfsB (*E. coli.*) and nicotinic acid shows the possibility of

NAD to stack over an isoalloxazine ring in a proximal orientation for hydride transfer from C4 of the NAD ring to N5 of the FMN.[66] Similar binding of substrate stacking above FMN was observed with dinitrodenzamide prodrugs and dicoumarol to an oxygen-insensitive nitroreductase NfsB,[67] binding of dicoumarol to flavin reductase (*Vibrio fischeri*)[68] and coordination of benzoate to nitroreductase from *Enterobacter cloacae*.[51] BluB, which shows the most structural similarity to IYD, holds its substrate, molecular oxygen, over the C4a-N5 bond of FMN_{hq}.[28] However, π-stacking of 2IP above FMN and close proximity of the C–I bond to the C4a-N5 bond of FMN cannot mediate 2IP turnover. This observation indicated that IYD requires suitable substrates to modulate a switch of FMN chemistry for the deiodination reaction.

The human IYD•I-Tyr structure showed that coordination of I-Tyr induces formation of a lid to generate a closed conformation of the I-Tyr–IYD complex. Binding of I-Tyr also triggers a side chain of Thr235 to move close to N5-FMN (3.1 Å) while Thr235 is away from N5-FMN in the human IYD without I-Tyr (4.9 Å) (Figure 3-2).[32] This hydrogen bonding is key for promoting one-electron chemistry in IYD and other related enzymes.[28, 32, 52] The structure of hhIYD•I-Tyr also exhibited the presence of an active site lid when I-Tyr is coordinated as observed in human IYD•I-Tyr. However, its equivalent Thr (Thr173) does not move to hydrogen bond with N5-FMN when I-Tyr is associated in the crystal structure. Instead, Thr173 presents in two different rotamers, both of which remain distal to the N5-FMN (3.6 – 4.0 Å) (Figure 3-6 A). The same orientations and distance of Thr173 to N5-FMN were observed in the structures of hhIYD and hhIYD•2IP (Figure 3-6 B). Rigidity of this region is likely introduced by the presence of Pro176,[61, 62] which is replaced by Asn in both mouse and human IYDs. However, this Thr173 is still essential to promote one-electron chemistry in hhIYD as evident by detection of FMN_{sq} during the reduction of hhIYD•F-Tyr. In addition, the hhIYD T173A mutant also suppresses I-Tyr turnover while promoting a two-electron process for reduction of a nitrotyrosine.[52] Undetectable accumulation of FMN_{sq} during reduction of hhIYD•2IP confirmed the indispensability of the zwitterion for IYD catalysis. The

correlation between FMN_{sq} stabilization and a hydrogen bonding of Thr173 to N5-FMN in hhIYD can be determined by crystallization of the hhIYD•F-Tyr in the reduced form.

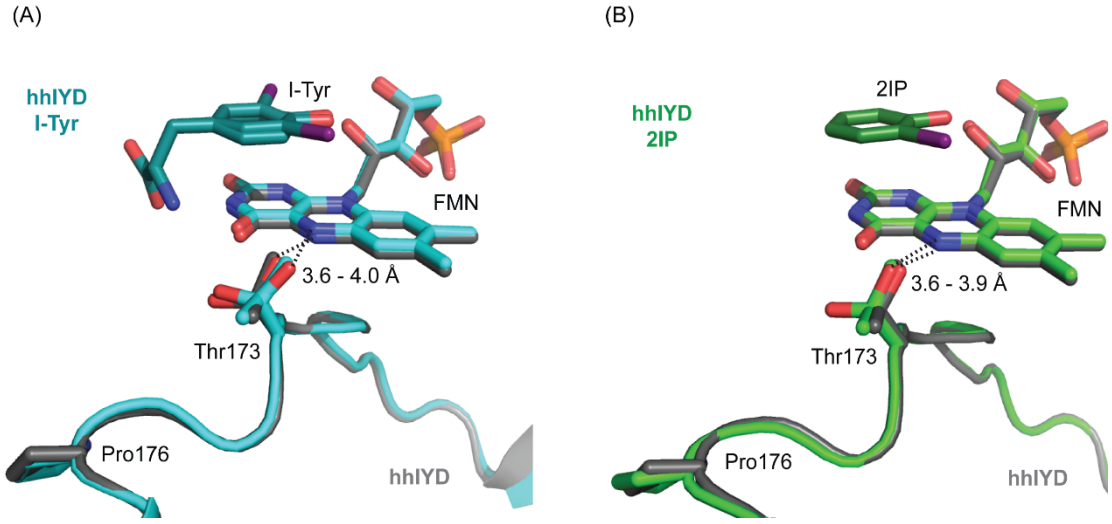

Figure 3-6. Superposition of a loop containing Thr173 of hhIYD structures. The overlay of the Thr173 loop region of hhIYD in the absence of ligand (gray) with that of (A) hhIYD•I-Tyr (blue) and (B) hhIYD•2IP (green).

3.5 Summary

Coordination of I-Tyr to hhIYD results in ordering of its active site lid through interactions between a substrate and active site residues in an arrangement similar to mammalian IYDs. However, I-Tyr is present in two conformations instead of a single conformation observed in mouse and human IYD. Crystallographic studies of hhIYD•2IP exhibited the presence of mobile 2IP with a single orientation similar to the aromatic ring of I-Tyr in mouse and human IYD. Unlike I-Tyr, 2IP lacks the ability to induce formation of the active site lid. The hhIYD•2IP complex is likely stabilized by π-stacking between 2IP and FMN and hydrogen bonding interactions from the phenolate to Ala64 and 2'OH-FMN. However, these interactions together with close proximity of the reaction position of the substrate (C–I bond) and the C4a-N5 bond of FMN are not sufficient to mediate IYD catalysis. The zwitterion of the substrate is key to induce closure of the active site lid and establish hydrogen bonding from the side chain of Thr to N5-FMN to promote the one-electron chemistry of FMN.

Chapter 4: Mutation of hhIYD to improve catalytic efficiency of turnover of 2-iodophenols

4.1 Introduction

Slow turnover of 2IP by the wild-type hhIYD indicated that its catalytic machinery is still designed for deiodination of I-Tyr. However, its basal affinity for 2IP and related derivatives is high enough to encourage us to engineer the enzyme to improve dehalogenation of iodophenols for bioremediation. Due to the lack of hhIYD crystal structures at the time of engineering, three mutants were designed using a predicted hhIYD structure (Figure 4-1). The designs focused on modifications of amino acid residues located in an active site lid consisting of the C-terminus of αC and αD regions (Figure 4-1) to either enhance stability of the lid or coordinate to the substrate and FMN for modulating the FMN chemistry. The best knowledge available at the time of these studies was employed for each hhIYD mutant since engineering was conducted concurrently with structural, binding and kinetic analysis of hhIYD.

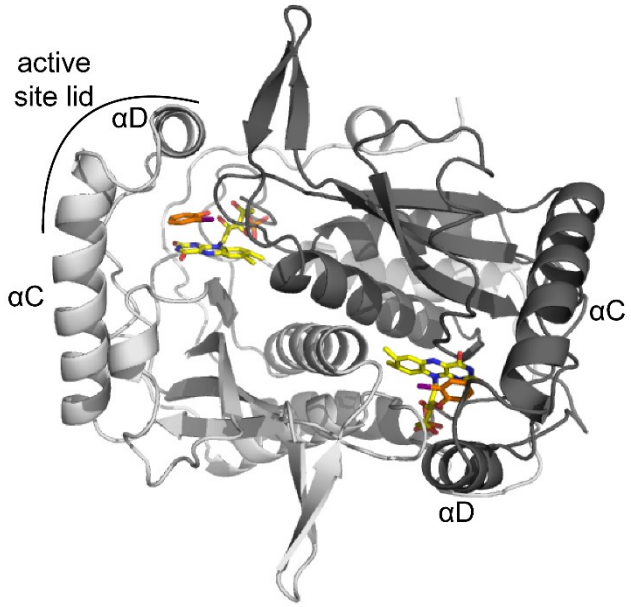

Figure 4-1. Predicted structure of hhIYD•2IP (gray) generated using Phyre2 (see 4.2.1). 2IP and FMN are indicated in orange and yellow (carbon atoms) respectively. The structure was generated with a closed active site lid consisting of the C-terminus of αC helix and αD helix.

Mutations of hhIYD were performed before we learned that substrate affinity is not the only determinant for IYD catalysis. Hence, our first aim was to increase active site affinity to potentially

improve IYD catalysis for 2-iodophenols. The first double mutation (mutant A: hhIYD A64F L107A) was generated to introduce a possible π-stacking above 2IP to improve affinity for the substrate. A64 was selected for mutation as it is located over 2IP (Figure 4-2 A). Although A64 is conserved in most IYD homologs and was considered one of the signature residues for deiodinase activity,[30] substitution of this Ala by Met in pfuIYD suggests that the conserved Ala is not necessary for IYD function (Figure 4-2 B).[31] Introduction of A64F created a potential π-stacking above the substrate 2IP and is also likely to increase the population of the closed lid conformation by establishing hydrophobic interactions with a number of hydrophobic residues (M99, W103, L107A, A64F and F110) located on αD region (Figure 4-2 B). Closure of the active site lid possibly mediates IYD catalysis toward iodophenols. L107A was introduced to avoid its potential steric clash with A64F (Figure 4-2 B).

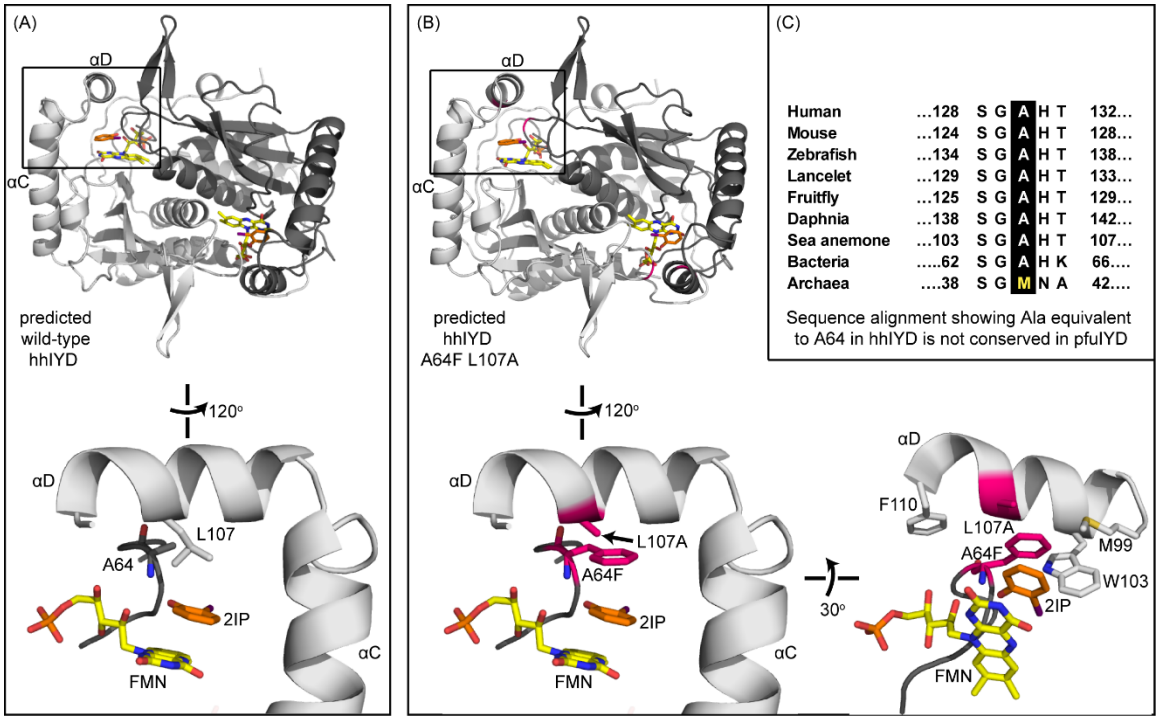

Figure 4-2. Predicted hhIYD structures (gray). (A) wild-type hhIYD and (B) hhIYD A64F L107A (mutant A). 2IP and FMN are presented in orange and yellow (carbon atoms) respectively. Mutated residues are highlighted in pink (carbon atom). (C) sequence alignment of IYD homologs exhibited a selected mutation site, A64, is replaced by M40 in pfuIYD (yellow).

Our second goal was to stabilize the lid region to potentially mimic a closed conformation of the lid as it appears in hhIYD•I-Tyr even though the coordinated substrate does not contain a zwitterion. The second mutant was designed to stabilize the C-terminus of the αC region to potentially induce an active site lid closure. To pursue this goal, a triple mutant (mutant B: hhIYD S94D N96R S175H) was created (Figure 4-3 A). N96R has the potential to establish an electrostatic interaction with Glu93. In addition, a positive charge introduced by N96R is likely to neutralize a negative dipole at the C terminus of its alpha helix (Figure 4-3 A).[69] These interactions potentially enhance the helix stability. Another pair of mutations was inspired from inter-chain interactions observed in BluB, which has the greatest structural similarity to IYD (Figure 4-3 B).[24, 28] Sequence and structural alignment of BluB and IYD revealed that BluB has the same active site lid position as that of IYD. However, the lid of BluB is always ordered whereas lid formation for IYD requires association of a zwitterionic substrate.[24, 28] Stability of the BluB active site lid is in part likely made by a number of inter-helix interactions (Figure 4-3 B). To add an inter-chain interaction to IYD, S94D and S175H were introduced to create mutant B (Figure 4-3). These intra- and inter-chain interactions in mutant B are intended to stabilize the C-terminus of the αC so that it can be structured upon coordination of 2IP. Enhanced stability of the C-terminus of αC was thought to possibly induce closure of αD via hydrophobic interactions between a hydrophobic substrate, 2IP, and hydrophobic residues of the αD region (Figure 4-4).

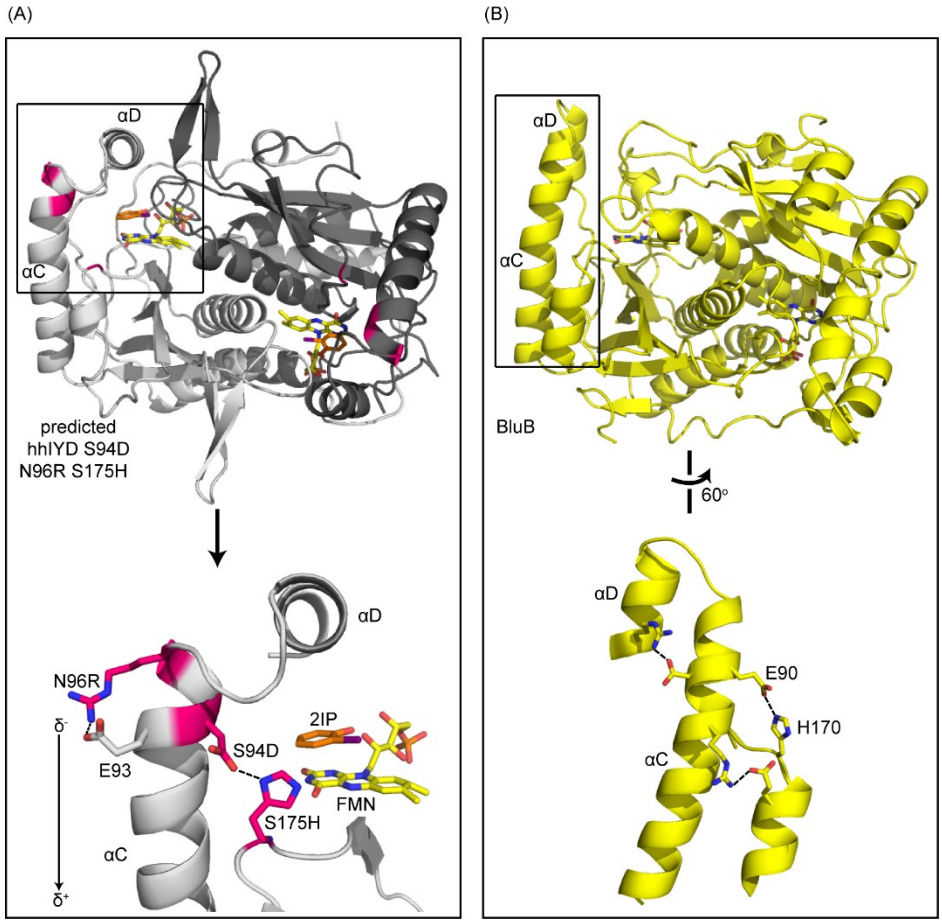

Figure 4-3. Predicted structure of mutant B, hhIYD S94D N96R S175H, and structure of BluB. Cartoon illustration of (A) predicted hhIYD S94D N96R S175H structure (gray) and (B) BluB structure (PDB: 2ISJ) (yellow). Mutated residues are highlighted in pink. 2IP and FMN in hhIYD are presented in orange and yellow (carbon atoms) respectively.

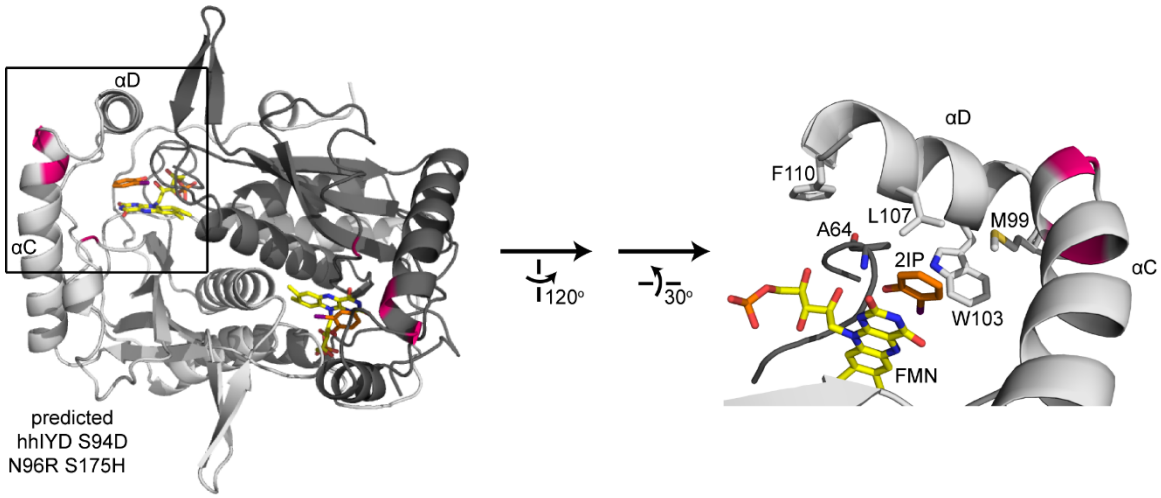

Figure 4-4. Predicted structure of mutant B, hhIYD S94D N96R S175H, exhibiting potential hydrophobic interactions among αD lid residues, A64 and 2IP. Mutated regions are highlighted in pink. 2IP and FMN are presented in orange and yellow (carbon atoms) respectively.

The last hhIYD mutant (mutant C: hhIYD E91R) was designed for a 2IPCOOH substrate by replacing a potentially repulsive force between E91 and the carboxylate group of 2IPCOOH with an attractive polar interaction with Arg (Figure 4-5). In addition, E91R is also likely to interact with FMN to possibly improve IYD catalysis for iodophenol compounds. As shown by some enzymes within the nitro-FMN reductase superfamily, the chemistry of FMN co-factor is controlled by coordination of amino acid sidechains to FMN.[51, 66, 68, 70-73] IYD is no exception. Coordination to N3- and O^4-FMN in IYD is established through the zwitterion of the substrate.[24, 32] Introduction of E91R potentially provides a polar interaction with the O^4-FMN (Figure 4-5 B). Even though E91 is one of the three active site lid residues assisting formation of the active site lid in a native hhIYD, this residue may not be necessary for a non-zwitterionic substrate like 2IPCOOH. R91 has the potential to mediate binding orientation of 2IPCOOH substrate, also coordinate O^4-FMN to possibly fine-tune its catalytic deiodination toward 2IPCOOH.

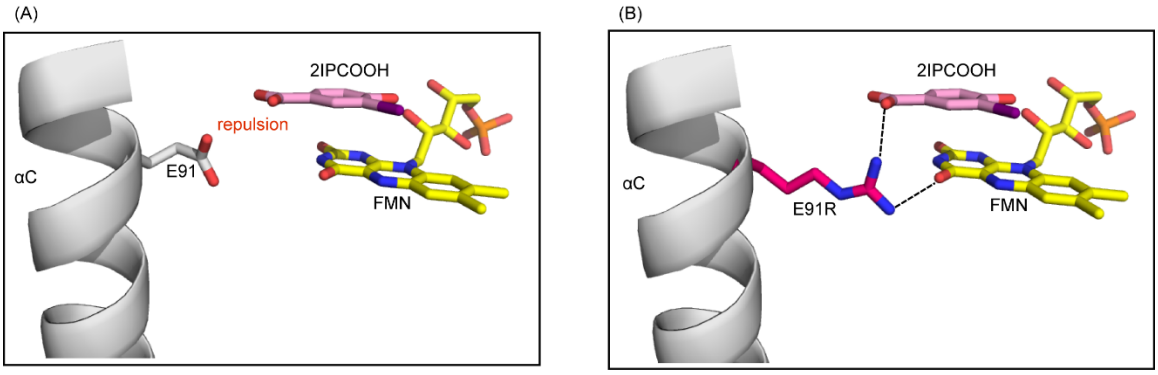

Figure 4-5. Active site region of the predicted hhIYD•2IPCOOH structures. (A) wild-type hhIYD and (B) mutant C, hhIYD E91R. A mutated residues E91R is highlighted in dark pink. 2IPCOOH and FMN are presented in light pink and yellow (carbon atoms) respectively.

In this Chapter, we used rational design to generate three hhIYD mutants as described above. Kinetic studies of the mutants describe their catalytic efficiency (k_{cat}/K_m) as well as their k_{cat} and K_m values for deiodination of 2IP and 2IPCOOH.

4.2 Experimental Procedures

4.2.1 Materials

The predicted structure of hhIYD was generated by Phyre2 intensive search[74] using an amino acid sequence of hhIYD as an input to provide its predicted structure in an *apo* monomer form. An *apo* biological dimer was then generated by Rosetta2[75] using C2 symmetry extracted from the structure of mouse IYD•I-Tyr (PDB: 3GFD)[24] (Calculation was performed by Dr. Michael Pacella, a former student in Dr. Jeffrey Gray's lab). The resulting dimer was aligned with the mouse IYD•I_2-Tyr structure (PDB: 3GH8) and a predicted hhIYD structure with the most similar folding to 3GH8 was selected. Coordinates of FMN and I_2-Tyr from PDB: 3GH8 were then merged with the predicted protein to create a hhIYD dimer in the presence of FMN and I_2-Tyr. hhIYD•2IP was generated by deleting the zwitterion and one iodo atom from I_2-Tyr, hence providing the predicted hhIYD•2IP complex. This resulting structure was used for the rational designs described above (Figure 4-1). Point mutations generated in the model were introduced using the mutagenesis feature in PyMOL without further optimization by Rosetta2.

Other materials are described in Chapter 2 (2.2.2). A detailed procedure for synthesis of 2IPCOOH is described in Chapter 2 (2.2.6).

4.2.2 Site-directed mutagenesis

Site-directed mutagenesis was performed as described in Chapter 2 (2.2.4) except for the modification of templates and primers described below. Vectors containing the hhIYD gene alternatively with SUMO (pSMT3-His_6-SUMO-hhIYD-His_6) and without SUMO (pET24a-hhIYD-His_6) were employed as the templates for site-directed mutagenesis. Each mutation was sequentially introduced using specified primers in the order provided below. The vectors with correct sequences after each round were used for the next round of a PCR reaction to introduce the next mutation to the templates. For mutant A, A64F was generated using a forward primer of 5'-CTCAA-GGCACCTTCAGGTTTTCACAAACAGCCTTGGACCT-3' and its reverse com-

plement. L107A was introduced after A64F by using a forward primer 5'CATGTCCAATG-AGTGGCTGGAAGATGCGCAGCCTTTTGGAA-3' and its reverse complement. For mutant B, S94D was first introduced using a forward primer 5'-GACAAGCTGCTGAAAAAGAGGAATTT-GAAGATTATAATGGCCGCATGTCCA-3' and its reverse complement. Then S175 was generated using a forward primer 5'-GTTTGGTGGCACTTACACATACCCCGCACCCAA-TGAATTTTTTGCAAAAAATT-3'and its reverse complement. Lastly, N96R was generated using a forward primer 5'-GCTGAAAAAGAGGAATTTGAAGATTATCGTGGCCGCATGTCCA-3' and its reverse complement. Note that a sequence of the forward primer GAT was modified from the *wild-type hhIYD* gene to maintain the previously introduced S94D mutation. For mutant C, E91R was created using a forward primer 5'- CGACAAGCTGCTGAAAAAGAGAGATTTG-AAAGCTATAATGGCCG-3' and its reverse complement. The mutated codons are indicated in red.

4.2.3 General methods

Expression and purification of the hhIYD mutants were performed following the procedures described in Chapter 2 (2.2.5). Concentration and FMN occupancy of each hhIYD mutant were measured following the method used for the wild-type hhIYD as described in Chapter 2 (2.2.2). Binding affinity of ligands for hhIYD was determined by their ability to quench the fluorescence of FMN_{ox} described in Chapter 2 (2.2.8). Catalytic deiodination of I-Tyr, 2IP and 2IPCOOH by hhIYD was quantified by formation of the deiodinated product after separation by the reverse-phase HPLC as described in Chapter 2 (2.2.9).

4.3 Results

4.3.1 Generation of the predicted hhIYD structure

Phyre2 intensive search initially provided 20 predicted structures of hhIYD based on 20 different models from the PDB data base. A predicted structure that had the closet folding to the model (mouse IYD•I_2-Tyr, PDB: 3GH8) was selected for engineering studies. The resulting structure appeared as an *apo* monomer with its active site lid in a closed position. This was

employed to generate a biological dimer form. The final predicted hhIYD dimer in the presence of FMN and 2IP is superimposable with the crystal structure of mouse IYD•I_2-Tyr (PDB: 3GH8 with RMSD of 1.83 Å for 369 Cα atom comparison) and its crystallographic structure, hhIYD•I-Tyr (PDB: 57O8 with RMSD of 1.37 Å for 367 Cα atom comparison).

4.3.2 Site-directed mutagenesis

All of the mutated codons were successfully generated except for introduction of N96R to the pSMT3-His_6-SUMO-hhIYD S94D S175H His_6 vector. Only a partial primer insertion was detected from the sequencing results. A successful hhIYD S94D N96R S175H mutant without SUMO fusion was used for protein expression and further kinetic studies.

4.3.3 Expression and purification

The hhIYD A64F L107A and hhIYD S94D N96R D175H triple mutants were expressed and purified with SUMO tag to yield 18 – 19 mg protein per 1 L of culture with FMN occupancy of 93 – 98%. The hhIYD E91R mutant was expressed and purified without the SUMO fusion and yielded ~13 mg protein per 1L of culture with ~92% FMN occupancy. Each mutant was obtained with purity of > 98% as evident from SDS-PAGE, Coomassie staining and ImageQuantTL analysis (Figure 4-6).

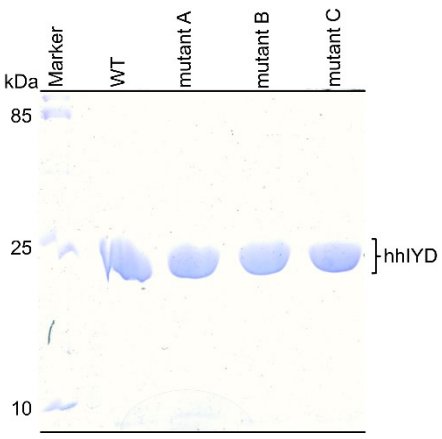

Figure 4-6. SDS-PAGE gels of the purified wild-type hhIYD and its mutants. Lane 1 is a marker with molecular weights of protein (kDa) indicated on the left. Lane 2 is wild-type hhIYD. Lane 3 is mutant A (hhIYD A64F L107A). Lane 4 is mutant B (hhIYD S94D N96R S175H). Lane 5 is mutant C (hhIYD E91R).

4.3.4 Affinity of I-Tyr and 2IP for the wide-type hhIYD and mutant A

Binding affinity was determined by monitoring fluorescence quenching of the FMN_{ox} upon association of the ligand. Studies were performed at pH 9.0 to enhance population of the phenolate anion, which has preferential binding to IYD.[32] The K_d of 2IP for mutant A is ~2 fold more than that of the wide-type while its K_d for I-Tyr is ~ 4-fold less (Table 4-1, Appendix Figure C1). The results revealed that affinity of the mutant A for 2IP cannot be improved indicating that a necessity of the zwitterion is still needed for binding to this mutant.

Table 4-1. Binding affinity of I-Tyr and 2IP for a wild-type hhIYD and mutant A

hhIYD	K_d [a] (μM)	
	2IP	I-Tyr
WT	14 ± 3	3.6 ± 0.5
A64F L107A	32 ± 2	0.9 ± 0.2

[a]Determined from the data of Appendix Figure C1. Errors derived from least squares fitting.

4.3.5 Catalytic deiodination of I-Tyr, 2IP and 2IPCOOH by hhIYD mutants

The initial rates of deiodination of I-Tyr, 2IP and 2IPCOOH by hhIYD mutants as a function of substrate concentrations were used to determine the steady-state kinetic parameters as shown in Table 4-2 (Appendix Figures A8 and C2-C4). The mutant A showed almost 3-fold decrease in a k_{cat}/K_m compared to that of the wild-type hhIYD (Table 4-2, Appendix Figure C2). The k_{cat} value of deiodination of 2IP by mutant A is almost 2.5-fold lower and its K_m is ~1.2 fold higher than that of the wild-type. The k_{cat} of the mutant B for 2IP is also ~9 fold lower as compared to that of the wild-type. However, the mutant B has a lower K_m for 2IP turnover by ~3 fold leading to the same catalytic efficiency as that of mutant A.

Table 4-2. Catalytic deiodination of 2IP, 2IPCOOH and I-Tyr by wild-type hhIYD and mutants

hhIYD	Substrate	k_{cat} (min^{-1})	K_m (μM)	k_{cat}/K_m (min^{-1} μM^{-1})
WT[a]	2IP	0.17 ± 0.02	4,100 ± 800	(4 ± 1) x 10^{-5}
mutant A[b]		0.07 ±0.01	5,000 ± 2,000	(1.4 ± 0.6) x 10^{-5}
mutant B[b]		0.02 ± 0.003	1,400 ± 700	(1.4 ± 0.8) x 10^{-5}
WT[a]	2IPCOOH	0.186 ± 0.006	7,100 ± 600	(2.6 ± 0.2)×10^{-5}
mutant A[b]		0.027 ± 0.007	17,000 ± 9,000	(1.6 ± 0.9)×10^{-6}
mutant B[b]		0.07 ± 0.03	20,000 ± 10,000	(3.5 ± 2.3)×10^{-6}
mutant C[b]		0.0152 ± 0.0005	1,700 ± 200	(0.89 ± 0.01) x 10^{-5}
WT[a]	I-Tyr	16 ± 1	12 ± 2	1.3 ± 0.3
mutant A[b]		7 ± 1	6 ± 2	1.2 ± 0.4

[a]Determined from the data of Appendix Figure A8. [b]Determined from the data of Appendix Figure C2 – C4. Errors derived from least squares fitting.

Deiodination rates of 2IPCOOH were first performed with mutant C that was designed to improve 2IPCOOH turnover. However, mutant A and B were also screened for their deiodinase activity for this substrate. The results demonstrated the k_{cat} values of three mutants for 2IPCOOH ranged between 0.01 – 0.07 min^{-1} which is 3 – 10 fold less than that of the wild-type hhIYD (Table 4-2, Appendix Figure A8 and C3). The K_m values of mutant A and B increased significantly by ~2 – 3 fold, resulting in decreases in k_{cat}/K_m by one order of magnitude as compared to that of the wild-type enzyme. However, the K_m for the mutant C is lower than that of the wild-type by 4 fold, leading to the k_{cat}/K_m within the same order of magnitude but ~3-fold lower than that of the wild-type.

Lastly, kinetics studies of the mutant A for I-Tyr were performed to learn whether its stronger affinity for I-Tyr than that of the wild-type hhIYD would increase its catalytic efficiency. The results exhibited that the both k_{cat} and K_m of mutant A decreased by ~2 fold compared to that of the wild-type. Hence, its k_{cat}/K_m for I-Tyr is almost identical to that of the wild-type hhIYD (Table 4-2, Appendix Figures A8 and C4).

4.4 Discussion

Decreases in affinity of 2IP for mutant A compared to that of the wild-type may result from steric hindrance of F64 that was introduced to the active site instead of the hope for adding π-stacking to 2IP. Increases in affinity of mutant A for I-Tyr compared to the wild-type may result from interactions between the zwitterion to the lid residues and FMN that can compensate with

possible bulkiness introduced by F64. However, the ~ 4-fold tighter affinity of mutant A for I-Tyr than that of wide-type still could not improve its catalytic efficiency as evident by almost identical k_{cat}/K_m values. This finding also supports the knowledge learned in Chapter 2 that tight binding does not ensure efficient catalysis.

Three ways to improve the k_{cat}/K_m for an enzymic transformation are to increase the k_{cat} and/or decrease the K_m value. For mutant A, the k_{cat} for deiodination of 2IP is 2.4 fold lower while the K_m is only 1.2 fold higher compared to that of the wild-type, leading to ~ 3 fold lower k_{cat}/K_m. Catalysis of 2IP by mutant A may be in part suppressed by its weaker affinity compared to the wild-type. The decrease in catalytic efficiency of 2IPCOOH by mutant A is even more drastic than 2IP compared to the wild-type as the k_{cat} for deiodination of 2IPCOOH by mutant A is ~7 fold lower and its K_m is ~ 2.4 fold higher than that of the wild-type leading to ~17 fold decrease in k_{cat}/K_m. In addition to possible steric hindrance introduced by F64, the increase in K_m and significant decrease in the k_{cat}/K_m of 2IPCOOH for mutant A may be explained by a repulsive force between the carboxylate of 2IPCOOH. This rationale is supported by smaller changes of the kinetic parameters for deiodination of 2IP by mutant A compared to those of 2IPCOOH.

For mutant B, its k_{cat} for deiodination of 2IP is 8.5 fold lower but the K_m is only ~3 fold lower compared to those of the wild-type. This change leads to ~ 3 fold lower k_{cat}/K_m than that of the wild-type. The reason for a decrease in catalysis of 2IP by mutant B is not known but we can speculate that either the C-terminus of the αC is not stabilized or it is stabilized but cannot serve FMN chemistry for deiodination. The k_{cat} of 2IPCOOH turnover by mutant B is ~ 2.7 fold lower while its K_m is almost 3 fold higher than that of the wild-type. This mutation resulted in almost 8-fold decrease in the k_{cat}/K_m. Again, the increase in the K_m and decrease in the k_{cat}/K_m for deiodination of 2IPCOOH by mutant B compared to the wild-type can be explained by a repulsive force between E91 and the carboxylate of 2IPCOOH. Kinetic studies of mutant C confirmed impaired catalysis caused by this repulsion as an introduced favorable interaction from E91R can decrease the K_m for deiodination of 2IPCOOH by ~ 4 fold compared to the wild-type. However,

the k_{cat} of 2IPCOOH by mutant C significantly drops by ~12 fold compared to that of the wild-type leading to ~3 fold lower k_{cat}/K_m. Significant decrease in the k_{cat} of deiodination of 2IPCOOH for mutant C implied that R91 may result from an electron withdrawing effect as evident by 10 fold greater k_{cat}/K_m for deiodination of 4-amino-2-iodophenol (4A2IP) by the wild-type hhIYD compared to that of 2IPCOOH. However, this cannot be concluded until the related studies are established.

4.5 Summary

The K_d of mutant A for 2IP is increased by ~2 fold while that of I-Tyr is decreased by ~4 fold compared to those of the wild-type hhIYD. We speculated that F64 may introduce steric hindrance to the active site, hence impair its affinity and catalysis for 2IP. However, the zwitterion is likely to assist binding of I-Tyr despite the presence of bulky F64. Again, improved affinity of I-Tyr for mutant A does not provide more efficient catalysis which confirmed that tight binding is not the only determinant for IYD catalysis. The k_{cat}/K_m values of 2IP and 2IPCOOH turnover by mutant A-C are generally lower than those of the wild-type. More profound decrease in k_{cat}/K_m and increase in K_m were observed in deiodination of 2IPCOOH compared to 2IP. This difference may be explained by repulsive interaction between E91 to the carboxylate of 2IPCOOH. This interaction also exists in the wild-type hhIYD. However, introduced mutations may not be favorable for catalysis of 2IPCOOH, hence deiodination of 2IPCOOH is even suppressed compared to the wild-type. However, decrease in the K_m of 2IPCOOH turnover for E91R mutant is likely explained by a favorable interaction between the substrate and R91. There is a similar observation from the studies of Drosophila IYD showing significant increase in the K_m of deiodination of I_2-Tyr by E154Q.[23] The increase in K_m is potentially due to removal of favorable electrostatic interaction between Glu154 and the zwitterion of I_2-Tyr. The studies indicated that Glu91 of hhIYD is potential for mutation to optimize the K_m value for iodophenol turnover.

Chapter 5: Analysis of IYD-related enzymes for affinity of 2-halophenols

5.1 Introduction

Sequence analysis identified IYD as a member of the nitro-FMN reductase superfamily which supports diverse redox reactions of varied substrates.[20, 76] Diversity of enzymatic reactions in the superfamily implied opportunities to develop other IYD-related enzymes to possess deiodinase activity. Here we studied two additional enzymes in the nitro-FMN reductase superfamily, BluB and 3EO8, to explore the possibility of developing deiodinase activity from their scaffold.

The BluB gene was previously identified in bacterium *Sinorhizobium meliloti* and found necessary for biosynthesis of a lower ligand of vitamin B_{12}.[28, 77] Determination of the first crystal structure of mouse IYD demonstrated that BluB has the most structural similarity to IYD (RMSD of 4.89 Å for 283 Cα atom comparison of PDB: 3GFD and 2ISJ) (Figure 5-1).[24, 28] Sequence alignment shows BluB and IYD share an active site lid derived from the same region of their primary structures (Figure 5-2 A), which is different from the other two subclasses (NOX and FRP).[24] Hence, BluB and IYD were placed into a new distinct subclass in the superfamily.[24] Structural analysis revealed that the lids of BluB and IYD are located in similar orientations, however the loop of BluB aligns in a different orientation from that of IYD as its loop is more buried into the active site to potentially accommodate only the small size of molecular oxygen (Figure 5-2 B).

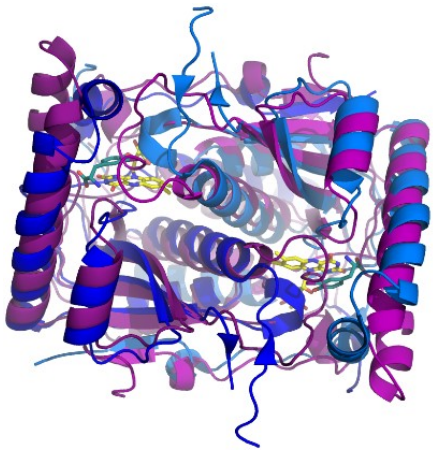

Figure 5-1. Superposition of BluB and IYD structures. Overlay of BluB (PDB 2ISJ) (purple) with mouse IYD (PDB 3GFD) (dark blue). FMN_{ox} and I-Tyr are presented in yellow and blue (carbon atoms) respectively.

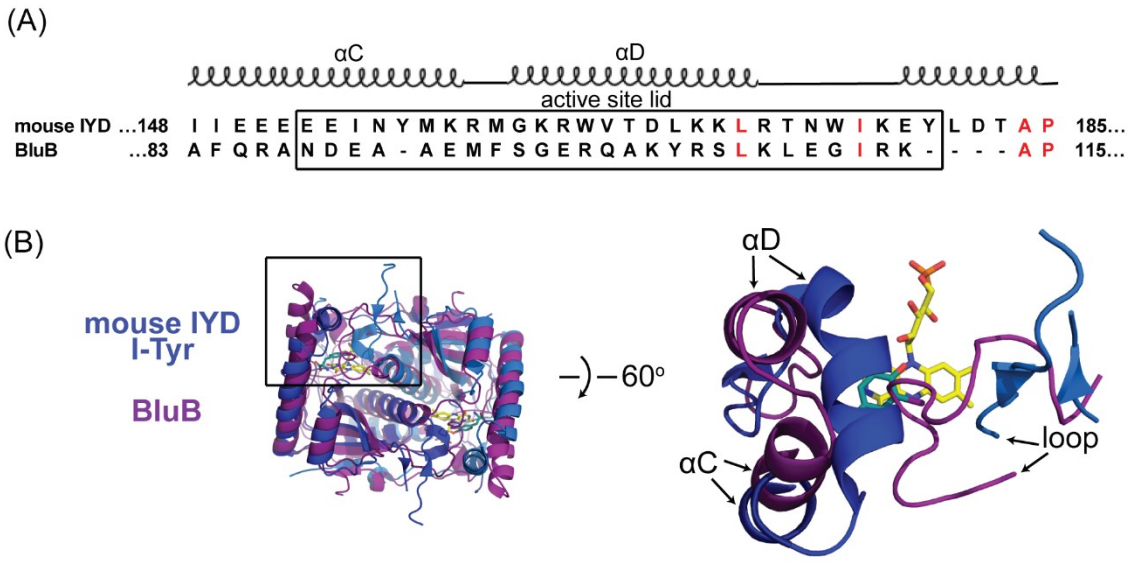

Figure 5-2. Sequence and structural comparison between mouse IYD and BluB. (A) amino acid sequence alignment of an active site lid region in mouse IYD and BluB. Numbers on the left and right indicate numbering for amino acid residues. Conserved residues are indicated in red. (B) superposition of mouse IYD (PDB 3GFD) (dark blue) and BluB (PDB 2ISJ) (purple). Figure on the right demonstrates the lid (αC and αD) and loop regions of mouse IYD (dark blue) and BluB (purple). FMN_{ox} and I-Tyr are presented in yellow and blue (carbon atoms) respectively.

Besides the structural similarity of BluB and IYD, they also exhibit the same one-electron mechanism as evident by consumption of molecular oxygen by BluB and detection of a FMN_{sq} intermediate in the presence of zwitterionic substrate or ligand in IYD.[22, 28, 32, 52] In addition, a side chain of Ser167 in BluB always provides a hydrogen bonding to N5-FMN that assists stabilization of the one electron process. This observation is borne out by similar distance between Ser167 to both N5-FMN_{ox} and N5-FMN_{hq} (3.2 – 3.4 Å) (Figure 5-3).[28] In contrast, this equivalent hydrogen bonding is not formed in IYD unless the zwitterionic substrate is bound.[32] The intact hydrogen bonding to N5-FMN in BluB suggest that the scaffold of BluB may be able to stabilize one-electron chemistry for deiodination of iodophenols. Moreover, the crystal structure of BluB with reduced FMN_{hq} and molecular oxygen also showed that an oxygen is aligned above the reactive site C4a-N5 bond equivalent to alignment of C–I bond of I-Tyr in a structure of IYD (Figure 5-4), which suggests that BluB and IYD have similar reaction sites.[24, 28, 32] Moreover, success in engineering BluB for IYD activity may provide an additional benefit to exploit a known reductase (SsuE) for an easy UV assay for deiodinase activity.

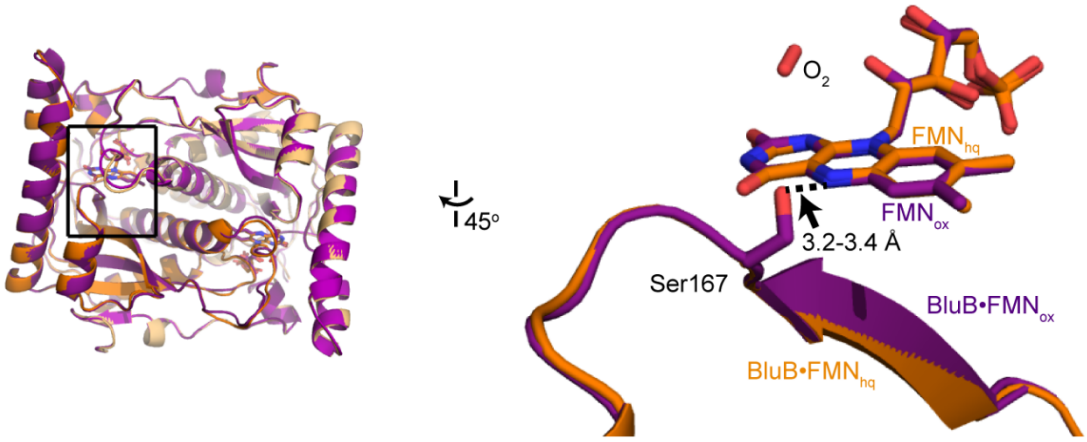

Figure 5-3. Superposition of the structures of FMN_{hq}-bound BluB in the presence of oxygen (PDB 2ISL) (orange) and FMN_{ox}-bound BluB (PDB 2ISJ) (purple). FMN_{hq} and FMN_{ox} are presented in orange and purple (carbon atoms) respectively. Oxygen is indicated in red. This structural comparison demonstrated no conformational change of a Ser167 upon reduction.

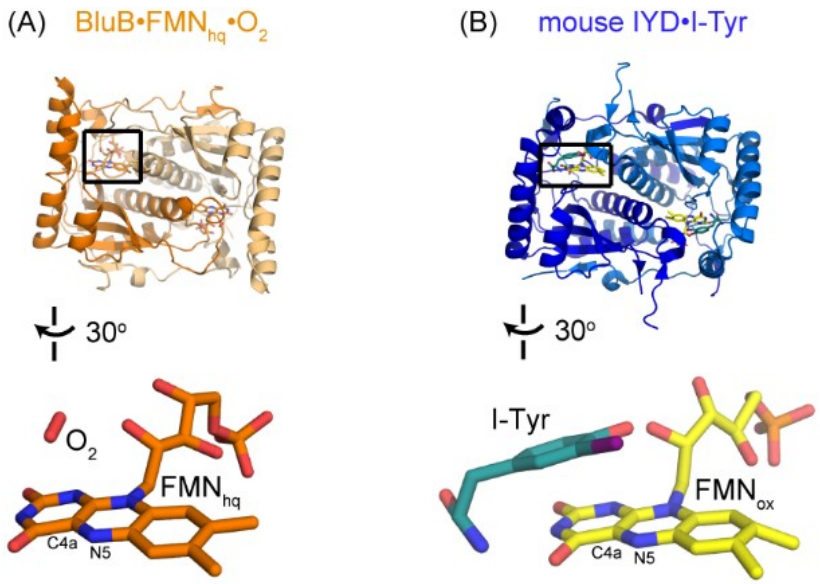

Figure 5-4. Similar alignment in substrates of BluB and IYD over a highly reactive center C4a–N5 bond of FMN. Alignment of the substrates (A) oxygen (red) and (B) C–I bond of I-Tyr (blue) of BluB and IYD above C4a–N5 bond of FMN_{hq} (pink) and FMN_{ox} (blue) respectively.

The second enzyme (Hub enzyme, PDB 3EO8) was selected based on a new classification for the nitro-FMN reductase superfamily. Recently, Babbitt and Copp et al. developed an exhaustive analysis of the entire FMN-dependent nitroreductase (NTR) superfamily using new integrative approaches to examine protein sequence, structure and function for comprehensive functional and

sequence evolutionary relationship.[78] Analysis of a large sequence set resulted in 22 major subgroups including BluB, IYD and a new central Hub topology directly connecting to most of other subgroups (Figure 5-5).[78]

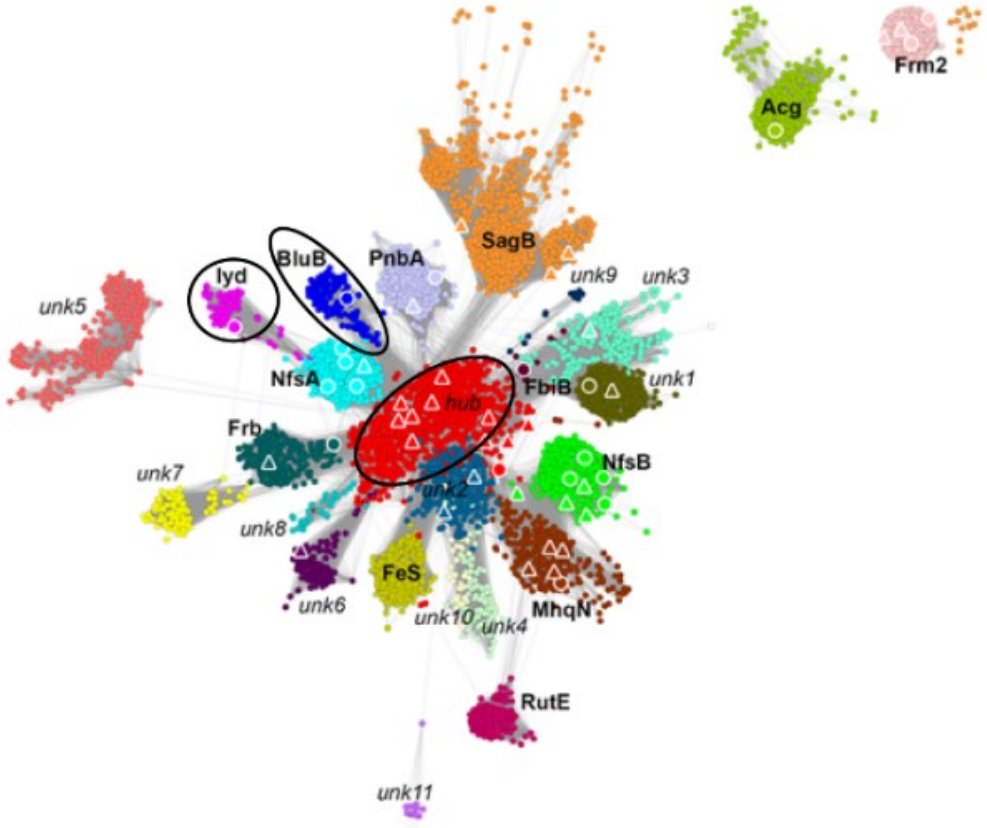

Figure 5-5. Cytoscape[79] demonstrating a representative sequences similarity network (SSN)[80, 81] of the nitroreductase superfamily. A total of 24,270 protein sequences are depicted by 5,337 nodes that represent proteins sharing >60% sequence identity using a stringency threshold value of e^{-18}. Node coloring represents subgroup classification including IYD (magenta), BluB (dark blue) and Hub (red) subgroups. Figure was adapted from Babbitt and Copp et al.[78]

The hub subgroup may represent an ancestral origin for contemporary NTR as most enzymes in the hub subgroup are from bacteria (88 %) and archaea (9 %).[78] Structural analysis revealed most of the hub enzymes display a minimal scaffold that is conserved throughout other NTR. The structures of BluB and IYD also represent this general minimal scaffold with additional insertions (active site lid) required for their specific activities.[24, 28, 78, 82] Analysis from Copp et al. indicated that 3EO8 is a hub protein that exhibits the closest structural similarity to IYD with RMSD of 3.62

Å for 221 Cα atom comparison of PDB: 3EO8 versus 3GFD (Figure 5-6). This enzyme has a crystal structure available (PDB 3EO8) that was annotated as a BluB-like enzyme, however, its actual biochemical function is still unknown. 3EO8 possesses an active site lid that is derived from the same region in its primary structure as that of IYD (Figure 5-7 A), but superposition of the 3EO8 and mouse IYD structures shows their different lid orientations (Figure 5-7 B). Moreover, the loop of 3EO8 is extended more than that of IYD by having two extra helices pointing away from its active site (Figure 5-7).

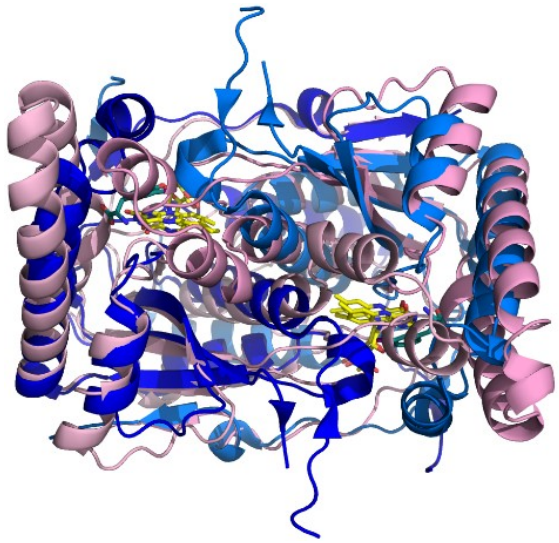

Figure 5-6. Superposition of 3EO8 and IYD structures. Overlay of 3EO8 (PDB 3EO8) (pink) with mouse IYD (PDB 3GFD) (dark blue). FMN_{ox} and I-Tyr are presented in yellow and blue (carbon atoms) respectively.

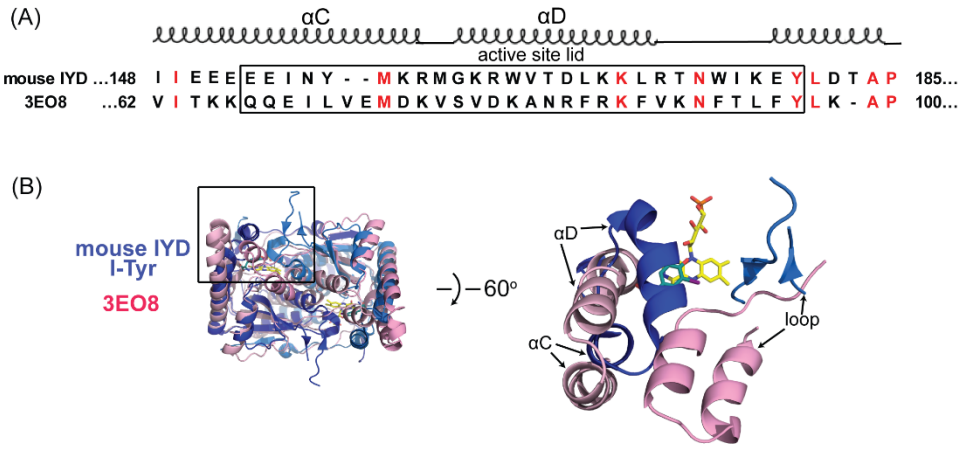

Figure 5-7. Sequence and structural comparison between mouse IYD and 3EO8. (A) amino acid sequence alignment of an active site lid region in mouse IYD and 3EO8. Numbers on the left and right indicate numbering for amino acid residues. Conserved residues are indicated in red. (B) superposition of mouse IYD (PDB 3GFD) (dark blue) and 3EO8 (PDB 3EO8) (pink). Figure on the right demonstrates the lid (αC and αD) and loop regions of mouse IYD (dark blue) and 3EO8 (pink). FMN_{ox} and I-Tyr are presented in yellow and blue (carbon atoms) respectively.

The structure of 3EO8 also suggested the possibility that 3EO8 supports one-electron chemistry since the side chain of Thr163 is likely to provide a hydrogen bonding to N5-FMN similar to that observed in BluB and IYD•I-Tyr (Figure 5-3 and 5-8).[24, 28, 32] Structural analysis of 3EO8 with placement of 2IP (see 5.2.1) demonstrated that the 2IP•3EO8 complex may be stabilized by similar interactions observed in the hhIYD•2IP complex (Figure 5-9). However, the active site of 3EO8 is relatively small compared to IYD suggesting that the wild-type 3EO8 may not be able to accommodate 2IP. Mutations in the active site region of 3EO8 are necessary to allow more access to 2IP into its active site.

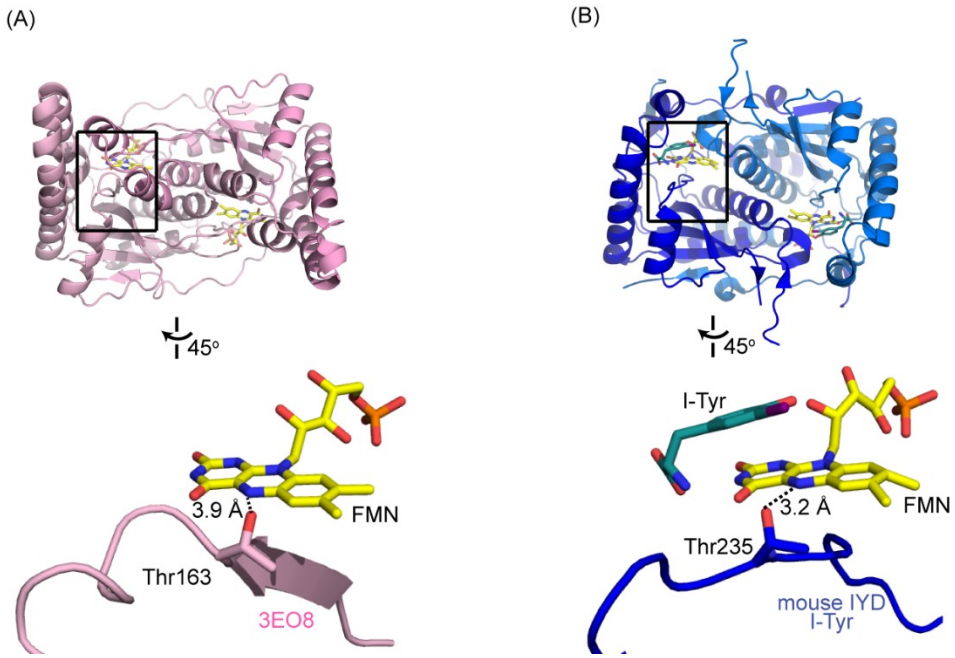

Figure 5-8. Orientation of a side chain of Thr toward N5-FMN in structures of (A) 3EO8 (PDB 3EO8) (pink) and (B) mouse•I-Tyr (PDB 3GFD) (dark blue). FMN and I-Tyr are presented in yellow and blue (carbon atoms) respectively.

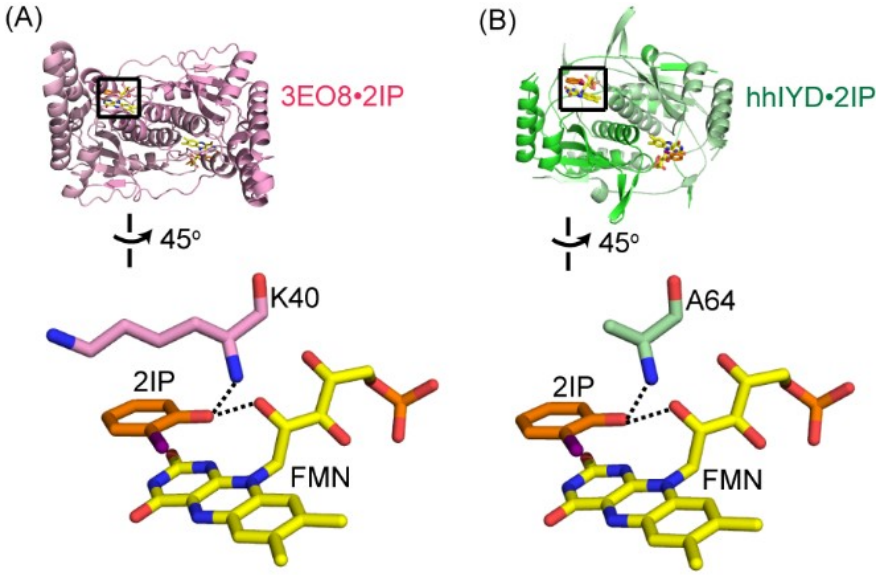

Figure 5-9. Possible interactions stabilizing 2IP•FMN complex in (A) 3EO8 (PDB 3EO8) (pink) and (B) IYD (PDB 3GFD) (dark blue). Dashed lines indicated hydrogen bonding distance within 2.7 – 2.8 Å. FMN and 2IP are presented in yellow and orange (carbon atoms) respectively.

In this chapter, the possibility of introducing deiodinase activity into BluB and 3EO8 is evaluated by screening affinity of 2IP for both wild-type enzymes. Eight individual 3EO8 mutants were generated in the hope of enlarging space in its active site for accommodation of 2IP. Affinity of 2IP for all 3EO8 mutants was also screened to determine the contribution from each mutation to affinity with 2IP.

5.2 Experimental Procedures

5.2.1 Materials

The plasmid encoding BluB gene (pET-11t/BluB–His_8) was kindly provided by Dr. M. E. Taga (UC Berkeley, Berkeley, CA). The enzyme SsuE was kindly provided by Dr. H. R. Ellis (Auburn University, Auburn, AL). DH5α *E. coli.* cells containing pSpeedET-wild-type 3EO8 gene was obtained from the DNASU plasmid respository (Arizona State University, Tempe, AZ). NADH and NADPH were obtained from Sigma-Aldrich. Other materials are listed in Chapter 2 (2.2.1). A 3EO8•2IP complex was generated in Coot[57] by transfering 2IP coordinates from hhIYD•2IP structure (PDB 5KRD) to a structure of 3EO8 (PDB 3EO8).

5.2.2 Site-directed mutagenesis of 3EO8 protein

Site-directed mutagenesis of 3EO8 was performed following the protocol described in Chapter 2 (2.2.4) with the templates and primers listed below. A vector containing wild-type 3EO8 gene (pSpeedET-His_6-3EO8) (Appendix Figure D1) was initially employed as a template for site-directed mutagenesis. Then, additional mutation(s) was sequentially introduced using specified primers provided below. Each resulting vector with correct mutation(s) was then used for the next round of a PCR reaction to introduce the next mutation. A total of 8 individual 3EO8 mutants were created with mutation(s) introduced to the 3EO8 gene in an order indicated in Table 5-1. F88A was generated using a forward primer 5'-GGCTAATAGATTTAGAAAAGCTGTTAAAAATTT-TACAC-3' and its reverse complement. F92A was generated using a forward primer 5'-GAAAA-TTTGTTAAAAATGCTACACTATTTTACTTAAAAGC-3' and its reverse complement. F88A F92A were simultaneously introduced using a forward primer 5'-GGCTAATAGATTTAGAAAA-

GCTGTTAAAAATGCTACACTATTTTAC-3'. Y110H was generated using a forward primer 5'GTTTTTACAAAGGTACATAATCCATCAGG-3' and its reverse complement. S113A was created using a forward primer 5'- TAATCCAGCAGGATATTATGAATTAG-3' and its reverse complement. K40A was introduced to a template using a forward primer 5'- CAGCACCATCAG-GCGCGAATATTCAA-3' and its reverse complement. K40Y was generated using a forward primer 5'-GCACCATCAGGC- TATAATATTCAAAAC-3' and its reverse complement. The last mutation, Y110S was generated using a forward primer 5'-GTTTTTACAAAGGTAAGTAATCC-ATCAGG-3' and its reverse complement. The mutated codons are indicated in red.

Table 5-1. List of 3EO8 mutants

Mutant	Mutation(s)
1	F88A
2	F92A
3	F88A F92A
4	F88A Y110H
5	F88A Y110H S113A
6	F88A Y110H K40A
7	F88A Y110H K40Y
8	F88A Y110S

5.2.3 Expression and purification of BluB and 3EO8 enzymes

BluB was expressed and purified with a method modified from the previously reported procedure.[77] Electrocompetent BL21 *E. coli.* cells were transformed with an expression construct, pET-11t/BluB–His_8. Single colonies were picked and inoculated into a seed culture of LB medium (25 ml) containing ampicillin (50 µg/ml). The culture was incubated with shaking at 37 ºC for ~14 h. The seed culture was then diluted by 50-fold into an expression culture of LB medium (1 L) with ampicillin (50 µg/ml). The expression culture was shaken at 37 ºC until OD_{600} of 0.9-1.0 was reached. Protein expression was performed by addition of IPTG (300 µM) with shaking for ~3 h at 37 ºC. The induced cells were then harvested by centrifugation (5,000 x g for 10 min). Cell pellets were washed with buffer (300 mM NaCl, 50 mM sodium phosphate pH 8.0), frozen in liquid nitrogen and stored at -80 ºC.

For purification, frozen cells were re-suspended in the same buffer and DNaseI (10 μg/ml), phenylmethylsulfonyl fluoride, PMSF (1 mM) and pepstatin A (10 μg/ml) were added. The cells were lyzed using Emulsiflex C3 homogenizer (Avestin) at pressure of 15,000 – 20,000 psi for 3 – 4 passages. Cell lysates were centrifuged at 57,000 x g for 1 h to precipitate cell debris. BluB was purified using Ni-NTA affinity with a flow rate of 1 ml/min. The supernatant (25 – 35 ml) was loaded onto a Ni-NTA column (7 ml) that was pre-equilibrated with the lysis buffer containing 20 mM imidazole (3 column volumes). The loaded sample was washed with lysis buffer containing 20 mM and 60 mM imidazole for 5 column volumes each before protein was eluted with lysis buffer containing 250 mM imidazole. The eluted fractions with > 95% purity were combined and dialysed three times (4 h, 4 h and 12 – 14 h) in dialysis buffer (50 mM NaCl, 50 mM sodium phosphate, pH 8) with 1:100 of protein to buffer volume (10 % glycerol was added into the final dialysis buffer). BluB was then concentrated using an Amicon ultra centrifugal filter unit with a 10 kDa cut-off. The final concentration of BluB was determined by measuring A_{280} using $\varepsilon_{280} = 44{,}710$ $M^{-1}cm^{-1}$ as determined by ExPASy ProtParam.[34]

3EO8 protein (Appendix Figure D2) was expressed and purified following the procedure used for IYD described in Chapter 2 (2.2.5). Only induction conditions were modified by increasing IPTG concentration from 20 μM to 40 μM and increasing the induction temperature from 16 ^{o}C to 20 ^{o}C but the same induction time was used (12-16 h). Purified protein was concentrated and its concentration was determined following the procedure described in Chapter 2 (2.2.2).

5.2.4 BluB activity assay

Native activity of BluB was tested by monitoring FMN depletion (445 nm) in the presence of a FMN reductase enzyme (SsuE) and NADPH as previously described.[77]

5.2.5 Binding affinity of BluB for FMN and 2IP

Determination of K_d values of BluB for FMN and 2IP was performed using an isothermal titration calorimetry (ITC) by measuring thermal energy associated with ligand binding. Affinity assays of BluB for FMN were carried out following a method previously described.[28] In brief, BluB

solution (25 μM, 1.5 ml) was loaded into a sample cell while degassed FMN (500 μM) was loaded onto an injection syringe. An apo-BluB was then titrated with 10 μl of FMN for 25 injections. The experiment was performed in buffer (10 mM NaCl, 10 mM Tris pH 8.0) at 23 ºC using a Microcal MCS ITC at Integrated Imaging Center (IIC), Johns Hopkins, Homewood campus. 5 min-interval was allowed between each injection for heat generated to re-equilibrate. Under similar conditions, determination of BluB affinity for 2IP was performed by titration of 10 μl of degassed 2IP (3 mM) for 55 injections into BluB-FMN solution (1.5 ml) containing BluB (70 μM) and FMN (140 μM). The data were fit using Origin ITC software (V. 5.0, Microcal Software Inc.) and the result was modeled to a single binding site per monomer to determine the K_d value.

5.2.6 NAD(P)H reduction assays

Reduction of FMN_{ox} bound to 3EO8 by NAD(P)H was determined by monitoring reduction of FMN_{ox}-bound 3EO8 (λ = 445 nm) in the alternative presence of NADH or NADPH. The protocol was modified from that previously described.[77] The UV spectrum of buffer (300 mM NaCl, 0.5 mM TCEP, 10 % glycerol, 50 mM sodium phosphate pH 7.4) containing NAD(P)H (10 mM) and 3EO8 (20 μM) was monitored over 30 min using a Hewlett-Packard 8453 spectrophotometer.

5.2.7 Binding affinity determination of 3EO8 protein for 2IP and 2FP

Binding affinity of 3EO8 for 2IP and 2FP was determined by the ability of the ligand to quench the fluorescence of FMN_{ox} in the active site of the protein (λ_{ex} = 450 nm and λ_{em} = 529 nm). Fluorescence binding assays were performed following a procedure described in Chapter 2 (2.2.8).

5.2.8 Oxygen sensitivity assays

Oxygen sensitivity of 3EO8 protein was determined by re-oxidation of reduced FMN_{hq} bound to 3EO8 to generate FMN_{ox} (λ = 445 nm) upon reacting with molecular oxygen. Buffer (300 mM NaCl, 0.5 mM TCEP, 10 % glycerol, 50 mM sodium phosphate pH 7.4) containing 3EO8 protein (20 μM) was purged with Ar for 30 min and a head space was then purged for an addition 20 min to remove molecular oxygen. Subsequently, stoichiometric amount of dithionite in 5 % $NaHCO_3$ solution was gradually added to this protein solution until FMN_{ox} was fully reduced (decrease in

A_{445}). The FMN_{hq} bound protein solution was then exposed to O_2 and mixed immediately followed by monitoring an increase in absorbance of FMN_{ox} (λ = 445 nm) every minute over 10 min. The solution was mixed again after every 5 min during the UV measurement.

5.3 Results

5.3.1 Expression and purification of BluB and 3EO8

BluB and all 3EO8 proteins were purified to homogeneity (Appendix Figure D3 – D4). Soluble BluB was expressed without a protein fusion in an *apo* form in a relatively high yield of 25 mg/L. 3EO8 wild-type and its 8 mutants were also expressed without a SUMO fusion. FMN occupancy of all 3EO8 proteins was relatively consistent between 60 – 73 % except for mutant 8, which had a FMN occupancy of only ~48 %. Under the same expression conditions, most 3EO8 proteins were obtained with in good yield of 13 – 17 mg/L except for a 3EO8 wild-type, mutant 2 and 4, which provided relatively low protein yields (5 – 8 mg/L).

5.3.2 Studies of a BluB enzyme

5.3.2.1 BluB activity

Native activity of BluB was first tested to ensure that the enzyme was active for further studies. Activity of BluB was determined by monitoring deletion of FMN_{ox} (λ = 445 nm). The expected FMN depletion was confirmed when BluB is present (Figure 5-10).

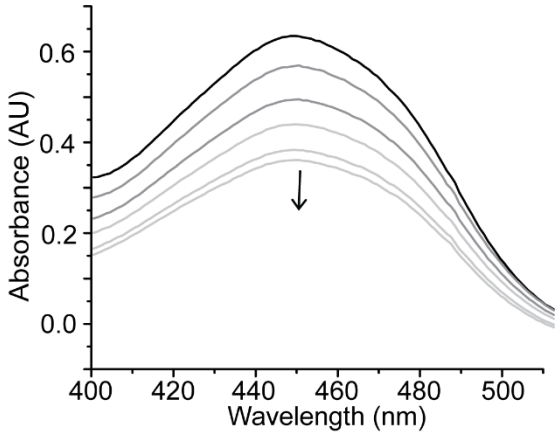

Figure 5-10. FMN depletion by BluB. BluB activity assay was performed as previously described[77] at room temperature. Reaction contained 50 μM FMN, 300 μM NADPH, 50 μM BluB, and 200 nM SsuE in 20 mM Tris–HCl, pH 8. Depletion of FMN was monitored over 10 min after the reaction was initiated by addition of SsuE reductase. Gradient of the spectrum (black to light gray) indicate decrease in maximum absorbance of FMN_{ox} at 445 nm.

5.3.2.1 Affinity of FMN and 2IP for BluB

Affinity of FMN and 2IP for BluB was determined by measuring thermal energy associated with ligand binding. Determination of FMN affinity to BluB was first performed to verify a protocol for the ITC experiment. The resulting K_d value and other thermodynamic parameters of FMN for BluB are in the same order of magnitude with those previously reported[28] (Table 5-2, Appendix Figure D5-A) indicating a proper protocol for affinity was determined. Then, titration of 2IP into the FMN-bound BluB solution was monitored to assess the ability of BluB to bind 2IP. In contrast to FMN, binding affinity of 2IP for BluB was not observed as exhibited by scattered plots of energy per injection versus molar ratio of 2IP (Appendix Figure D5-B).

Table 5-2. K_d value and thermodynamic parameters of BluB for FMN

Enzyme	K_d [a] (μM)	ΔH^a (kcal/mol)	ΔS^a (cal/mol K)
BluB	3.6 (1.6)	-16.2 (-15.0)	-29.6 (-23.6)

[a]Determined from the data of Appendix Figure D5-A. Parameters derived from a single experiment. Values indicated in parenthesis are previously reported.[28]

5.3.3 Studies of 3EO8 proteins

5.3.3.1 NAD(P)H-dependent FMN reduction of 3EO8

Reduction of FMN-bound 3EO8 (WT) in the presence of NAP(P)H was performed to determine if the hub 3EO8 protein is capable of catalyzing NAD(P)H-dependent FMN reduction. The result confirmed that 3EO8 (WT) lacks this ability as no depletion of FMN_{ox}-bound 3EO8 (WT) was observed when NAD(P)H was present (Figure 5-11).

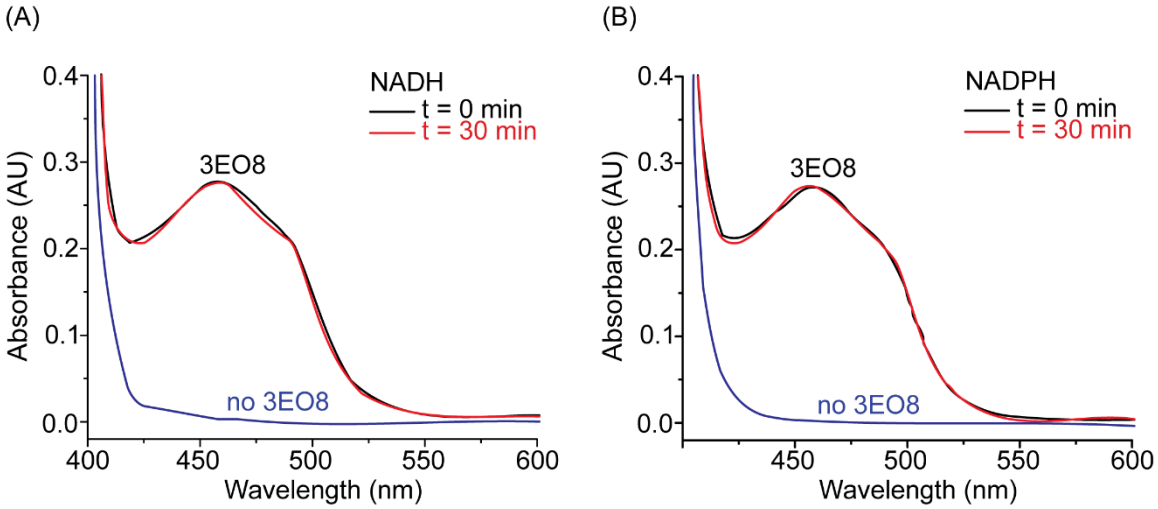

Figure 5-11. UV spectra during the reduction of 3EO8-FMN_{ox} in the presence of NAD(P)H. No depletion of 3EO8-FMN_{ox} by (A) NADH and (B) NADPH was observed at λ = 445 nm over 30 min. Reactions containing buffer (300 mM NaCl, 0.5 mM TCEP, 10 % glycerol, 50 mM sodium phosphate pH 7.4), 10 mM NAD(P)H and 20 µM 3EO8 (WT) were performed at room temperature.

5.3.3.2 Affinity to 2-iodophenol (2IP) and 2-fluorophenol (2FP) for the wild-type 3EO8 and its mutants

Affinity assays of 2IP and 2FP for the wild-type 3EO8 and its mutants were carried out to determine if affinity of 2IP and 2FP for the engineered 3EO8 proteins with higher active site accessibility was improved compared to that of the wild-type. Affinity was determined by monitoring quenching of the fluorescence of FMN_{ox} bound to the proteins upon coordination of 2IP. Since incomplete fluorescence quenching due to the solubility limit of 2IP did not allow determination of the K_d values, binding affinity of 2IP for each 3EO8 protein was evaluated by % fluorescence quenching at ~ 10 mM 2IP.

The results demonstrated that wild-type 3EO8 cannot bind 2IP (Figure 5-12). The increase in fluorescence emission at high concentration of 2IP (≥ 5 mM) is likely explained by the release of a bound FMN into the protein solution. The release of FMN is potentially caused by instability of the protein at high concentration of 2IP which may lead to partial protein unfolding. Affinity studies of the mutants with 2IP exhibited that only mutant 4, 5 and 8 display slightly decreases in F/F_0 compared to that of the wild-type (~ 10 – 20 % fluorescence quenching at ~10 mM 2IP) while other 3EO8 mutants could not improve affinity to 2IP as evident from no fluorescence (Figure 5-12).

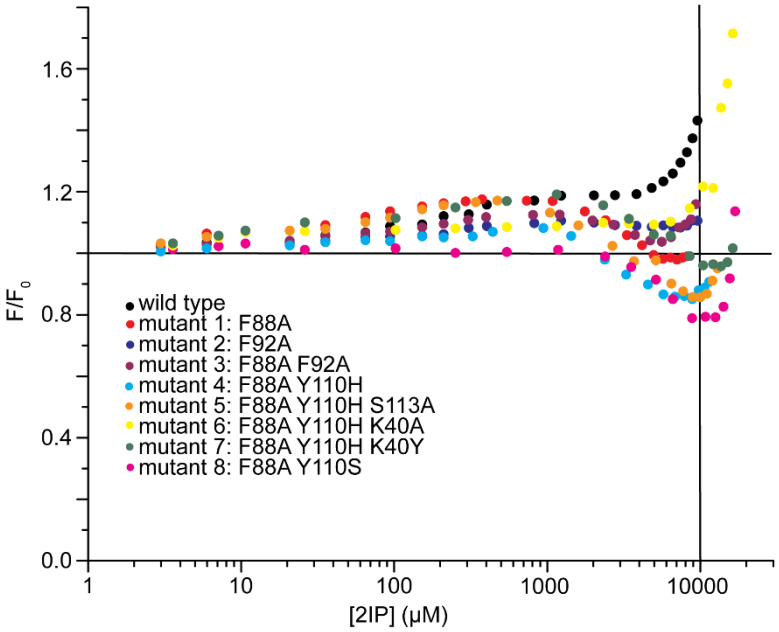

Figure 5-12. Quenching of FMN_{ox} fluorescence in the presence of 2IP to wild-type 3EO8 and 8 indicated mutants at 25 ºC. 3EO8 (5 µM) in 100 mM potassium phosphate, pH 7.4 were stirred at 25 ºC for 30 min prior to addition of 2IP. Black solid lines mark at $F/F_0 = 1$ and [2IP] = 10 mM for easy comparison of fluorescence intensity among different proteins.

Affinity of 2FP for the wild-type 3EO8 and mutants 1-3 was determined to guide the next mutation for 3EO8 enzyme. The results showed that % fluorescence quenching at 10 mM 2FP is similar to that of 2IP at the same concentration but significant fluorescence quenching was observed for the wild-type and all 3 mutants at high concentration of 2FP (~40 – 60 % quenching at ~57 mM 2FP) (Figure 5-13). As expected, the binding curves of 2FP to 3EO8 proteins were more

experimentally distinguishable than that of 2IP. The results showed that mutant 1 gained the most fluorescence quenching 60% at ~57 mM 2FP while the wild-type showed ~40% quenching.

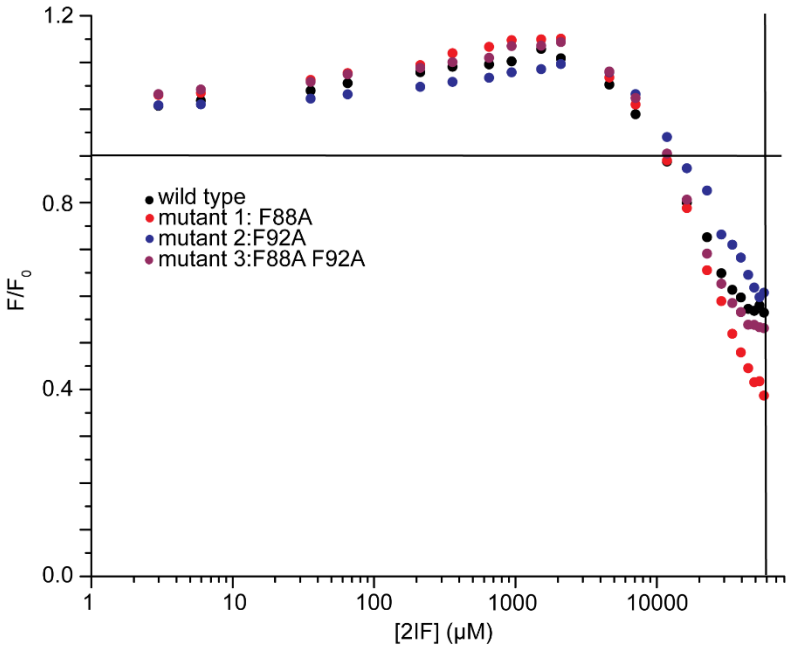

Figure 5-13. Quenching of FMN_{ox} fluorescence upon binding of 2FP to wild-type 3EO8 and 3 indicated mutants at 25 ºC. 3EO8 (5 μM) in 100 mM potassium phosphate, pH 7.4 were stirred at 25 ºC for 30 min prior to addition of 2FP. Black solid lines mark at $F/F_0 = 1$ and [2FP] = ~57 mM for easy comparison of fluorescence intensity among different proteins.

5.3.3.3 Oxygen sensitivity of 3EO8

Oxygen sensitivity of the wild-type and 3EO8 mutant 6 (F88A Y110H K40A) with the greatest active site accessibility was determined by measuring re-oxidation of FMN_{hq} after mixing the reduced protein with molecular oxygen. The results showed the increase of FMN_{ox} over time (6 min) after the reduced enzymes were mixed with O_2. This experiment indicated that 3EO8 is an oxygen sensitive enzyme.

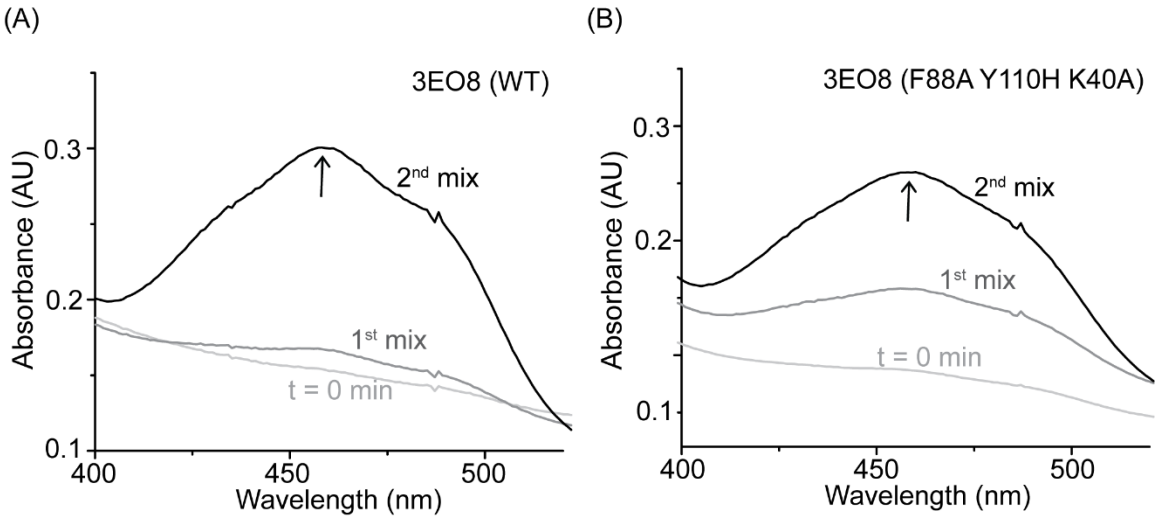

Figure 5-14. Oxidation of FMN_{hq}-bound 3EO8 protein by oxygen. Oxidation of (A) FMN_{hq}-bound 3EO8 (WT) and (B) FMN_{hq}-bound 3EO8 mutant 6 (F88A Y110H K40A) in the presence of oxygen. Buffer (300 mM NaCl, 0.5 mM TCEP, 10 % glycerol, 50 mM sodium phosphate pH 7.4) containing 20 μM 3EO8 was purged with Ar to remove O_2 prior to addition of ~ 20 μM dithionite. The solution was monitored at λ = 445 nm to observe increase of FMN_{ox}. Spectrum at time = 0 min (light gray) was recorded prior to mixing with O_2. The solution was then mixed immediately after being exposed to O_2 and the spectra were recorded continuously for every 1 min. Mixing was introduced every 5 min during the measurement. The selected spectra represent the data after the 1st mix (gray) and the 2nd mix (black) which demonstrates fully oxidized FMN_{ox}.

5.4 Discussion

Binding studies revealed that a native BluB did not bind 2IP in its active site. The lack of binding of 2IP to BluB is consistent with its crystal structure exhibiting a loop of BluB that is more buried into its active site resulting in a small binding pocket to exclude bulky substrates larger than molecular oxygen (Figure 5-2 B). A wild-type 3EO8 also exhibited no detectable binding to 2IP as expected for its inaccessible and small active site (Figure 5-15 A-B). Hence, 8 3EO8 mutants were generated to either open its active site entrance or enlarge the active site volume to increase its possibility to bind 2IP (Figure 5-15 and 5-16). Mutant 1 (F88A) and 2 (F92A) modify the entrance of the active site to allow more access to 2IP (Figure 5-15 C-F). However, very minimal fluorescence quenching (~1-2 %) of mutant 1 and no detectable quenching of mutant 2 was observed at the end of 2IP titration (Figure 5-12). A combination of F88A and F92A still did not improve affinity with 2IP. Binding studies of 2IP for mutants 1 – 3 were not experimentally

distinguishable and were still limited by solubility of 2IP, further affinity assays with 2-fluorophenol (2FP) for these three mutants were performed. 2FP was selected as its higher solubility than 2IP that allowed us to determine affinity of the ligand at higher concentrations (~57 mM) compared to 2IP (~10 mM). The smaller fluoro atom also occupies less space than an iodo atom, hence 2FP is more likely to incorporate the active site of 3EO8 proteins better than 2IP. The results revealed that mutant 1 exhibited the greatest fluorescence quenching (62 %) among the three mutants (Figure 5-13). Hence, mutant 1 was selected for the next round of mutation.

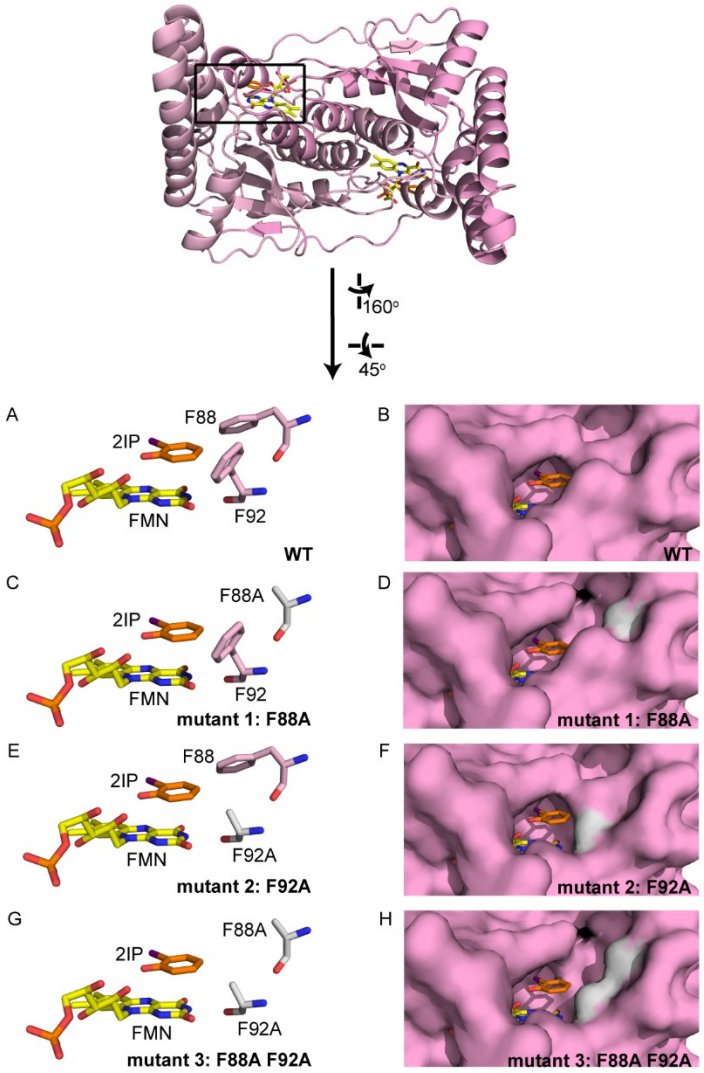

Figure 5-15. Active site region of 3EO8 protein with a placement of 2IP. Active site region of (A-B) 3EO8 (WT), (C-D) 3EO8 mutant 1 (F88A), (E-F) 3EO8 mutant 2 (F92A) and (G-H) 3EO8 mutant 3 (F88A F92A). The active sites are shown in stick representation to exhibit mutation site(s) (left panel) and surface representation to exhibit active site accessibility (right panel). The native amino acid residues are shown in pink and the mutated residues are presented in gray (carbon atoms). FMN and 2IP are presented in yellow and orange respectively.

Y110 was selected as the next mutation site because it is located nearby the iodo atom of 2IP (Figure 5-16). Introduction of Y110H was thought to provide sufficient space for an iodo atom of 2IP (4.2 Å) (Figure 5-16 A). Histidine was selected to maintain a possible halogen bonding to the iodo atom of 2IP as possibly provided by Y110 in the native protein (2.8 Å) (Figure 5-16 A). Binding affinity of mutant 4 to 2IP showed about ~10 % quenching (at 2IP ~ 10 mM) indicating a

little increase in affinity with 2IP compared to the wild-type. Another mutation site (S113A) close to C–I bond was also generated in combination with F88A Y110H (mutant 5: F88A Y110H S113A) (Figure 5-16 B), but a similar lack of fluorescence quenching to that of mutant 4 was observed. Two additional mutants were generated to allow more access for 2IP to enter the active site (mutant 6: F88A Y110H K40A) or to introduce possible π-stacking interaction to potentially increase affinity with 2IP (mutant 7: F88A Y110H K40Y) (5-16 C-D). However, neither of these two mutants could increase the affinity for 2IP since no fluorescence quenching was observed at the end of the titration of (~10 mM 2IP) (Figure 5-12). As introduction of Y110H provided significant fluorescence quenching upon addition of 2IP, this mutation site was re-considered for the introduction of a small amino acid to allow more space near the C–I bond of 2IP.

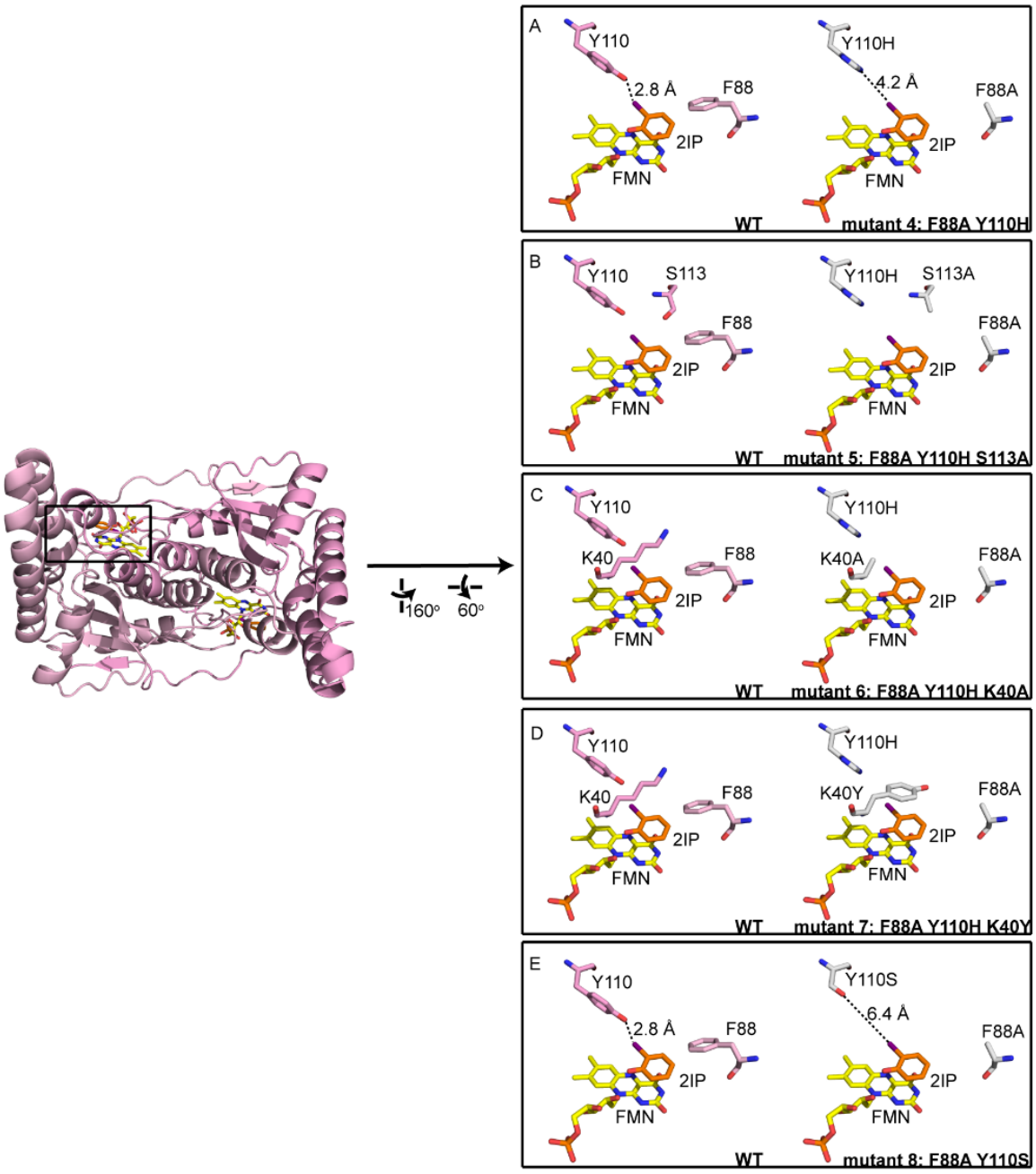

Figure 5-16. Active site region of 3EO8 with the placement of 2IP. Stick illustration of active site region indicating mutation sites of (A) mutant 4 (F88A Y110H), (B) mutant 5 (F88A Y110H S113A), (C) mutant 6 (F88A Y110H K40A), (D) mutant 7 (F88A Y110H K40Y) and (D) mutant 8 (F88A Y110S). The native amino acid residues are shown in pink and the mutated residues are presented in gray (carbon atoms). FMN and 2IP are presented in yellow and orange respectively.

Initially, Y110H was thought to provide enough space for an iodo atom of 2IP as the nitrogen atom of His is quite distant from the iodo atom of 2IP (4.2 Å) (Figure 5-16 A). However, its affinity

for 2IP was only increased by 10 % at ~10 mM 2IP. Hence, another mutation with a further decrease in size (Y110S) was introduced into the 3EO8 F88A gene to generate mutant 8 (F88A Y110S) (Figure 5-16 E). Binding assays of mutant 8 with 2IP showed more fluorescence quenching (~20% at ~10 mM 2IP) compared to F88A Y110H. However, no further attempts to mutate 3EO8 were pursued since all potential residues near the predicted position of 2IP were already mutated to smaller amino acids compared to the wild-type, but only ~20% fluorescence quenching was observed at ~10 mM 2IP. This finding indicated that the modified active sites of 3EO8 proteins cannot efficiently accommodate 2IP. Perhaps, thermodynamically favorable interactions were not established in the mutants. Specific orientations of the active site lid and loop may be required to accommodate 2IP. In contrast to IYD, the lid and loop of 3EO8 protrude away from the modelled position of 2IP and would not likely cover 2IP (Figure 5-7 B). Good affinity of 2IP to hhIYD (K_d = 67 μM) may in part be mediated by incorporation of the lid and loop of hhIYD. The lid of hhIYD may be partially formed upon binding of 2IP and cover the 2IP-FMN complex and therefore maintains 2IP in the active site. Partial lid formation can be determined by performing a limited proteolysis experiment to evaluate the dynamics of the protein structure.

Binding studies implied that the active site of 3EO8 was possibly not designed for any substrates as large as 2IP. However, this enzyme seems to share two common features with IYD and BluB. Inability of 3EO8 to catalyze NAD(P)H-dependent FMN reduction suggested that 3EO8 may require a specific reductase to transfer electrons from NAD(P)H to FMN_{ox} similar to that needed for BluB and IYD. A reductase, SsuE, was already identified for BluB while that of IYD is still unknown.[15, 28, 83] Hence, dithionite has been used as an alternative reductant in most IYD analyses. The second BluB-, IYD- like feature of 3EO8 is the likely use of one-electron chemistry for catalysis as it is sensitive to molecular oxygen (Figure 5-14). This condition is consistent with hydrogen bonding to N5-FMN that is potentially established by a side chain Thr163 of 3EO8 (Figure 5-8 A). Recovery of FMN_{ox} bound to 3EO8 in the presence of oxygen also confirmed that 3EO8 does not have a BluB-like activity as annotated in the PDB database.

5.5 Summary

Binding experiments indicated that BluB and 3EO8 do not have affinity for 2IP. Eight individual 3EO8 mutants did not increase affinity with 2IP as no more than 20 % fluorescence quenching was observed. Mutant 5 (3EO8 F88A Y110S) appeared to have the best affinity with 2IP with ~20 % fluorescence quenching after titration of 2IP (~10 mM). Binding of 2IP may in part require proper orientation of the lid and loop as that appears in IYD. Sufficient space for 2IP alone may not be enough to improve the affinity for 2IP as this enzyme exhibits different orientations of the lid and loop from those of IYD. However, 3EO8 likely drives one-electron process as its FMN_{hq} is able to be re-oxidized to FMN_{ox} in the presence of O_2 indicating this enzyme is oxygen sentitive. Recovery of FMN_{ox} also indicated that activity of 3EO8 is different from BluB which fragments the FMN_{hq} for a synthesis of the lower ligand of vitamin B_{12}.[28] Similar to BluB and IYD, 3EO8 may require reductase for FMN reduction as the native 3EO8-bound FMN cannot be directly reduced by NAD(P)H.

Chapter 6: Conclusions

The selected IYDs from an eukaryote (human IYD) and two prokaryotes (hhIYD and pfuIYD) demonstrated different binding selectivity but surprisingly similar catalytic specificity. Both hhIYD and pfuIYD share more binding promiscuity with 2IP compared to human IYD as indicated by their K_d values (K_d = 67 μM (hhIYD), 79 μM (pfuIYD) and 1,410 μM (human IYD)). The reasons for the different affinity of the three IYDs for 2IP are still unclear. However, significant differences in the affinity of hhIYD and human IYD for 2IP may be apparent from their crystal structures. Tight affinity of hhIYD for 2IP may be explained the presence of a pre-organized loop near the active site of hhIYD, which is not maintained in human IYD (Appendix Figure B2). However, high affinity of hhIYD and pfuIYD for 2IP does not increase their catalytic efficiency as shown by the k_{cat}/K_m values of 2IP and I-Tyr that remain within an order of magnitude of those of human IYD. Catalysis of all three IYDs is still very selective for iodotyrosines (I-Tyr and I_2-Tyr) as evident by k_{cat}/K_m values for deiodination of iodotyrosines that are 4 – 5 orders of magnitude greater than those of 2IP.

hhIYD exhibits the least difference in affinity for I-Tyr and 2IP as shown by the only 8-fold difference in their K_d values. Initially, the zwitterion of I-Tyr was not thought to be necessary for binding or even for catalysis of hhIYD. Further binding studies of hhIYD with 2IP derivatives revealed that the phenolate anion of the ligand is key for affinity to hhIYD. More acidic phenolic protons lead to stronger affinity with hhIYD. However, high affinity for the active site does not ensure efficient catalysis as demonstrated by the lack of turnover of 2IPCN despite its affinity with hhIYD that rivals an equivalent affinity of I-Tyr. Tight binding to the active site is therefore not the only determinant for IYD catalysis.

Slow turnover of 2IP by hhIYD can be explained by crystallographic and redox studies. Similar to human IYD, the zwitterion of halotyrosines is also essential for hhIYD to stabilize one electron chemistry, which is key for efficient deiodination. Crystal structures of hhIYD demonstrated that coordination of I-Tyr can induce formation of an active site lid. The co-crystal of hhIYD•I-Tyr

does not show hydrogen bonding from a side chain of Thr173 to N5-FMN, which potentially stabilizes a radical intermediate FMN_{sq}. However, a switch from two- to one-electron chemistry was evident by detection of FMN_{sq} during reduction of hhIYD in the presence of a substrate analog, F-Tyr.

A co-crystal structure of hhIYD•2IP shows that 2IP aligns similar to the conformation of the aromatic ring of I-Tyr. However, 2IP is not able to trigger formation of the active site lid of hhIYD. It also lacks the ability to stabilize accumulation of FMN_{sq} during reduction of hhIYD in the presence of 2IP. These results indicated that π-stacking interaction between 2IP and FMN together with close proximity of the reaction sites (C–I bond of 2IP and C4a–N5 FMN) are not sufficient for effective IYD catalysis. These observations explain the slow catalysis of hhIYD for 2IP despite its decent affinity.

Engineering of IYD was performed to increase the k_{cat}/K_m values for catalysis of iodophenols for bioremediation. Phyre2 provided a good model of hhIYD for engineering studies as indicated by superimposable structures of the predicted hhIYD in the absence of ligand and a crystal structure of hhIYD•I-Tyr (RMSD of 1.374 Å for 367 Cα atom comparison of the Phyre2 model and PDB: 5KO8). The selected residues for engineering would still be the best to change if the actual crystal structure were used for an engineering design as those residues of the hhIYD model are aligned with those of the crystal structure. However, modifications of hhIYD to increase affinity for 2IP (mutant A: A64F L107A), to stabilize the C-terminus of αC lid region (mutant B: S94D N96R S175H), and to introduce an attractive interaction between the active site lid and the carboxylate of 2IPCOOH (mutant C: E91R) did not increase the catalytic efficiency for deiodination of iodophenols as evident by decrease in k_{cat}/K_m values for 2IP and 2IPCOOH by 3 – 16 fold compared to those of the wild-type. However, replacement of a repulsive interaction with 2IPCOOH by an attractive interaction (E91R) did significantly decrease the K_m value by ~4 fold compared to that of the wild-type. The previous studies of Drosophila IYD showed in contrast that mutation of this

equivalent (E154Q) significantly increased the K_m for deiodination of I_2-Tyr which is likely because a favorable electrostatic interaction between Glu and the zwitterion of I_2-Tyr was removed. Site-directed mutagenesis of hhIYD and Drosophila IYD both revealed that this substitution of Glu may help to optimize the K_m value for deiodination of different non-physiological substrates. Hence, a site-saturation mutagenesis at this residue to fine-tune the K_m values for deiodination of iodophenols is recommended for future study.

The hub enzyme with most structural similarity to IYD, 3EO8, was also selected to engineer for deiodination of iodophenols. Modifications were introduced to increase the volume of the active site, which was thought to be too small to accommodate of 2IP. However, none of the mutants exhibited a significant increase in affinity for 2IP compared to the wild-type. Differences in the orientation of the lid and loop of 3EO8 versus those of IYD (Figure 5-7) may explain the inability to accommodate 2IP despite the increased active site volume. The lid and loop of 3EO8 do not cover its active site in contrast to those of hhIYD. This observation suggested that placement of the lid and loop of hhIYD may be suitable for 2IP binding and also supported that its pre-organized loop may contribute to the greater affinity for 2IP compared to that of human IYD in which the equivalent loop is disordered.

Initial engineering studies of IYD and 3EO8 suggested that optimizing deiodinase activity for catalysis of the non-native substrates is not straightforward. Efficient IYD activity involves structural changes upon binding of the zwitterionic substrate to maintain its high substrate specificity. A computational design is a powerful tool for engineering catalysis as it can identify novel amino acid sequences and can predict various mutations that may induce cooperative for substrate binding and/or catalysis. An alternative directed evolution approach could explore huge sequence space in fine-tuning IYD catalysis for iodophenols. However, a fast and sensitive screening system for selection is necessary to test large numbers of the mutants. Identification of a specific reductase for reduction of IYD-bound FMN would enable a fast screening for IYD activity by monitoring the absorbance for depletion of NAD(P)H. Currently, finding good candidates for

engineering is also a key to success. Development of the sequence similarity network (SSN) is also a powerful tool to search for useful candidates for engineering as SSN allows analysis of huge native sequence assemblies that have been discovered to date. This method enhances the possibility to identify IYD variants with different catalytic specificity. For example, the nitro-FMN reductase superfamily was analyzed by Dr. Akiva (Dr. Babbit Lab, University of California at San Francisco) to generate the SSN. A couple of IYD homologs were selected from proteins that belong to a cluster of IYD enzymes by Dr. Janine Copp (University of British Columbia, Vancouver) and one of the selected homologs, an IYD from *Thermotoga neopolitiana* (tnIYD), was studied for deiodination rates of 2IP at 60 ºC by Jamie Alley. The results showed that tnIYD exhibited ~ 5-fold higher k_{cat} and ~2.5 fold higher k_{cat}/K_m compared to those of pfuIYD at the same temperature. These results suggested that tnIYD is another good candidate to improve deiodination rates for iodophenols. These various approaches demonstrate their own unique set of advantages and disadvantages for engineering studies. Integration of multiple approaches should increase our chances to enhance a deiodinase activity for halophenols.

Appendices

Appendix A: Supporting information for Chapter 2

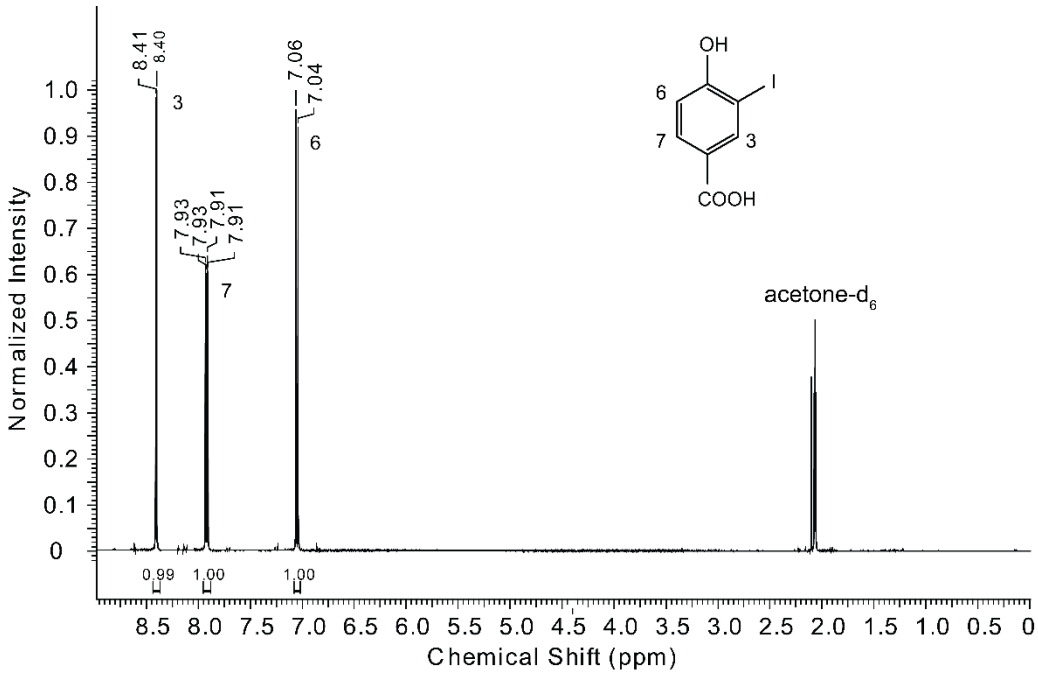

Figure A1. ^{1}H NMR (400 MHz) of 2IPCOOH in acetone-d_6.

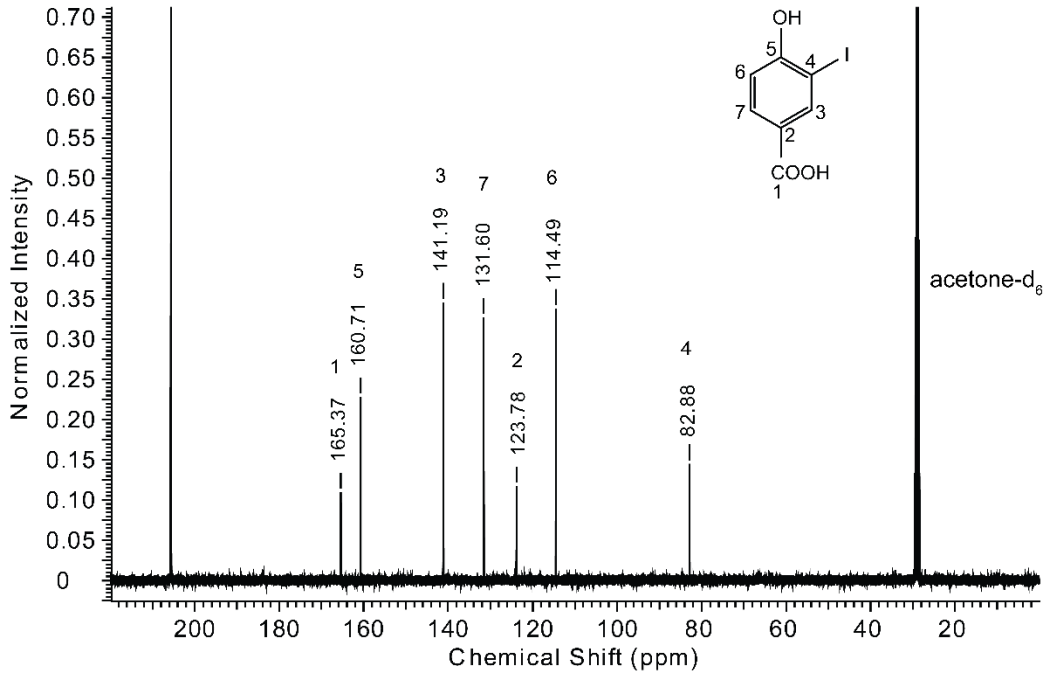

Figure A2. ^{13}C NMR (101 MHz) of 2IPCOOH in acetone-d_6.

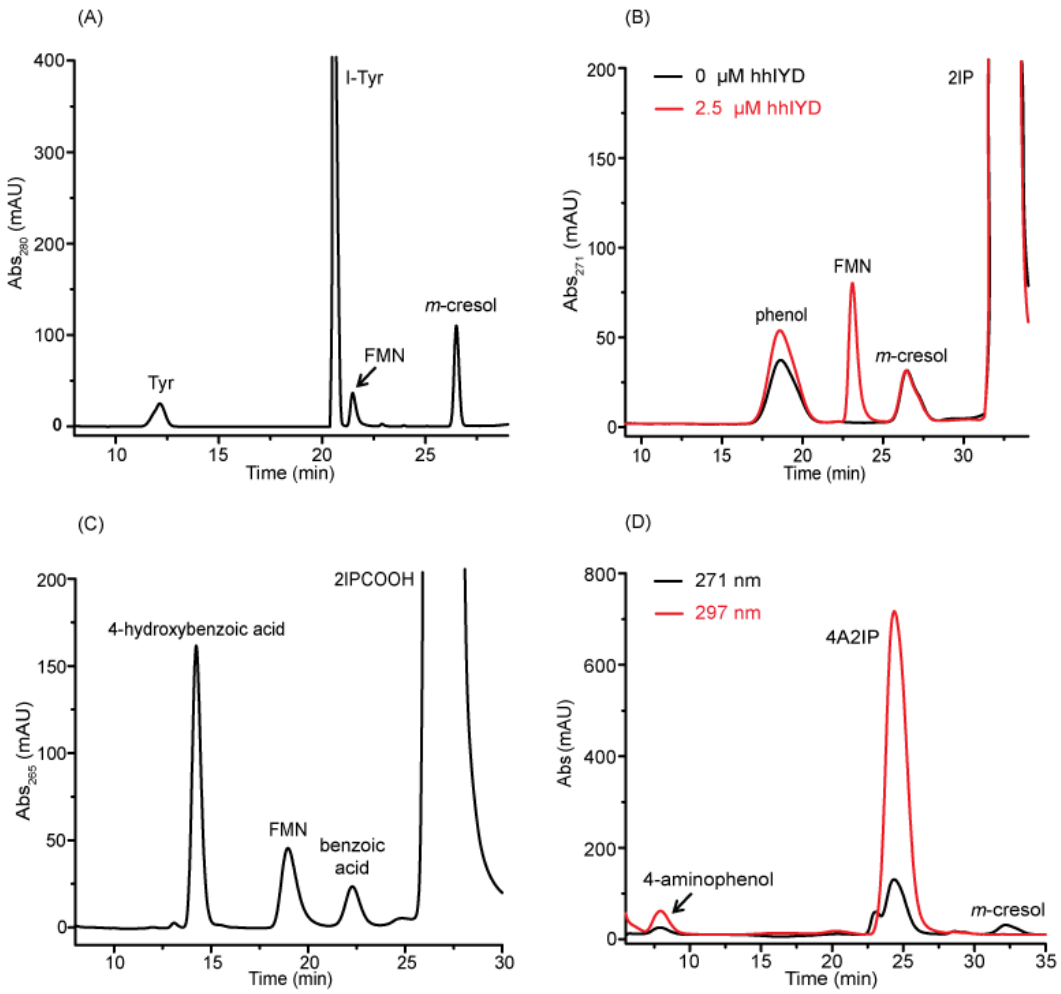

Figure A3. Standards used to identify components of deiodination reactions by IYD. The following mixtures were incubated under the same condition containing 111 mM potassium phosphate pH 7.4 (900 µl) with addition of 5% dithionite in 5% sodium bicarbonate (100 µl) to a final volume of 1 ml. The mixtures were then incubated at 25 °C for an indicated period of time followed by quenching with 88% formic acid (50 µl) except for (D) that was directly injected onto HPLC without addition of 88% formic acid to maintain pH of the mixture similar to that of elution buffer. Each mixture was subject to reverse phase HPLC using a flow rate 1 ml/min, solvent A: 0.44% aq. formic acid and solvent B: 0.44% formic acid in acetonitrile according to indicated gradients (A) 100 µM I-Tyr, 1 µM hhIYD, 30 µM *m*-cresol, incubated for 15 mins, gradient: 0-5% B for 10 min, 5-60% B for 15 min and a wash (60-95% B for 5 min and 95% B for 10 min); (B) 5 mM 2IP, 0 and 2.5 µM hhIYD (black and red lines), 30 mM *m*-cresol, incubated for 2 hours, gradient: 0-7% B for 10 min, 7-35% B for 15 min and a wash (35-95% B for 5 min and 95% B for 10 min); (C) 1 mM 2IPCOOH, 2.5 µM hhIYD, 30 µM benzoic acid, incubated for 3 hours, gradient: 0-10% B for 5 min, 10-30% B for 25 min and a wash (35-95% B for 5 min and 95% B for 10 min). 2IP has a phenol product contaminated (1.2 %). Contributions to product signals were subtracted prior to analysis.; (D) 0.8 mM 4A2IP, 2 µM hhIYD, 30 µM *m*-cresol, incubated for 2 hours, solvent A: 10 mM ammonium formate, pH 6.8 and solvent B: acetonitrile, gradient: 0% B for 10 min, 0-30% B for 20 min and a wash (30-95% B for 5 min and 95% B for 10 min). The signal identified as FMN derives from hhIYD.

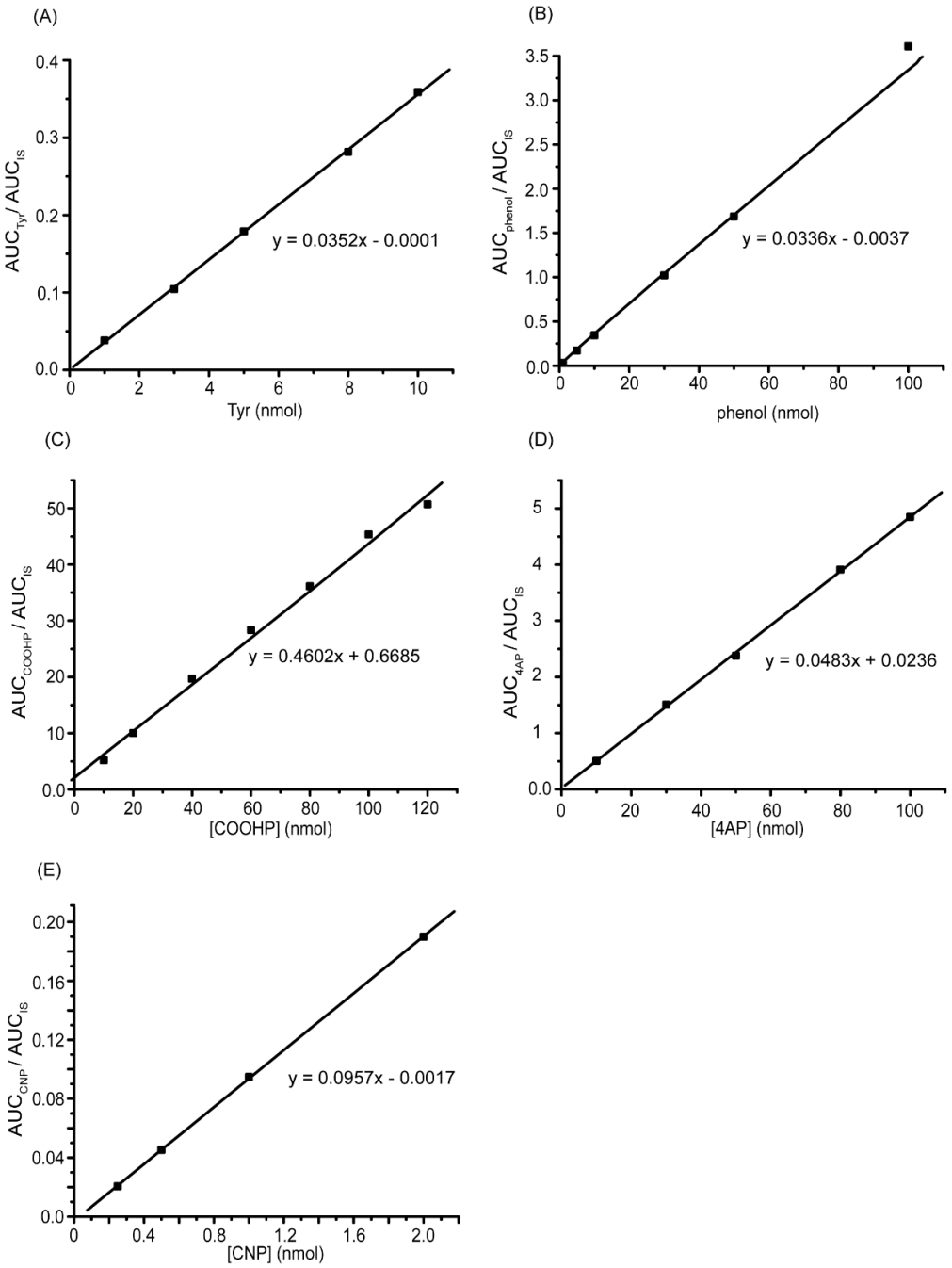

Figure A4. Standard curves for determination of a deiodinated product produced by IYD (A) Tyr (B) phenol (C) 4-hydroxybenzoate, COOHP (D) 4-aminophenol, 4AP (E) 4-hydroxybenzonitrile, CNP. Known concentrations of each deiodinated product were spiked into the reaction mixtures without its substrate and the mixtures were analyzed by HPLC. The ratios of AUC of the deiodinated product to AUC of IS were plotted against the known concentrations of spiked product. Each point represents an average of two individual measurements. Each indicated equation was determined from linear regression and used for calculation of each product produced by IYD.

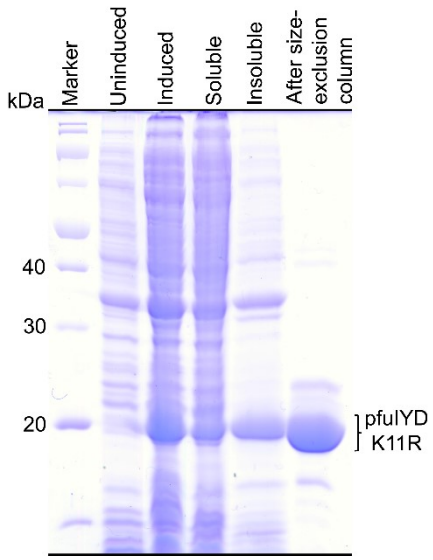

Figure A5. SDS-PAGE gel of the purified pfuIYD K11R mutant. Lane 1 is marker with molecular weights of protein (kDa) indicated on the left. Lane 2 – 5 exhibited fractions containing an uninduced protein, induced protein, soluble fraction and insoluble fraction, respectively. Lane 6 is the purified pfuIYD K11R protein.

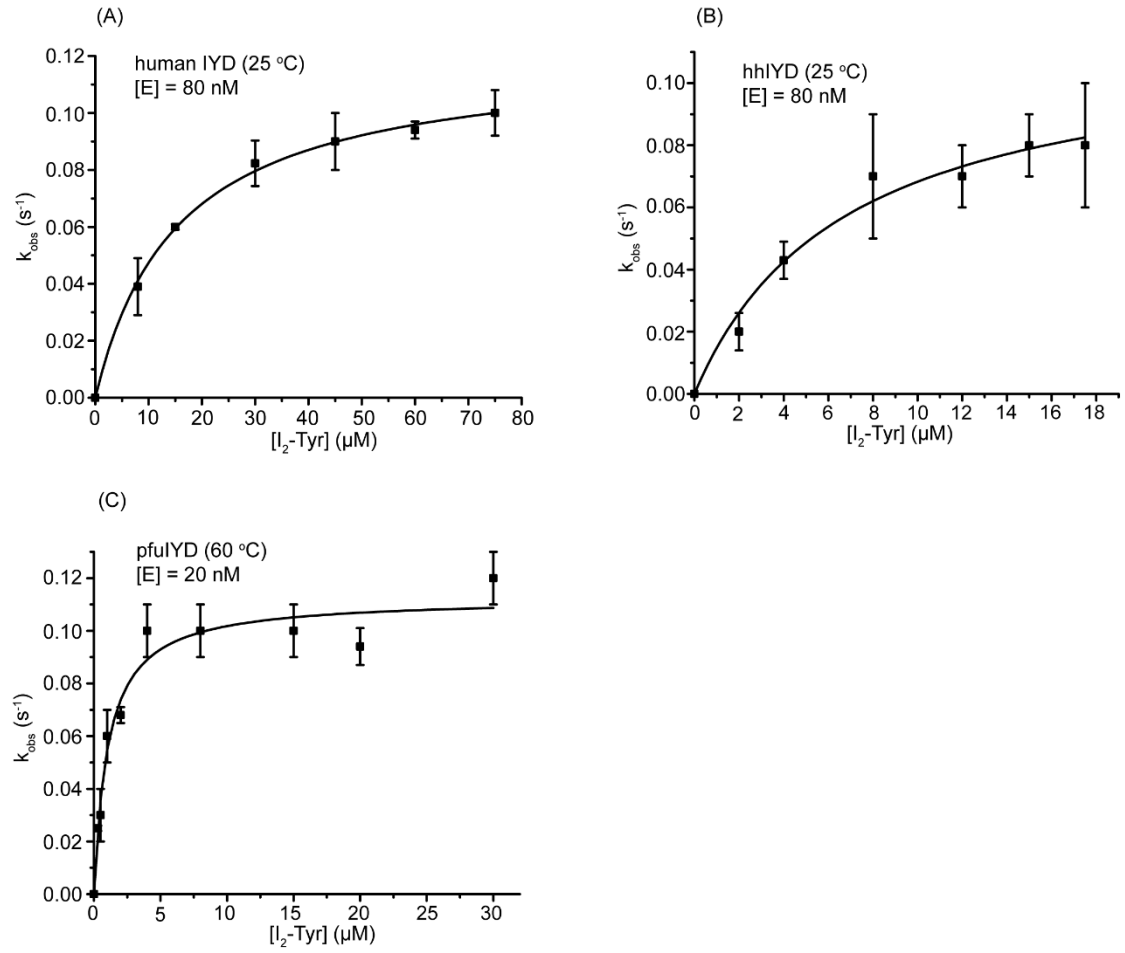

Figure A6. Steady-state kinetics of ^{125}I-[I_2-Tyr] turnover by IYD homologs. Initial rates of deiodination were determined by quantifying $^{125}I^-$ released by IYD. Each data point represents an average of two individual observations and error bars represent the standard deviations from the average. The kinetic parameters were determined from the best fit of data (solid lines) to the Michaelis-Menten equation 2-3 using Origin 6.0.

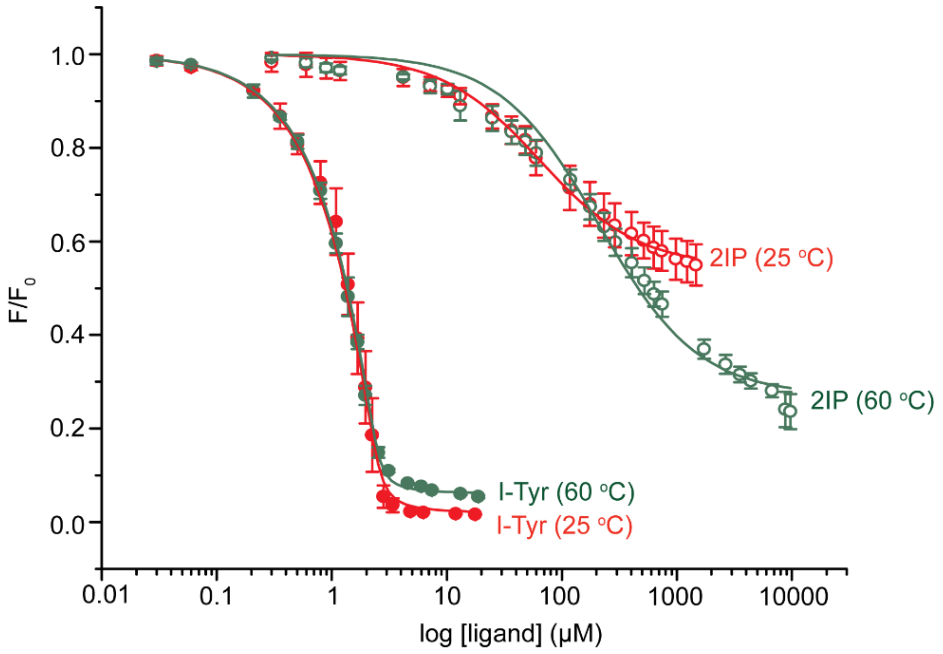

Figure A7. Quenching of FMN_{ox} fluorescence upon ligand binding to pfuIYD at 25 °C and 60 °C. pfuIYD (2.5 μM) in 100 mM potassium phosphate, pH 6.9 were stirred at 25 °C for 30 min or 60 °C for 10-15 min prior to addition of the indicated ligand. The K_d values derived from the best fit of the data (solid lines) to equation 2-4. Complete fluorescence quenching by 2IP was limited by its solubility.

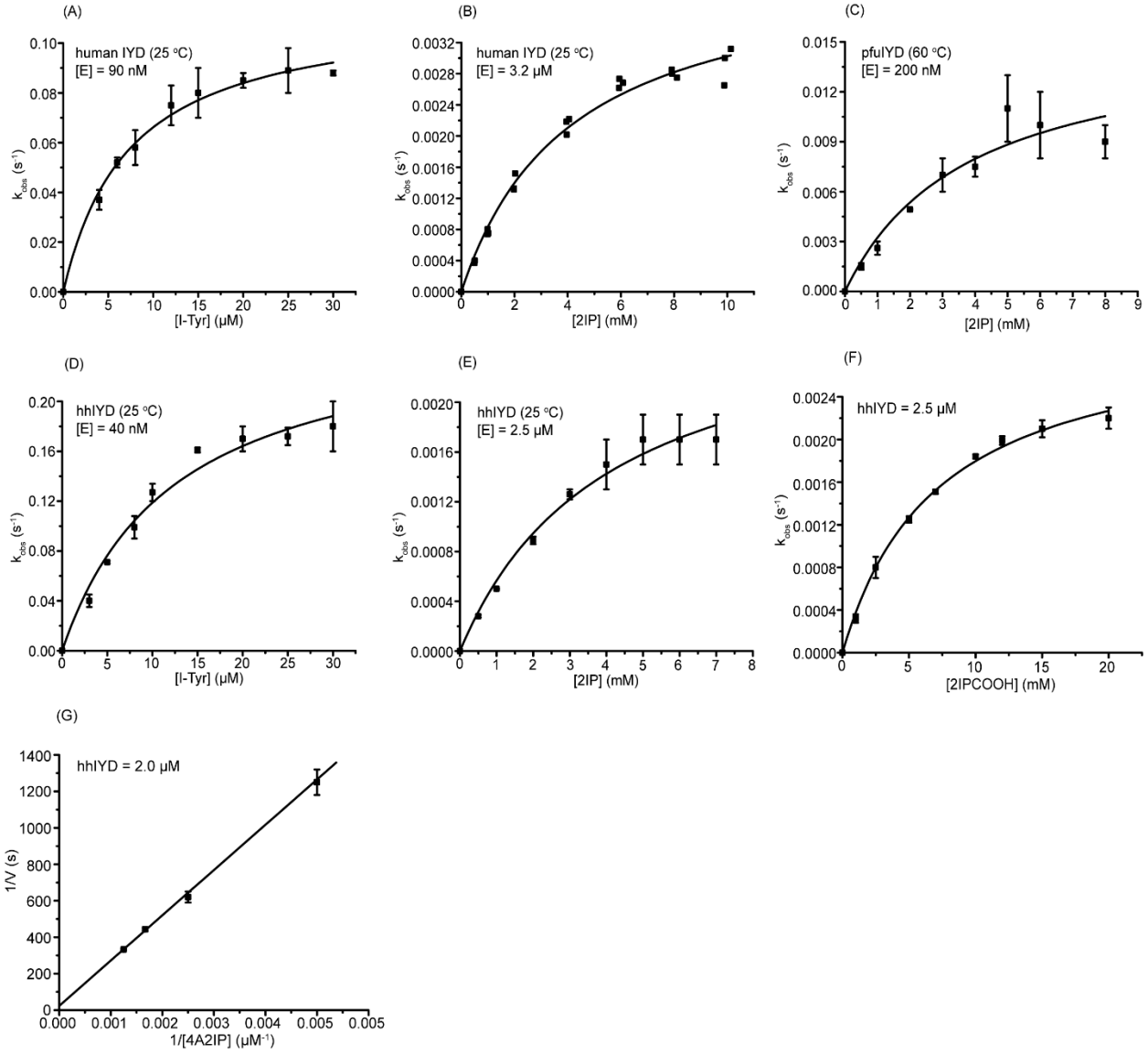

Figure A8. Steady-state kinetics of I-Tyr, 2IP and 2IP derivatives by IYD. Initial rates of deiodination were determined by quantifying the deiodinated products after separation by reverse-phase HPLC. Low solubility of 4A2IP (≤ 1mM) in 100 mM potassium phosphate, pH 7.4 limited the studies at substrate saturation. Hence, its k_{cat}/K_m was estimated from a Lineweaver-Burk plot at 4A2IP concentrations of 0-0.8 mM. Each data point represents an average of three individual observations and error bars represent the standard deviations from the average except for (B) where the data points are from three independent determinations performed at different set of substrate concentrations. The kinetic parameters were determined from the best fit of data (solid lines) to the Michaelis-Menten equation 2-3 using Origin 6.0.

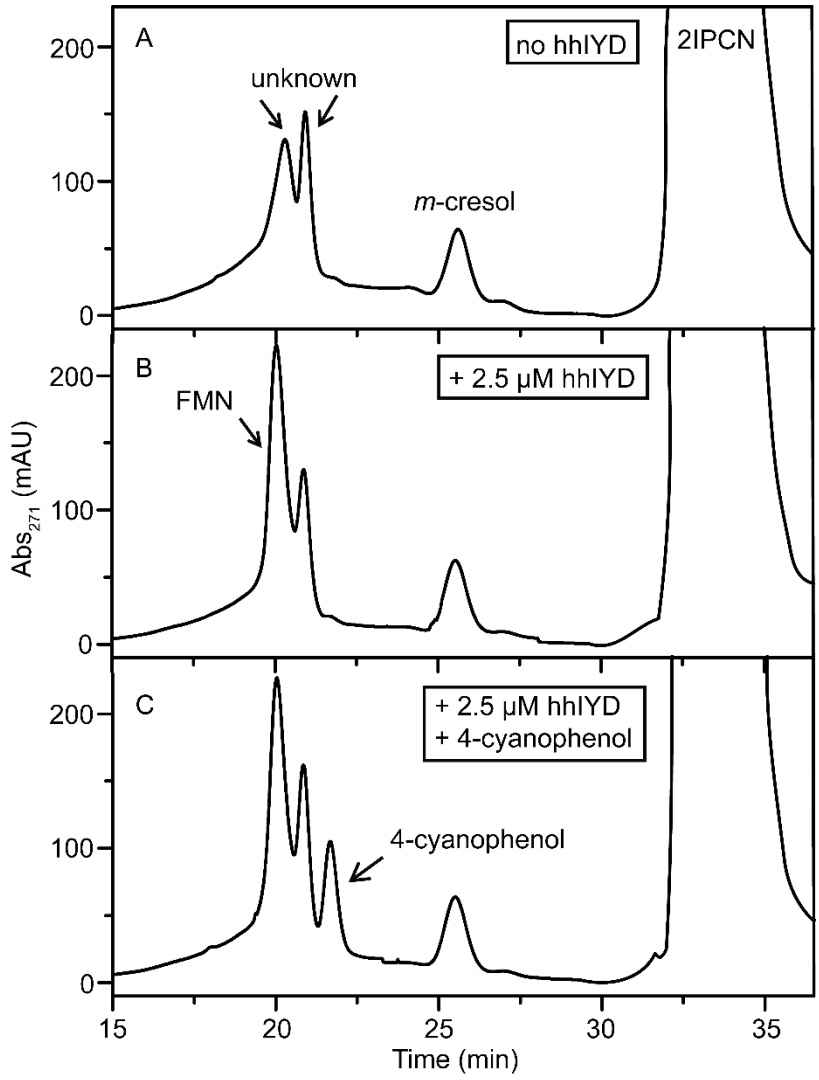

Figure A9. HPLC chromatogram of deiodination of 2IPCN by hhIYD. A mixture of 2IPCN (10 mM), m-cresol (30 µM) in 111 mM potassium phosphate buffer pH 7.4 (900 µl) together with (A) hhIYD (0 µM), (B) hhIYD (2.5 µM), (C) hhIYD (2.5 µM), standard 4-cyanophenol (10 µM) was incubated at 25 ^{o}C for 5 mins prior to addition of dithionite in 5% sodium bicarbonate solution (100 µl) to the final volume of 1 ml. After 4 h, each mixture was quenched by addition of 88% formic acid (50 µl). The entire mixture (1050 µl) was subjected to reverse phase HPLC using solvent A: 0.44% aq. formic acid and solvent B: 0.44% formic acid in acetonitrile. A product was separated using a gradient; 0-25 % B for 10 min, 25 % B for 10 min (0.8 ml/min) and a wash (25-60% B for 10 min, 60-95% for 5 min and 95% B for 10 min (1 ml/min).

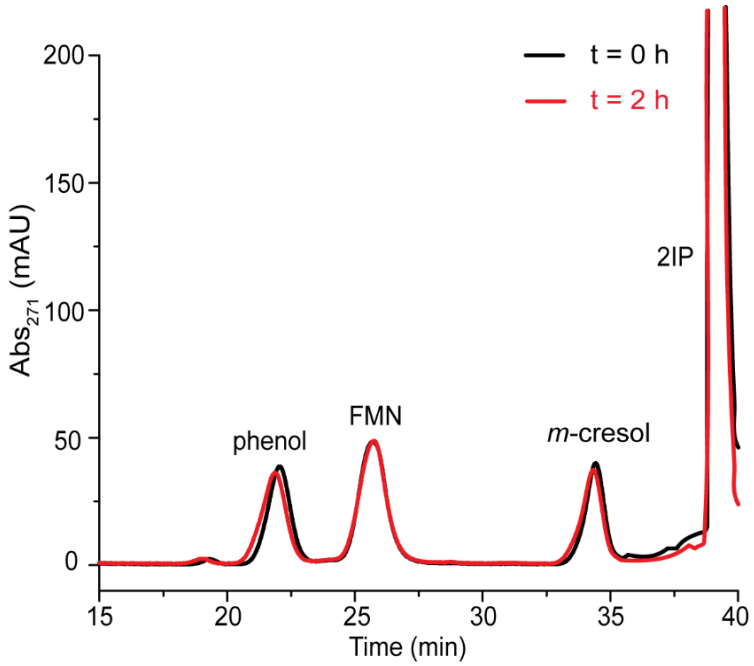

Figure A10. Chromatogram of 2IP incubated with free FMN. A mixture containing FMN (2.5 µM), 2IP (5 mM), m-cresol (30 µM) in 111 mM potassium phosphate buffer (900 µl) was incubated at 25 ºC for 5 mins prior to addition of dithionite in 5% sodium bicarbonate solution (100 µl) to the final volume of 1 ml. The mixtures were continued with incubation at 25 ºC for 0 h (black line) and 2 h (red line) followed by quenching with 88% formic acid (50 µl) prior to analysis by HPLC. See Figure A3 for HPLC solvents and gradients used for analysis. 2IP has a phenol contaminated (0.8%). Similar amount of phenol (~40 nmol) at t = 0 and 2 h indicates no phenol formation by free FMN.

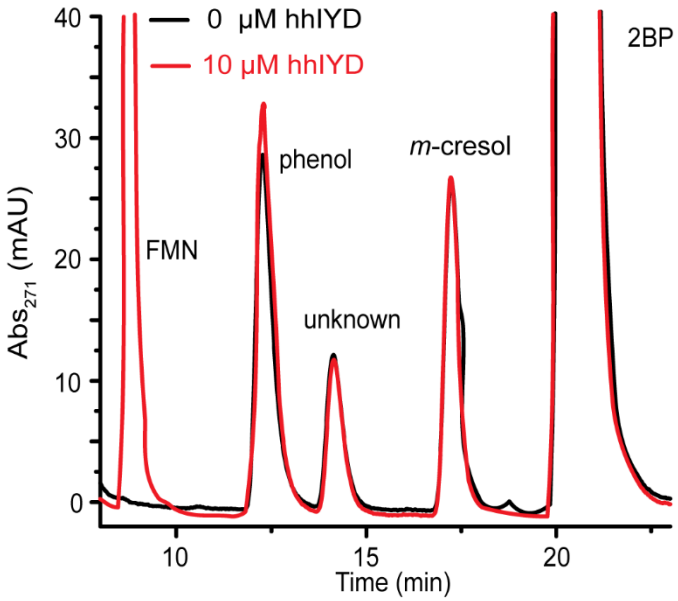

Figure A11. Chromatogram of 2BP turnover by hhIYD. A mixture containing hhIYD (0 µM, black line and 10 µM, red line), 2BP (2 mM), m-cresol (20 µM) in 111 mM potassium phosphate buffer (900 µl) was incubated at 25 °C for 5 mins prior to addition of dithionite in 5% sodium bicarbonate solution (100 µl) to the final volume of 1 ml. The mixtures were continued with incubation at 25 °C for 4 h followed by quenching with 88% formic acid (50 µl). The entire mixture (1050 µl) was subjected to reverse phase HPLC (1 ml/min) using solvent A: 10 mM triethylamine acetate, pH 4.0 and solvent B: acetonitrile. A product was separated using a gradient; 10 – 60 % B for 30 min, 60 – 100 % B for 5 min and a wash (100% B for 10 min). 2-bromophenol (2BP) has a phenol contaminated (0.6%). No phenol produced more than a threshold of 5 nmol over 4 h indicating very slow 2BP turnover by hhIYD.

Appendix B: Supporting information for Chapter 3

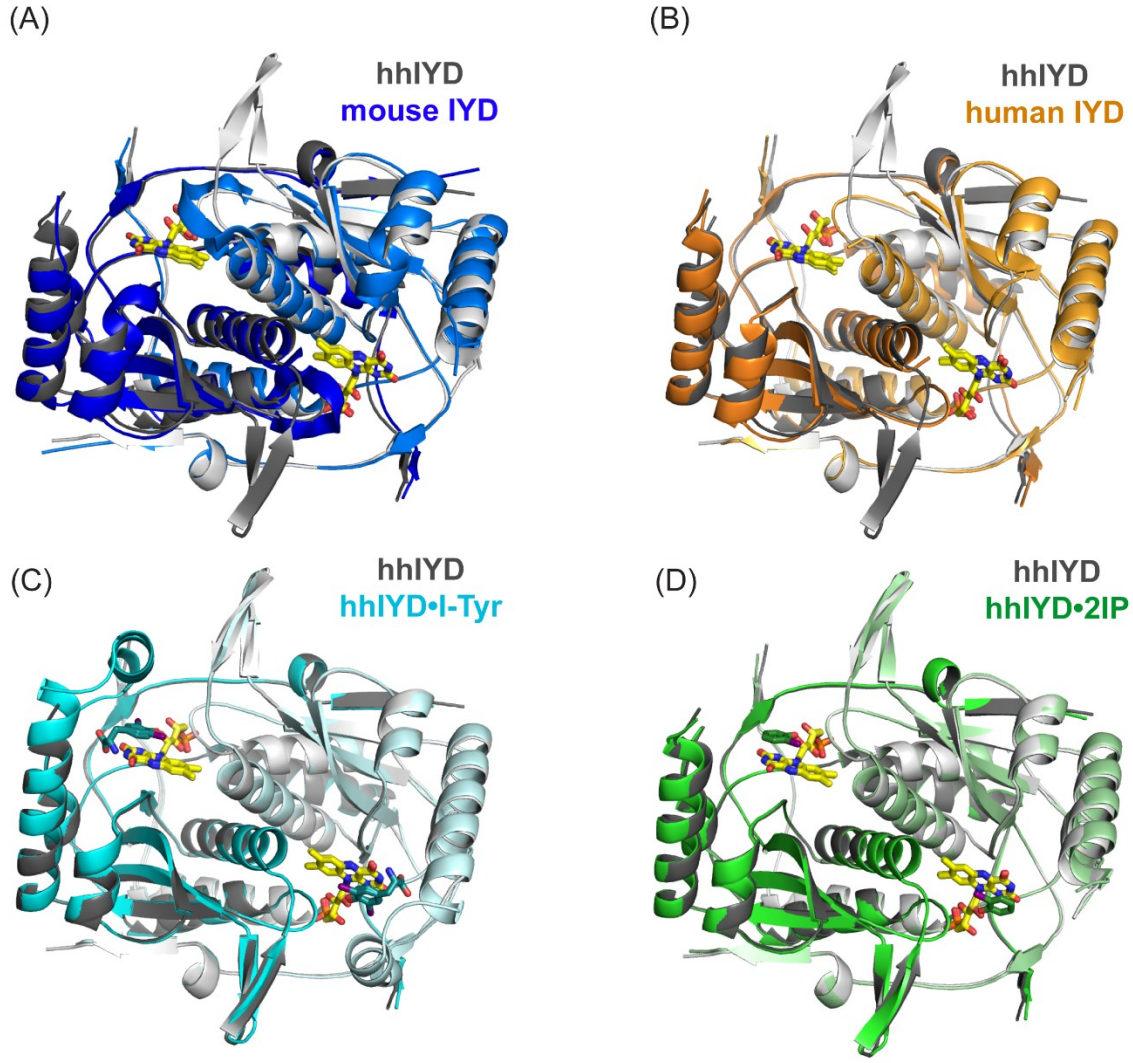

Figure B1. Superposition of IYD structures. Overlay of the hhIYD structure (PDB: 5KO7, grey) with (A) mouse IYD (PDB: 3GB5, dark blue) (B) human IYD (PDB: 4TTB, orange) (C) hhIYD•I-Tyr (PDB: 5KO8, cyan) and (D) hhIYD•2IP (PDB: 5KRD, green). FMN_{ox}, I-Tyr and 2IP are presented in yellow, cyan and green respectively by their carbon atoms.

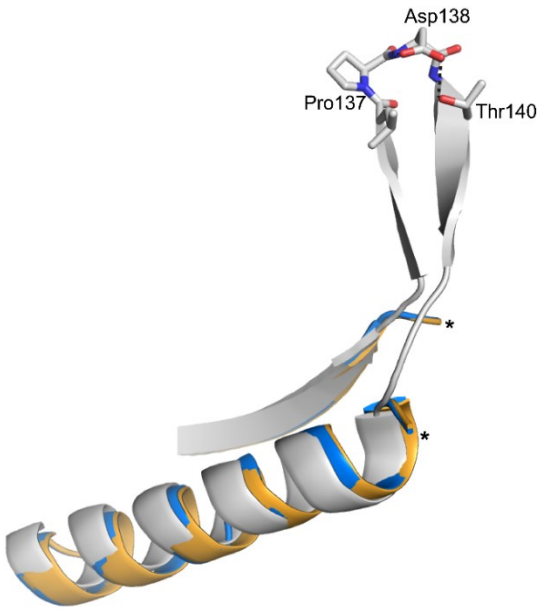

Figure B2. Superimposition of the loop region in IYD homologs. The loop of hhIYD (PDB: 5KO7, grey) is exist while the equivalent loops of mouse IYD (PDB: 3GB5, dark blue) and human IYD (PDB: 4TTB, orange) are undetectable. Discontinuous ends are generated as indicated by (*). The presence of Pro137, and hydrogen bonding (dashed line) are likely to stabilize the loop structure.

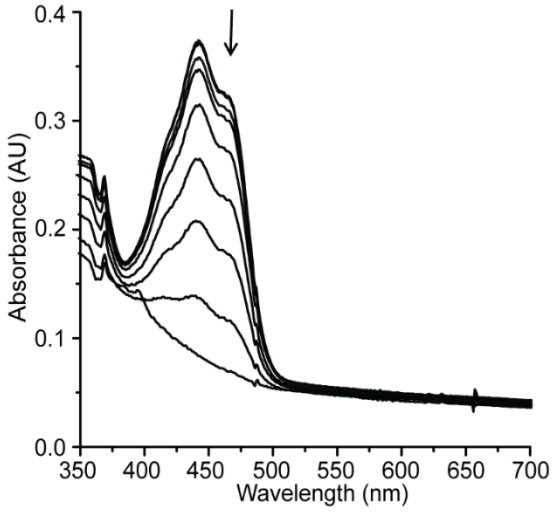

Figure B3. UV spectrum monitoring reduction of FMN bound to hhIYD in the absence of ligand. FMN_{ox} (446 nm) is decreased upon reduction and no FMN_{sq} accumulation was detected (590 nm). Solution contained xanthine (1 mM), methyl viologen (13 µM), hhIYD (20 µM), potassium phosphate (100 mM) pH 7.4, sodium chloride (500 mM) and glycerol (10% v/v). Reduction was initiated by addition of xanthine oxidase (140 µg/ml, final). The experiment was performed at pH 7.4, room temperature. UV-Vis spectral changes (lines) represent some spectra over 40 min.

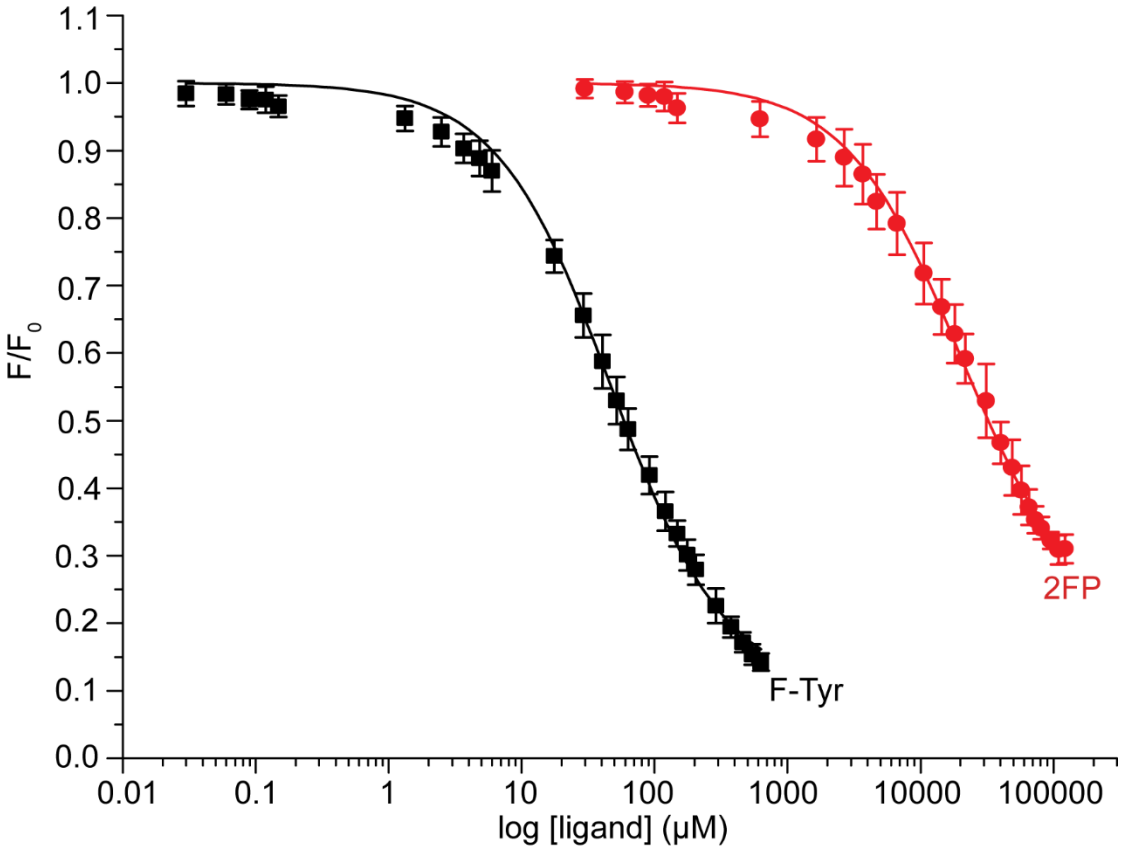

Figure B4. Quenching of FMN_{ox} fluorescence upon ligand binding to hhIYD. hhIYD (2.5 μM) in 100 mM potassium phosphate, pH 7.4 was stirred at 25 °C for 30 min prior to addition of the indicated ligand. The K_d values derived from the best fit of the data (solid lines) to equation 2-4.

Appendix C: Supporting information for Chapter 4

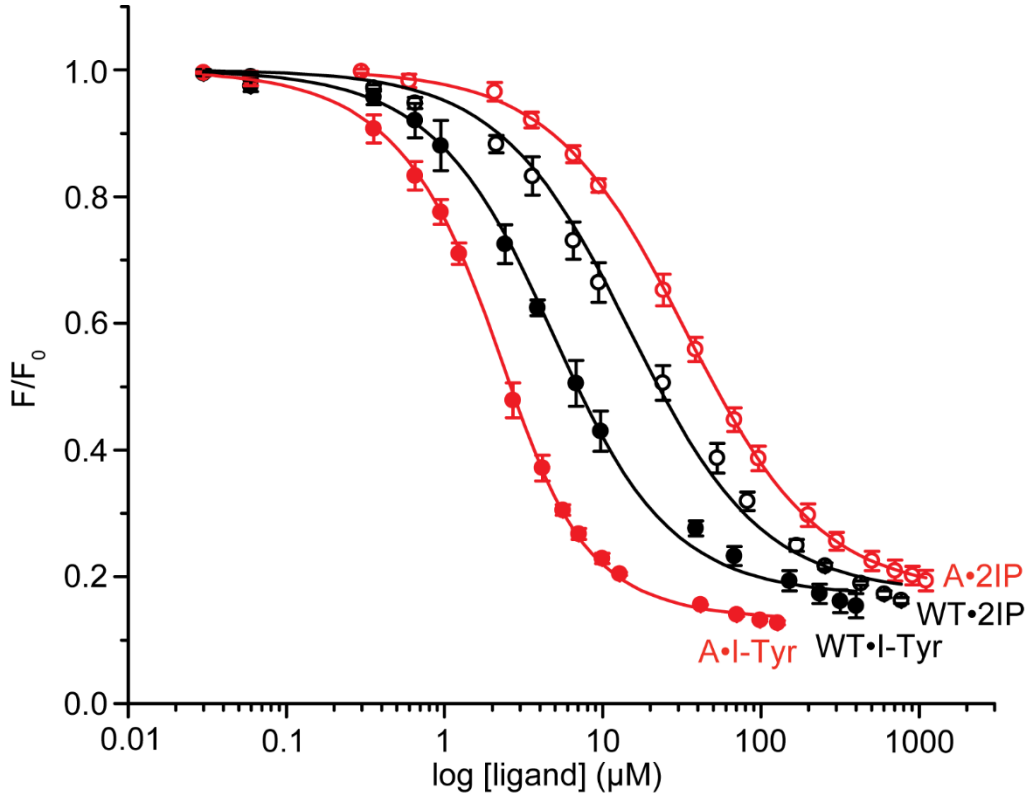

Figure C1. Quenching of FMN_{ox} fluorescence upon ligand binding to hhIYD: wild type (black) and mutant A, hhIYD A64F L107A (red). hhIYD (2.5 μM) in 100 mM glycine-KOH and 114 mM KCl, pH 9.0 was stirred at 25 °C for 30 min prior to addition of the indicated ligand. The K_d values derived from the best fit of the data (solid lines) to equation 2-4.

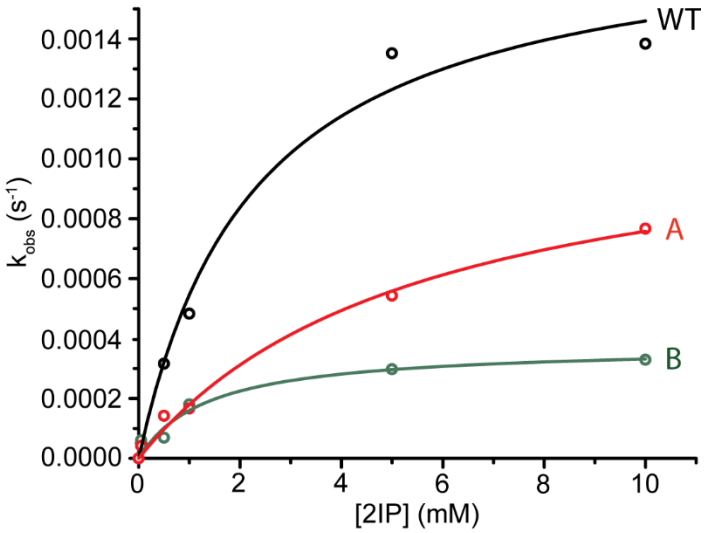

Figure C2. Steady-state kinetics of 2IP. Deiodination of 2IP by wild-type hhIYD (2.5 μM) (black), mutant A, hhIYD A64F L107A (2.5 μM) (red) and mutant B, hhIYD S94D N96R S175H (2.5 μM) (green). Initial rates of deiodination were determined by quantifying phenol product after separation by reverse-phase HPLC. Each data point represents a single observation. The kinetic parameters were determined from the best fit of data (solid lines) to the Michaelis-Menten equation 2-3 using Origin 6.0.

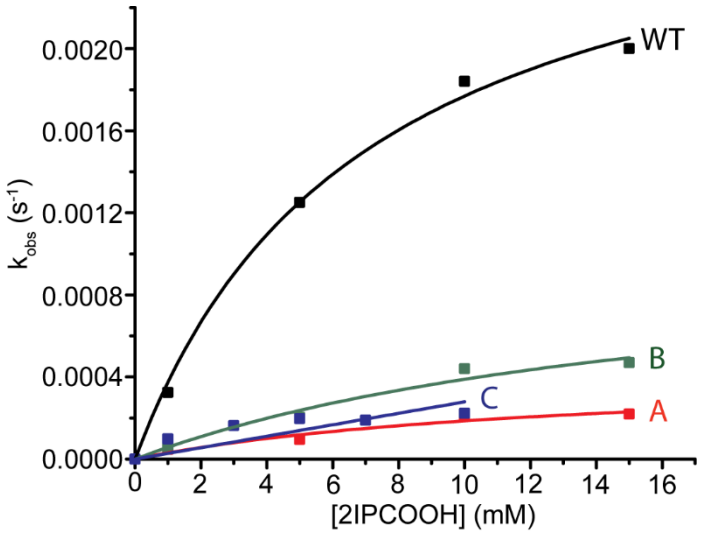

Figure C3. Steady-state kinetics of 2IPCOOH. Deiodination of 2IPCOOH by wild-type hhIYD (2.5 μM) (black), mutant A, hhIYD A64F L107A (2.5 μM) (red), mutant B, hhIYD S94D N96R S175H (2.5 μM) (green) and mutant C, hhIYD E91R (3.5 μM) (blue). Initial rates of deiodination were determined by quantifying 4-hydroxybenzoate product after separation by reverse-phase HPLC. Each data point represents a single observation. The kinetic parameters were determined from the best fit of data (solid lines) to the Michaelis-Menten equation 2-3 using Origin 6.0.

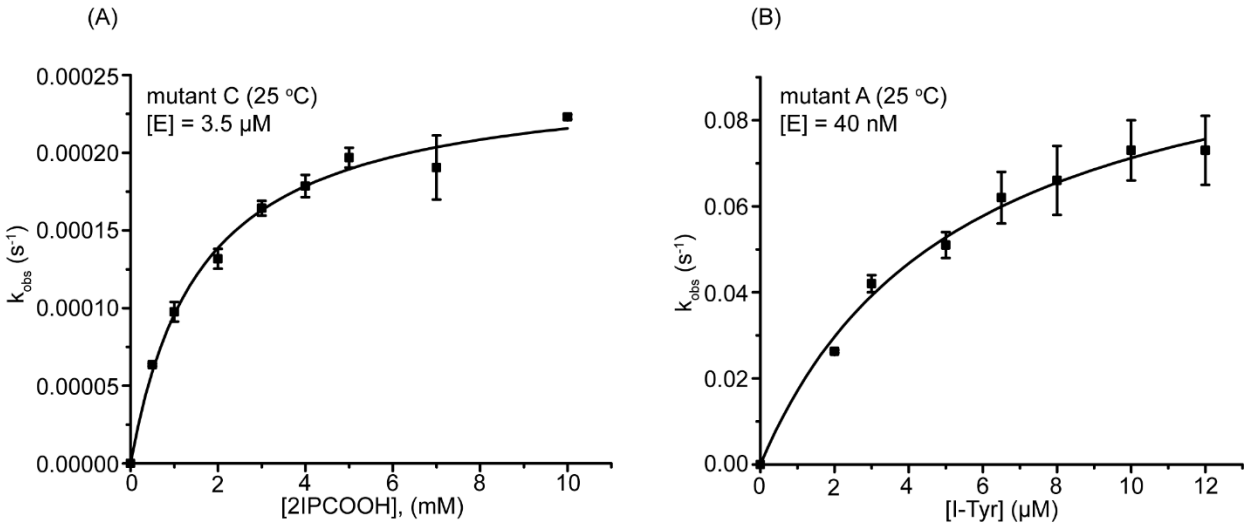

Figure C4. Steady-state kinetics of 2IPCOOH and I-Tyr by hhIYD mutants. Deiodination of (A) 2IPCOOH by mutant C (hhIYD E91R) and (**B**) I-Tyr by mutant A hhIYD A64F L107A. Initial rates of deiodination were determined by quantifying the deiodinated product after separation by reverse-phase HPLC. Each data point represents an average of three individual observations and error bars represent the standard deviations from the average. The kinetic parameters were determined from the best fit of data (solid lines) to the Michaelis-Menten equation 2-3 using Origin 6.0.

Appendix D: Supporting information for Chapter 5

ATGGGATCTGATAAAATTCATCATCATCATCATCACGAAAACCTGTACTTCCAGGGC
ATGGAATTACAAGATACTATTTTTAAAAGACAAAGTGTAAGAAAGTTTAAAAATCAAG
ATGTATCAGATGAAGATATTTTAAAAATGATAAAAGCAGCAGGTGCAGCACCATCAG
GCAAGAATATTCAAAACTGGCATTTTGTTGTTATAAAACGCCGTGATTTAATGGAAA
AGATAGCAGATGTGATAACTAAAAAGCAACAAGAAATACTTGTAGAAATGGATAAAG
TATCAGTGGATAAGGCTAATAGATTTAGAAAATTTGTTAAAAATTTTACACTATTTTAC
TTAAAAGCTCCAGTTTTAGTATTAGTTTTTACAAAGGTATATAATCCATCAGGATATT
ATGAATTAGAGCTTATAGATGCACCTAAGGAGACTATAGATAAATTATTTATAAGAAA
TCCAGGTATGCAGAGTCTAGGTGCTGCAATTGAAAACTTTACACTATCAGCAATTGA
ACTTGGATATGGTTCTTGTTGGTTGACAAGTCAAAACTATGCAGCAGATGAGATAGA
AGCTGTTTTAGAAGCAGAAACTGGTTTTGAAAAGGGAGAGTATTTTTTAGGTGCAAT
GTTAGCTCTTGGAGTGCCAGAGGACAATTTGAAGAGTCCATCTAAAAAACCAGTAG
AAGAAATATGTACATTTATAAAATAA

Figure D1. Translated gene sequence of a pSpeedET vector containing a wild-type 3EO8 gene. The translated sequence includes the 3EO8 gene (accession YP_001089088.1) (codons in black), the N-terminal His_6 (codons in red) and extra codons derived from the pSpeedET plasmid (codons in blue).

MGSDKIHHHHHHENLYFQGMELQDTIFKRQSVRKFKNQDVSDEDILKMIKAAGAAPSG
KNIQNWHFVVIKRRDLMEKIADVITKKQQEILVEMDKVSVDKANRFRKFVKNFTLFYLKA
PVLVLVFTKVYNPSGYYELELIDAPKETIDKLFIRNPGMQSLGAAIENFTLSAIELGYGSC
WLTSQNYAADEIEAVLEAETGFEKGEYFLGAMLALGVPEDNLKSPSKKPVEEICTFIK

Figure D2. Protein corresponding to the translated sequence containing 3EO8 gene shown in Figure D1. The expressed protein includes the 3EO8 protein (black) with His_6 (red) and another 13 extra amino acids (blue) at the N-terminus.

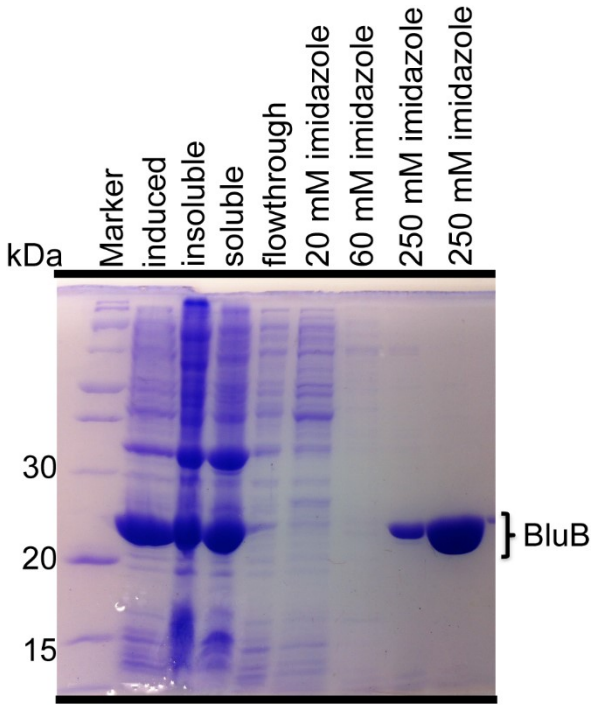

Figure D3. SDS-PAGE gels of purified BluB protein. Lane 1 is marker with molecular weights of protein (kDa) indicated on the left. Lane 2 – 5 exhibited fractions containing induced protein, insoluble proteins, soluble proteins and contaminated proteins of the flowthrough from Ni-NTA affinity column respectively. Lane 6 – 7 were from a step-wise washes from Ni-NTA purification with buffer containing 20 and 60 mM imidazole respectively. Lane 8 – 9 are purified BluB enzyme from 250 mM imidazole elution.

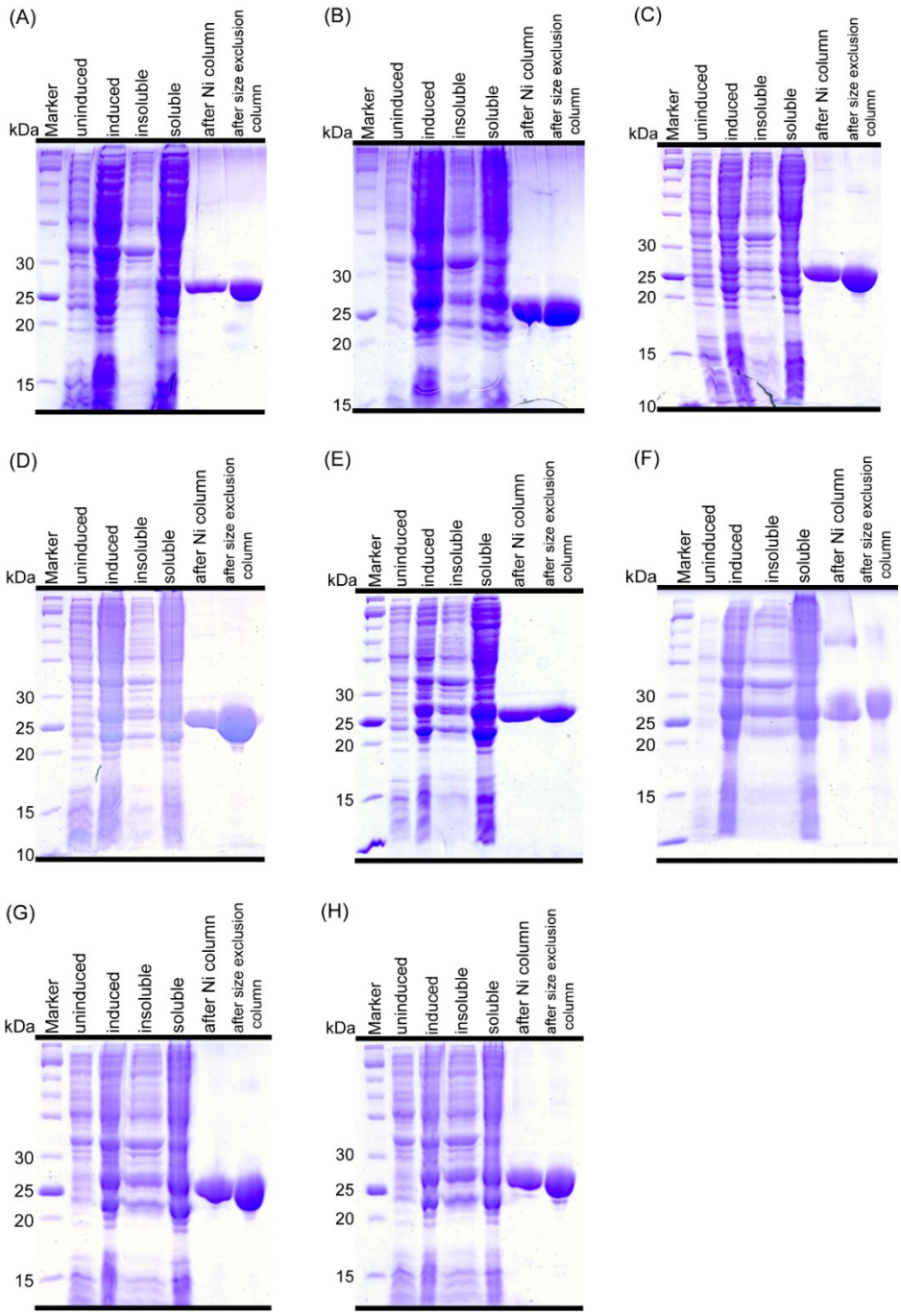

Figure D4. SDS-PAGE gels of purified 3EO8 proteins. (A) wild-type (B) mutant 1 (F88A) (C) mutant 2 (F92A) (D) mutant 3 (F88A F92A) (E) mutant 4 (F88A Y110H) (F) mutant 5 (F88A Y110H S113) (G) mutant 6 (F88A Y110H K40A) (H) mutant 8 (F88A Y110S). Lane 1 is marker with molecular weights of protein (kDa) indicated on the left. Lane 2 – 5 exhibited fractions containing an uninduced protein, induced protein, insoluble proteins and soluble proteins, respectively. Lane 6 – 7 are purified 3EO8 after Ni-NTA affinity column and size-exclusion column, respectively.

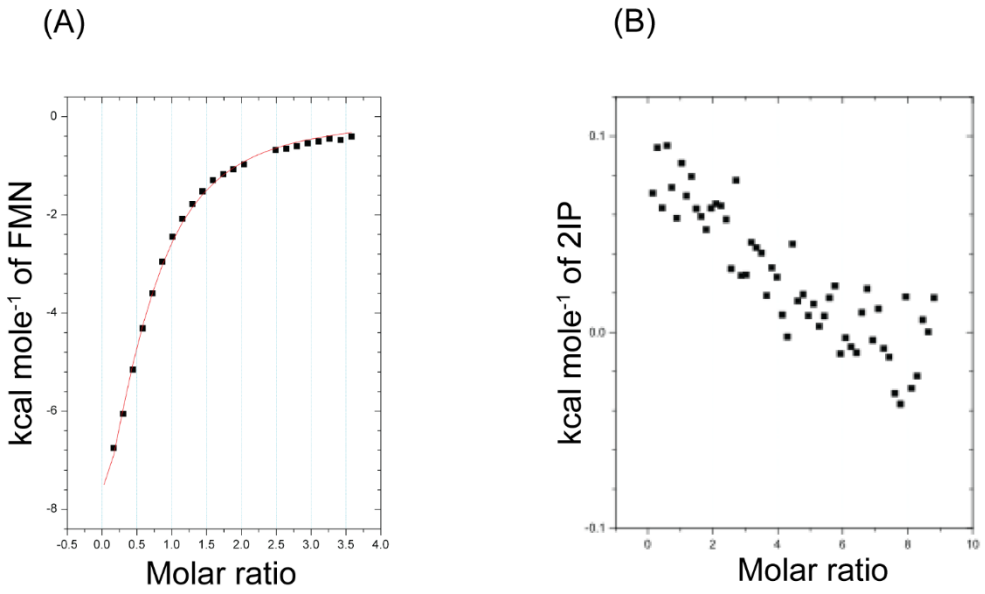

Figure D5. ITC binding measurement for titration of a ligand into BluB. ITC binding isotherm of (A) FMN (~70 μM) titrated into BluB solution (25 μM, 1.5 ml) and (B) 2IP (~ 1 mM) titrated into BluB-FMN solution (BluB = 70 μM, 1.5 ml; FMN = 140 μM). Assays were performed in buffer containing 10 mM Tris pH 8.0, 10 mM NaCl at 23°C. Data from a single experiment were fitted to a single-binding site model 32 using Origin ITC software (V. 5.0, Microcal Software Inc.) and the result was modeled to a single binding site per monomer to determine the K_d value.

Bibilography

1. Whiteley, C. G.; Lee, D. J. Enzyme technology and biological remediation. *Enzyme Microb. Technol.* 2006, 38, 291-316.

2. Haggblom, M. M.; Bossert, I. D. Dehalogenation microbial processes and environmental applications. Kluwer Academic Publishers, Boston, 2003.

3. Adrian, L.; Szewzyk, U.; Wecke, J.; Gorisch, H. Bacterial dehalorespiration with chlorinated benzenes. *Nature* 2000, 408 (6812), 580-583.

4. Bunge, M.; Adrian, L.; Kraus, A.; Opel, M.; Lorenz, W. G.; Andreesen, J. R.; Gorisch, H.; Lechner, U. Reductive dehalogenation of chlorinated dioxins by an anaerobic bacterium. *Nature* 2003, 421 (6921), 357-360.

5. Holliger, C.; Wohlfarth, G.; Diekert, G. Reductive dechlorination in the energy metabolism of anaerobic bacteria. FEMS Microbiol. Rev. 1998, 22 (5), 383.

6. Ruggaber, T. P. T., J. W., Enhancing bioremediation with enzymatic processes: a review. *J. Hazard. Toxic Radioact. Waste.* 2006, 10 (2), 73-85.

7. Copley, S. D., Diverse mechanistic approaches to difficult chemical transformations: microbial dehalogenation of chlorinated aromatic compounds. *Chem. Biol.* 1997, 4, 169-174.

8. Fetzner, S. Bacterial dehalogenation. *Appl. Microbiol. Biotechnol.* 1998, 50, 633-657.

9. Junko, H. Chemical degradation of chlorinated organic pollutants for in situ remediation and evaluation of natural attenuation, organic pollutants ten year after Stockholm convention-environmental and analytical update. InTech, Rijeka, Croatia Publisher: 2012.

10. Cline, R. E.; Hill, R. H.; Phillips, D. L.; Needham, L. L. Pentachlorophenol measurements in body fluids of people in log homes and workplaces. *Arch. Env. Contam. Toxicol.* 1989, 18, 475-481.

11. Scholten, J. D.; Chang, K. H.; Babbitt, P. C.; Charest, H.; Sylvestre, M.; Dunaway-Mariano, D., Novel enzymic hydrolytic dehalogenation of a chlorinated aromatic. *Science.* 1991, 253 (5016), 182.

12. Willett, W. S.; Copley, S. D., Identification of oxidative damage and its effect on the reaction catalyzed by tetrachlorohydroquinone dehalogenase. *Protein. Eng.* 1997, 10, 69.

13. Goswami, A.; Rosenberg, I. N., Studies on a soluble thyroid iodotyrosine deiodinase: Activation by NADPH and electron carriers. *J. Endocrinol.* 1977, 101 (2), 331-341.

14. Rosenberg, I. N.; Goswami, A., Purification and characterization of a flavoprotein from bovine thyroid with iodotyrosine deiodinase activity. *J. Biol. Chem.* 1979, 254 (24), 12318-12325.

15. Zimmermann, M. B. Iodine deficiency. *Endocr. Rev.* 2008, 30 (4), 376-408.

16. Zimmermann, M. B.; Jooste, P. L.; Pandav, C. S. Iodine-deficiency disorders. *The Lancet.* 2008, 372 (9645), 1251-1262.

17. Moreno, J. C.; Klootwijk, W.; van Toor, H.; Pinto, G.; D'Alessandro, M.; Lèger, A.; Goudie, D.; Polak, M.; Grüters, A.; Visser, T. J. Mutations in the iodotyrosine deiodinase gene and hypothyroidism. *New. Engl. J. Med.* 2008, 358 (17), 1811-1818.

18. St. Germain, D. L.; Galton, V. A.; Hernandez, A. Defining the roles of the iodothyronine deiodinases: Current concepts and challenges. *J. Endocrinol.* 2009, 150 (3), 1097-1107.

19. Berry, M. J.; Kieffer, J. D.; Harney, J. W.; Larsen, P. R. Selenocysteine confers the biochemical properties characteristic of the type I iodothyronine deiodinase. *J. Biol. Chem.* 1991, 266 (22), 14155-14158.

20. Friedman, J. E.; Watson, J. A.; Lam, D. W. H.; Rokita, S. E. Iodotyrosine deiodinase is the first mammalian member of the NADH oxidase/flavin reductase superfamily. *J. Biol. Chem.* 2006, 281 (5), 2812-2819.

21. Ruma, B.; Stephen, R. W., The many faces of vitamin B_{12}: Catalysis by cobalamin-dependent enzymes. *Biochemistry* 2003, 72, 209 - 247.

22. McTamney, P. M.; Rokita, S. E. A mammalian reductive deiodinase has broad power to dehalogenate chlorinated and brominated substrates. *J. Am. Chem. Soc.* 2009, 131 (40), 14212-14213.

23. Phatarphekar, A.; Rokita, S. E. Functional analysis of iodotyrosine deiodinase from *drosophila melanogaster*. *Protein Sci.* 2016, 25 (12), 2187–2195.

24. Thomas, S. R.; McTamney, P. M.; Adler, J. M.; LaRonde-LeBlanc, N.; Rokita, S. E. Crystal structure of iodotyrosine deiodinase, a novel flavoprotein responsible for iodide salvage in thyroid glands. *J. Biol. Chem.* 2009, 284 (29), 19659-19667.

25. Buss, J. M.; McTamney, P. M.; Rokita, S. E. Expression of a soluble form of iodotyrosine deiodinase for active site characterization by engineering the native membrane protein from *Mus musculus. Protein Sci.* 2012, 21 (3), 351-361.

26. Amachi, S.; Mishima, Y.; Shinoyama, H.; Muramatsu, Y.; Fujii, T. Active transport and accumulation of iodide by newly isolated marine bacteria. *Appl. Environ. Microbiol.* 2005, 71 (2), 741-745.

27. Kotay, S. M.; Datta, T.; Choi, J.; Goel, R. Biocontrol of biomass bulking caused by *Haliscomenobacter hydrossis* using a newly isolated lytic bacteriophage. *Water Res.* 2011, 45 (2), 694-704.

28. Taga, M. E.; Larsen, N. A.; Howard-Jones, A. R.; Walsh, C. T.; Walker, G. C. BluB cannibalizes flavin to form the lower ligand of vitamin B_{12}. *Nature*. 2007, 446, 449-453.

29. Rokita, S. E., Flavoprotein dehalogenases , in Handbook of Flavoproteins. Hille, R.; Miller, S. M.; Palfey, B. Eds. DeGruyter: Berlin, 2013: pp 337–350.

30. Phatarphekar, A.; Buss, J. M.; Rokita, S. E. Iodotyrosine deiodinase: A unique flavoprotein present in organisms of diverse phyla. *Mol. Biosyst.* 2014, 10 (1), 86-92.

31. Phatarphekar, A. The ubiquity of iodotyrosine deiodinase: Identification of its signature sequence and functional analysis in a model invertebrate. Johns Hopkins University, 2016.

32. Hu, J.; Chuenchor, W.; Rokita, S. E. A switch between one- and two-electron chemistry of the human flavoprotein iodotyrosine deiodinase is controlled by substrate. *J. Biol. Chem.* 2015, 290 (1), 590-600.

33. Buss, J. M. Iodotyrosine deiodinase from selected phyla engineered for bacterial expression. University of Maryland, College Park, 2012.

34. Gasteiger, E.; Hoogland, C.; Gattiker, A.; Duvaud, S. E.; Wilkins, M. R.; Appel, R. D.; Bairoch, A., Protein identification and analysis tools on the ExPASy server. In *The Proteomics Protocols Handbook*, Walker, J. M., Ed. Humana Press: Totowa, NJ, 2005;pp 571-607.

35. Kozioł, J., Fluorometric analyses of riboflavin and its coenzymes. In *Methods Enzymol.* Academic Press: 1971; 18, Part B, pp 253-285.

36. Edgar, K. J.; Falling, S. N., An efficient and selective method for the preparation of iodophenols. *J. Org. Chem.* 1990, 55 (18), 5287-5291.

37. Rosenberg, I. N.; Goswami, A. Iodotyrosine deiodinase from bovine thyroid. In *Methods Enzymol.*, Academic Press: 1984; 107, pp 488-500.

38. Warner, J. R.; Copley, S. D. Pre-steady-state kinetic studies of the reductive dehalogenation catalyzed by tetrachlorohydroquinone dehalogenase. *Biochemistry.* 2007, 46 (45), 13211-13222.

39. Heo, J. H.; Kim, S. W. Cloning the Pfu DNA polymerase from DNA contaminants in preparations of commercial Pfu DNA polymerase. *Afr. J. Microbiol. Res.* 2013, 7, 745-750.

40. Penhoat, M. Scope and limitations of a ^{1}H NMR method for the prediction of substituted phenols pK_a values in water, CH_3CN, DMF, DMSO and i-PrOH. *Tetrahedron Lett.* 2013, 54 (21), 2571-2574.

41. Stradins, J.; Hasanli, B., Anodic voltammetry of phenol and benzenethiol derivatives. *J. Electroanal. Chem.* 1993, *353* (1), 57-69.

42. Das, T. N. Redox chemistry of 3-iodotyrosine in aqueous medium. *J. Phys. Chem. A.* 1998, *102* (2), 426-433.

43. McTamney, P. M.; Rokita, S. E. A mammalian reductive deiodinase has broad power to dehalogenate

chlorinated and brominated substrates. *J. Am. Chem. Soc.* 2009, 131 (40), 14212-14213.

44. Fiala, G.; Stetter, K. O. *Pyrococcus furiosus sp.* represents a novel genus of marine heterotrophic archaebacteria growing optimally at 100°C. *Arch. Microbiol.* 1986, 145 (1), 56-61.

45. Hu, J. The interplay of substrate, protein and its cofactor in controlling the catalytic properties of human iodotyrosine deiodinase. University of Maryland, College Park, 2014.

46. Massey, V. The chemical and biological versatility of riboflavin. *Biochem. Soc. Trans.* 2000, 28 (4), 283-296.

47. Fraaije, M. W.; Mattevi, A. Flavoenzymes: diverse catalysts with recurrent features. *Trends Biochem. Sci.* 2000, 25 (3), 126-132.

48. Mansoorabadi, S. O.; Thibodeaux, C. J.; Liu, H.-W. The diverse roles of flavin coenzymes. Nature's most versatile thespians. *J. Org. Chem.* 2007**,** 72 (17), 6329-6342.

49. Fagan, R. L.; Palfey, B. A. In Chapter 3: Flavin-dependent enzymes In *Comprehensive Natural Products II*, Begley, T. P., Ed. Elsevier, Oxford: 2010; pp 37-114.

50. Silverman, R. B. The organic chemistry of enzyme-catalyzed reactions. Academic Press: 2002.

51. Haynes, C. A.; Koder, R. L.; Miller, A.-F.; Rodgers, D. W., Structures of nitroreductase in three states: Effect of inhibitor binding and reduction. *J. Biol. Chem.* 2002**,** 277 (13), 11513-11520.

52. Mukherjee, A.; Rokita, S. E. Single amino acid switch between a flavin-dependent dehalogenase and nitroreductase. *J. Am. Chem. Soc.* 2015**,** 137 (49), 15342-15345.

53. Koder, R. L.; Haynes, C. A.; Rodgers, M. E.; Rodgers, D. W.; Miller, A.-F. Flavin thermodynamics explain the oxygen insensitivity of enteric nitroreductases. *Biochemistry* 2002**,** 41 (48), 14197-14205.

54. Kabsch, W. Automatic processing of rotation diffraction data from crystals of initially unknown symmetry and cell constants. *J. Appl. Crystallogr.* 1993**,** 26 (6), 795-800.

55. Otwinowski, Z.; Minor, W. [20] Processing of X-ray diffraction data collected in oscillation mode. In *Methods Enzymol.*, Academic Press: 1997; Vol. 276, pp 307-326.

56. McCoy, A. J.; Grosse-Kunstleve, R. W.; Adams, P. D.; Winn, M. D.; Storoni, L. C.; Read, R. J. Phaser crystallographic software. *J. Appl. Crystallogr.* 2007**,** 40 (4), 658-674.

57. Emsley, P.; Cowtan, K. Coot: Model-building tools for molecular graphics. *Acta. Cryst.* 2004**,** 60, 2126-2132.

58. Adams, P. D.; Afonine, P. V.; Bunkóczi, G.; Chen, V. B.; Davis, I. W.; Echols, N.; Headd, J. J.; Hung, L.-W.; Kapral, G. J.; Grosse-Kunstleve, R. W.; McCoy, A. J.; Moriarty, N. W.; Oeffner, R.; Read, R. J.; Richardson, D. C.; Richardson, J. S.; Terwilligere, T. C.; Zwarta, P. H. PHENIX: a comprehensive Python-based system for macromolecular structure solution. *Acta. Cryst.* 2010**,** 66, 213-221.

59. Massey, V. A. In simple method for the determination of redox potentials, *Flavins Flavoproteins Proc*. Int. Symp., Berlin, Curti, B.; Ronchi, S.; Zanetti, G., Eds. Gruyter & Co.: Berlin, 1991; pp 59-66.

60. Van den Heuvel, R. H. H.; Fraaije, M. W.; Van Berkel, W. J. H. Redox properties of vanillyl-alcohol oxidase. *Methods Enzymol.* 2002**,** 353, 177-186.

61. Li, Y. R., P. J.; Ford, C. Effect of introducing proline residues on the stability of *Aspergillus awamori*. *Protein Eng.* 1997**,** 10, 1199-1204.

62. Nelson, D. L.; Cox, M. M., in Chapter 3: Amino acids, peptides and proteins. In *Principles of Biochemistry*, Ahr, K.; Ryan, M.; O'Neill, J.; Wong, V.; Ciprioni, J.; Mays, M.; Tymoczko, N., Eds. Sara Tenney: 2005; pp 78-79.

63. Gilday, L. C.; Robinson, S. W.; Barendt, T. A.; Langton, M. J.; Mullaney, B. R.; Beer, P. D. Halogen bonding in supramolecular chemistry. *Chem. Rev.* 2015, 115 (15), 7118-7195.

64. Breinlinger, E. C.; Rotello, V. M. Model systems for flavoenzyme activity. Modulation of flavin redox potentials through π-stacking interactions. *J. Am. Chem. Soc.* 1997, 119, 1165-1166.

65. Seo, D.; Naito, H.; Nishimura, E.; Sakurai, T. Replacement of Tyr50 stacked on the si-face of the isoalloxazine ring of the flavin adenine dinucleotide prosthetic group modulates *Bacillus subtilis* ferredoxin-$NADP^+$ oxidoreductase activity toward NADPH. *Photosynth. Res.* 2015, 125 (1), 321-328.

66. Lovering, A. L.; Hyde, E. I.; Searle, P. F.; White, S. A. The structure of *Escherichia coli* nitroreductase complexed with nicotinic acid: three crystal forms at 1.7 Å, 1.8 Å and 2.4 Å resolution. *J. Mol. Biol.* 2001, 309 (1), 203-213.

67. Johansson, E.; Parkinson, G. N.; Denny, W. A.; Neidle, S. Studies on the nitroreductase prodrug-activating system. Crystal structures of complexes with the inhibitor dicoumarol and dinitrobenzamide prodrugs and of the enzyme active form. *J. Med. Chem.* 2003, 46 (19), 4009-4020.

68. Koike, H.; Sasaki, H.; Kobori, T.; Zenno, S.; Saigo, K.; Murphy, M. E. P.; Adman, E. T.; Tanokura, M. 1.8 Å crystal structure of the major NAD(P)H: FMN oxidoreductase of a bioluminescent bacterium, *Vibrio fischeri*: overall structure, cofactor and substrate-analog binding, and comparison with related flavoproteins. *J. Mol. Biol.* 1998, 280 (2), 259-273.

69. Fersht, A. Structure and mechanism in protein science: a guide to enzyme catalysis and protein folding. W. H. Freeman and Conpany: New York, 1999.

70. Parkinson, G. N.; Skelly, J. V.; Neidle, S. Crystal structure of FMN-dependent nitroreductase from *Escherichia coli B*: A prodrug-activating enzyme. *J. Med. Chem.* 2000, 43 (20), 3624-3631.

71. Tanner, J. J.; Lei, B.; Tu, S.-C.; Krause, K. L. Flavin reductase P: Structure of a dimeric enzyme that reduces flavin. *Biochemistry* 1996, 35 (42), 13531-13539.

72. Hecht, H. J.; Erdmann, H.; Park, H. J.; Sprinzl, M.; Schmid, R. D. Crystal structure of NADH oxidase from *Thermus thermophilus*. *Nat. Struct. Mol. Biol.* 1995, 2 (12), 1109-1114.

73. Kobori, T.; Sasaki, H.; Lee, W. C.; Zenno, S.; Saigo, K.; Murphy, M. E. P.; Tanokura, M. Structure and site-directed mutagenesis of a flavoprotein from *Escherichia coli* that reduces nitrocompounds: Alteration of pyridine nucleotide binding by a single amino acid substitution. *J. Biol. Chem.* 2001, 276 (4), 2816-2823.

74. Kelley, L. A.; Sternberg, M. J. E. Protein structure prediction on the web: a case study using the Phyre server. *Nat. Protocols*. 2009, 4 (3), 363-371.

75. Ó Conchúir, S.; Barlow, K. A.; Pache, R. A.; Ollikainen, N.; Kundert, K.; O'Meara, M. J.; Smith, C. A.; Kortemme, T. A web resource for standardized benchmark datasets, metrics, and Rosetta protocols for macromolecular modeling and design. *PLoS ONE* 2015, 10 (9), e0130433.

76. Gnidehou, S.; Caillou, B.; Talbot, M.; Ohayon, R.; Kaniewski, J.; NoËL-Hudson, M.-S.; Morand, S.; Agnangji, D.; Sezan, A.; Courtin, F.; Virion, A.; Dupuy, C. Iodotyrosine dehalogenase 1 (DEHAL1) is a transmembrane protein involved in the recycling of iodide close to the thyroglobulin iodination site. *FASEB* 2004, 18 (13), 1574-1576.

77. Yu, T.-Y.; Mok, K. C.; Kennedy, K. J.; Valton, J.; Anderson, K. S.; Walker, G. C.; Taga, M. E. Active site residues critical for flavin binding and 5,6-dimethylbenzimidazole biosynthesis in the flavin destructase enzyme BluB. *Protein Sci.* 2012, 21 (6), 839-849.

78. Akiva, E.; Copp, J. N.; Tokuriki, N.; Babbitt, P. C., Evolution of new function from a minimal structural scaffold: structure-function transitions in the nitroreductase superfamily. Manucript in preparation.

79. Markiel, A.; Schwikowski, B.; Ideker, T.; Wang, T.; Shannon, P.; Ramage, A.; Ozier, O.; Amin, N. D.; Baliga, N., Cytoscape: a software environment for integrated models of biomolecular interaction networks.

80. Baier, F.; Copp, J. N.; Tokuriki, N. Evolution of enzyme superfamilies: comprehensive exploration of sequence–function relationships. *Biochemistry* 2016, 55 (46), 6375-6388.

81. Atkinson, H. J.; Morris, J. H.; Ferrin, T. E.; Babbitt, P. C. Using Sequence Similarity Networks for visualization of relationships across diverse protein superfamilies. *PLoS ONE* 2009, 4, e4345.

82. Akiva, E.; Copp, J. N.; Tokuriki, N.; Babbitt, P. C., Evolution of new function from a minimal structural scaffold: structure-function transitions in the nitroreductase superfamily. Manucript in preparation.

83. Watson, J. A.; McTamney, P. M.; Adler, J. M.; Rokita, S. E. Flavoprotein iodotyrosine deiodinase functions without cysteine residues. *ChemBioChem.* 2008, 9 (4), 504-506.

Curriculum Vitae

Nattha Ingavat
Johns Hopkins University
Department of Chemistry, Remsen 122
Baltimore, MD 21218
ing.nattha@gmail.com, mobile: 443-939-1036

Education

Johns Hopkins University, Krieger School of Arts and Sciences, Baltimore, MD
PhD Candidate (Chemistry) – expected graduation March 2017
Advisor: Prof. Steven E. Rokita

Chulabhorn Graduate Institute, Bangkok, Thailand
Master of Sciences, Chemical Biology, August 2009
Cumulative GPA: 3.93 on a scale of 4.0
Advisor: Dr. Prasat Kittakoop

Kasetsart University, Bangkok, Thailand
Bachelor of Sciences, Chemistry, May 2006
First-class honors

Research Experience

Rokita lab, Johns Hopkins University, January 2012 – present
PhD research involves binding and catalytic characterization of iodotyrosine dehalogenase from a bacterium, *Haliscomenobacter hydrossis*. Cloning, site-directed mutagenesis, protein expression and purification. Use of HPLC, FPLC, UV and fluorometer. Protein crystallization in collaboration with Asst. Prof. Jennifer Kavran, Department of Biochemistry and Molecular Biology, Johns Hopkins Bloomberg School of Public Health, Baltimore MD.

Research Assistant, Chulabhorn Graduate Institute, January 2007 – August 2009
Isolation and characterization of bioactive metabolites from marine-derived fungi. Column chromatography, use of HPLC and NMR.

Teaching experience

- Organic chemistry lecture: Teaching a group of 20 – 25 students at Johns Hopkins University.
- Introduction to chemistry: Holding help sessions for a group of 5 – 10 students at Johns Hopkins University.
- Organic chemistry laboratory: Briefing laboratory procedures for a group of 10 – 15 students at Johns Hopkins University.

Publications

Nattha Ingavat, Jennifer M. Kavran, Zuodong Sun, Steven E. Rokita. Active site binding is not sufficient for reductive deiodination by iodotyrosine deiodinase. *Biochemistry* 2017, 56 (8), 1130 – 1139.

Acharavadee Pansanit, Nattha Ingavat, Thammarat Aree, Chulabhorn Mahidol, Somsak Ruchirawat, Prasat Kittakoop. Nitrone formation in phosphate buffer and aqueous solutions: novel chemistry inspired by a natural product. *Tetrahedron Lett.* 2012, 53(16), 2129 – 2131.

Nattha Ingavat, Chulabhorn Mahidol, Somsak Ruchirawat, Prasat Kittakoop. Asperaculin A, a sesquiterpenoid from a Marine-derived fungus, *Aspergillus aculeatus*. *J. Nat. Prod.* 2011, 74(7), 1650 – 1652.

Nattha Ingavat, Jeffrey Dobereiner, Suthep Wiyakrutta, Chulabhorn Mahidol, Somsak Ruchirawat, Prasat Kittakoop. Aspergillusol A, an α-glucosidase inhibitor from the marine-derived fungus *Aspergillus aculeatus*. *J. Nat. Prod.* 2009, 72(11), 2049 – 2052.

Presentations

- Poster presentation: 30th Anniversary Symposium of the Protein Society (2016), Hyatt Regency Baltimore, MD. Title "Active site binding is not sufficient for reductive deiodination by iodotyrosine deiodinase"
- Poster presentation: 45th Mid-Atlantic Protein Crystallography Meeting (2015), Johns Hopkins University, Homewood Campus, Baltimore MD. Title "Engineering iodotyrosine deiodinase to broaden the substrate specificity"

Honors and Awards

- Full scholarship, Center of Excellence on Environmental Health, Toxicology and Management of Chemicals (ETM) and Chulabhorn Research Institute, June 2007 – August 2009
- Certificates from Dr. Tab Nilanidhi Foundation, 2004 and 2007
- Full scholarship, Faculty of Science, Kasetsart University May 2004 – May 2006